2

International Workshop on

Discrete Time Domain Modelling of Electromagnetic Fields and Networks

DAJA 45-91-M-0311.
R&D 6794-EE-02.

The German IEEE MTT/AP Joint Chapter and
the German IEEE CAS Chapter
Munich, October 24-25, 1991

International Workshop on

Discrete Time Domain Modelling of Electromagnetic Fields and Networks

The German IEEE MTT/AP Joint Chapter and the German IEEE CAS Chapter

Munich
October 24-25 1991

International Workshop of the German IEEE MTT/AP Joint Chapter
and the German IEEE CAS Chapter
on

Discrete Time Domain Modelling of Electromagnetic Fields and Networks

October 24-25, 1991.

Technical University Munich
Hörsaal 0606 (Theresianum)

The workshop will be organized by P. Russer and J. Nossek (both Technical University Munich) under sponsorship of the European Research Office (ERO) of the U.S. Army.

Program:

Thursday,	October 24, 1991:	
	SESSION A1 (Chairman: Prof. J.A. Nossek)	
10 00	Opening Session	K. Steinbach
10:10	Overview of Discrete Time Domain Modelling of Electromagnetic Fields	P. Russer
11:00	Radiation and Scattering of Transient Electromagnetic Fields	L B. Felsen
11:50	- Break -	
	SESSION A2 (Chairman: Prof. P. Russer)	
13:20	Finite Difference Time Domain Modelling of Electromagnetic Fields	I Wolff
14:10	TLM Modelling of Electromagnetic Fields	W.J.R. Hoefer
15.00	- Break -	
15·30	Multi-Dimensional Wave Digital Filters	A. Fettweis
16:20	Recent Developments in Numerical Integration of Differential Equations	W. Mathis
	SOCIAL EVENT (at Seehaus/Kleinhesseloher See, Munich 40)	
19 00	Song Recital with Piano and afterwards Dinner	
Friday,	October 25, 1991:	
	SESSION B1 (Chairman: Prof. W.J.R. Hoefer)	
8.30	Cellular Automata	L. Thiele
9.20	Cellular Automata	G Wunsch
10·10	- Break -	
10:40	Analysis of Nonlinear Microwave Circuits via the Time Domain Voltage-Update Method	T. Itoh
11:30	Nonlinear Time Domain Modelling of Networks	M. Sobhy
12.20	- Break -	

SESSION B2 (Chairman: Prof. A. Fettweis)

	Short contributions:	
13 10	Efficient Analytical-Numerical Modeling of Ultra-Wideband Pulsed Plane Wave Scattering from a Large Strip Grating	L.B. Felsen, L. Carin
13.25	Transient Currents and Fields of Wire Antennas with Diodes	N. Scheffer
13·40	Calculating Frequency Domain Data by Time Domain Methods	M. Dehler
13·55	– Break–	
14·15	Time Domain Analysis of Inhomogeneously Loaded Structures Using Eigenfunction Expansion	M. Mrozowski
14:30	The Hilbert Space Formulation of the TLM-Method	M. Krumpholz, P. Russer
14.45	Late Contributions	

CONCLUDING SESSION

16 00 Open Forum,
Panel Discussion

Further short contributions will be accepted at the workshop.

LIST OF PARTICIPANTS

Invited speakers:

name	
Prof. Dr. L.B. Felsen	Polytechn Univ. Farmingdale New York
Prof. Dr. A. Fettweis	Ruhr-Univ. Bochum
Prof. Dr. W.J.R. Hoefer	Univ. of Ottawa
Prof. Dr. T. Itoh	Univ. California Los Angeles
Prof. Dr. W. Mathis	GH Wuppertal
Prof. Dr. P. Russer	TU München
Prof. Dr. M.I. Sobhy	Univ. of Kent
Prof. Dr. L. Thiele	Univ. Saarbrücken
Prof. Dr. I. Wolff	Univ. Duisburg
Prof. Dr. G. Wunsch	Univ. Radebeul

Further participants:

name	
W. Anzill	TU München
H. Bender	TU München
Prof. Bex	FH Aachen
Dr. E. Biebl	TU München
Chr. Bornkessel	Univ. Karlsruhe
C. Ciotti	TH Aachen
Prof. Dalichau	Univ. d. Bundeswehr München
Dr. M. Dehler	TH Darmstadt
Prof. Dr. Entenmann	TU München
Prof. Dr. I. Frost	Univ. of York
T. Felgentreff	TU München
G. Gotthard	Univ. Karlsruhe
J. Graul	Texas Instruments
V. Güngerich	TU München
Prof. Dr. H.L. Hartnagel	TH Darmstadt
Dr. Heidler	Univ. d. Bundeswehr München
Prof Dr. E. Holzhauer	Univ. Stuttgart
Hüper	TU München
B. Isele	TU München
Prof. Dr. R.H. Jansen	Jansen Microwave
M. König	TU München
M. Krumpholz	TU München
Dr. J.F. Luy	Daimler Benz

name	
Prof. Dr G. Mahler	Univ. Stuttgart
H. Meier	TU München
H. Meinel	DASA
Dr. M. Mrozowski	TU Gdansk
Dr. J.W. Mink	ARO/US.Army
S. Müller	TU München
G. Nitsche	Ruhr-Uni. Bochum
Prof. Dr. J.A. Nossek	TU München
Dr. G. Olbrich	TU München
Hr. Paul	TU München
E. Parzich	Parzich GmbH
G. Rohrbach	Univ. Stuttgart
F. Rostan	Univ. Karlsruhe
Dr. N. Scheffer	Telefunken Systemtechnik
M. Schneider	MBB
Prof. Dr. R. Sorrentino	Univ. Perugia
Dr. K. Steinbach	ERO/US.Army
R. Stephan	TH Ilmenau
W. Tewes	DLR Oberpfaffenhofen
Prof. Thim	Univ. Linz
W Thomann	TU München
Dr. K H. Türkner	
Prof. Uhlmann	TH Ilmenau
Dr. R. Weigel	TU München
Dr. N. Zhu	Univ. Stuttgart
Th. Zundl	Univ. d. Bundeswehr München

Overview over Discrete Time Domain Methods in Electromagnetic Field Computation

Peter Russer [1]

Abstract

The modelling of fields in the time domain describes the evolution of physical quantities in a natural way. Transient phenomena, nonlinear and dispersive behaviour, the characteristics of systems with moving boundaries or with time dependent properties are best described in the time domain. In this contribution different approaches for time domain modelling of electromagnetic fields are compared.

1 Introduction

For electromagnetic field modelling numerous techniques have been developed [1,2,3]. The modelling of fields and networks in the time domain is highly attractive since it describes the evolution of physical quantities in a natural way. Time domain modelling is especially advantageous in the case of transient electromagnetic fields, fields in nonlinear, dispersive or time-dependend media or in regions with moving boundaries. One of the main advantages of time-domain modelling of electromagnetic fields is the local dependence of the field variables on space as well as on time. Within discretized space and time the state of the field in a given point and at a given time depends only on the field states of the neighbouring points at previous times This allows a highly parallel computation of the time evolution of the discretized field.

In modelling of high frequency circuits we have to deal with the network as well with the field concept (Table 1). Whereas the field has a spatial structure the network structure is topological. However if the field is described by a discrete set of base functions as it is done for example in the method of moments [4,5] or if the field is discretized with respect to space we obtain topological relations between the state variables of the field This allows to apply network-theoretical methods to field problems.

[1]Lehrstuhl für Hochfrequenztechnik, Technische Universität München, Arcisstrasse 21, D-8000 Munich 2, Fed. Rep Germany

Table 1: Concepts of Field Theory and Network Theory

NETWORK	FIELD
Topological structure	Spatial structure
Time, Amplitude	Time, Amplitude, Space
Continuous	
• Analog Network	• Electromagnetic Field
Discrete	
• Digital network	• Cellular Automata
• Discrete modelling of analog networks	• Discrete Modelling of fields

In the following we shall focus our attention on four approaches for time domain modelling of electromagnetic fields.

- The finite-difference time-domain (FDTD) method
- The transmission line matrix (TLM) method
- The field modelling by cellular automata
- The field modelling by multi-dimensional wave digital filters (MDWDF)

2 The Finite-Difference Time-Domain Method

The finite-difference time domain (FDTD) method is the mathematical approach for the solution of partial differential equations [6]. The partial derivatives are simply replaced by finite differences. In 1966 Yee has first given a finite-difference time-domain scheme for solution of the Maxwell equations [7,8,9]. In the FDTD method space and time are discretized with increments Δl and Δt, respectively. The field component placement in the FDTD unit cell is shown in Fig. 1. The side length of a unit cell in our notation is $2\Delta l$

Space and time coordinates are given by $x = l\,\Delta l$, $y = m\Delta l$, $z = n\,\Delta l$ and $t = k\,\Delta t$. The FDTD scheme for the solution of the Maxwell's equations is then given by

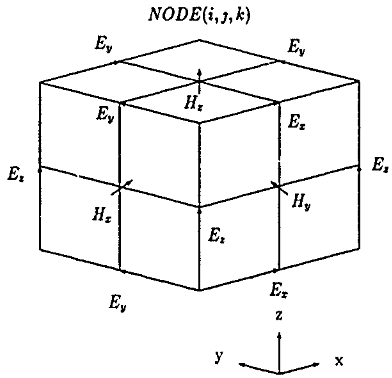

Figure 1: Field components in the FDTD unit cell.

$$
\begin{aligned}
H_x^{k+1}(l,m+1,n+1) &= H_x^{k-1}(l,m+1,n+1) + \\
&+\frac{s}{\mu}\Big[E_y^k(l,m+1,n+2) - E_y^k(l,m+1,n) + \\
&\quad + E_z^k(l,m,n+1) - E_z^k(l,m+2,n+1)\Big] \qquad (1)\\
H_y^{k+1}(l+1,m,n+1) &= H_y^{k-1}(l+1,m,n+1) + \\
&+\frac{s}{\mu}\Big[E_z^k(l+2,m,n+1) - E_z^k(l,m,n+1) + \\
&\quad + E_x^k(l+1,m,n) - E_x^k(l+1,m,n+2)\Big] \qquad (2)\\
H_z^{k+1}(l+1,m+1,n) &= H_z^{k-1}(l+1,m+1,n) + \\
&+\frac{s}{\mu}\Big[E_x^k(l+1,m+2,n) - E_x^k(l+1,m,n) + \\
&\quad + E_y^k(l,m+1,n) - E_y^k(l+2,m+1,n)\Big] \qquad (3)\\
E_x^{k+2}(l+1,m,n) &= E_x^k(l+1,m,n) + \\
&+\frac{s}{\epsilon}\Big[H_z^{k+1}(l+1,m+1,n) - H_z^{k+1}(l+1,m-1,n) + \\
&\quad + H_y^{k+1}(l+1,m,n-1) - H_y^{k+1}(l+1,m,n+1)\Big] \qquad (4)\\
E_y^{k+2}(l,m+1,n) &= E_y^k(l,m+1,n) + \\
&+\frac{s}{\epsilon}\Big[H_x^{k+1}(l,m+1,n+1) - H_x^{k+1}(l,m+1,n-1) + \\
&\quad + H_z^{k+1}(l-1,m+1,n) - H_z^{k+1}(l+1,m+1,n)\Big] \qquad (5)
\end{aligned}
$$

$$
\begin{aligned}
E_z^{k+2}(l,m,n+1) \;=\; & E_z^k(l,m,n+1) + \\
& +\frac{s}{\epsilon}\Big[H_y^{k+1}(l+1,m,n+1) - H_y^{k+1}(l-1,m,n+1) + \\
& +H_x^{k+1}(l,m-1,n+1) - H_x^{k+1}(l,m+1,n+1)\Big] \qquad (6)
\end{aligned}
$$

with the stability factor

$$s = \frac{2c\Delta t}{\Delta l} \quad , \qquad (7)$$

where c is the velocity of light, Δt is the time interval, Δl is the length interval. The condition for stability is given by

$$s \le \frac{1}{\sqrt{3}} \qquad (8)$$

The FDTD scheme gives the new field state at the time $k\,\Delta t$ as a function of the field states at $(k-1)\,\Delta t$ and $(k-2)\,\Delta t$. Also the new spatial components at l, m and n are related to the spatial components at $l \pm 1$, $l \pm 2$, $m \pm 1$, $m \pm 2$, $n \pm 1$ and $n \pm 2$. However all electrical field components with even values of k, are only related to the magnetic field components with odd values of k and vice versa.

Investigating planar circuits within the magnetic wall model a two-dimensional finite difference scheme may be applied [10]. For the circuit plane parallel to the $x-y$-plane the electric field exhibits only the z-component and the magnetic field exhibits only the x- and y- components The surface current $\mathbf{J}$ flowing in the upper plane of the planar circuit is given by

$$\mathbf{J} = -\mathbf{e}_z \times \mathbf{H} \qquad (9)$$

where $\mathbf{e}_z$ is the unit vector in z direction. The voltage V between the plates is given by

$$V = -dE_z \qquad (10)$$

where d is the distance between the plates.

$$\nabla V(x,y,t) = -jL_s\frac{\partial \mathbf{J}(x,y,t)}{\partial t} \qquad (11)$$

$$\nabla \cdot \mathbf{J}(x,y,t) = -jC_s\frac{\partial V(x,y,t)}{\partial t} \qquad (12)$$

C_s is the capacitance and L_s is the inductance of an arbitrary square element of the two-dimensional parallel plate line.

$$
\begin{aligned}
J_x^{k+1}(m,n) \;=\; & J_x^{k-1}((m,n) + \\
& +\frac{\Delta t}{L_s h}\Big[V^k(m+1,n) - V^k(m+1,n)\Big] \qquad (13) \\
J_y^{k+1}(m,n) \;=\; & J_y^{k-1}((m,n) + \\
& +\frac{\Delta t}{L_s h}\Big[V^k(m,n+1) - V^k(m,n+1)\Big] \qquad (14)
\end{aligned}
$$

$$\begin{aligned} V^{k+1}(m,n) &= V^{k-1}((m,n) - \\ &-\frac{\Delta t}{C_s h}\Big[J_x^k(m+1,n) - J_x^k(m-1,n) + \\ &+J_y^k(m,n+1) - J_y^k(m,n-1)\Big] \end{aligned} \tag{15}$$

Nonrectangular grids have been treated for the FD method [11]. The analysis of radiating structures requires the termination of the grid with absorbing boundaries [11,12,13].

3 The TLM (Transmission Line Matrix) Method

The transmission line matrix (TLM) method was developed and first published in 1971 by Johns and Beurle [14,15,16,17]. In the TLM method the physical analogy and the isomorphism in the mathematical description between the electromagnetic field and a mesh of transmission lines is used. The field evolution is modelled by voltage pulses propagating on the mesh lines and being scattered in the mesh nodes. Field theoretically the TLM method is based on the Huygens principle [18,19]

In the TLM model space and time are discretized in length intervals Δl and time intervals Δt. The intervals Δl and Δt correspond to the real space and time intervals without scaling if $\Delta l = \sqrt{2}c_0\Delta t/\sqrt{\epsilon_r}$ is chosen, where ϵ_r is the relative permittivity. Fig. (2) shows the port numbering of a two-dimensional TLM shunt node.

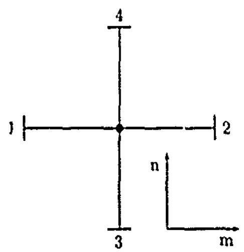

Figure 2: A two-dimensional TLM shunt node.

The scattering of impulses at a shunt nodeis described by the following equation:

$$_k\begin{bmatrix} V_1 \\ V_2 \\ V_3 \\ V_4 \end{bmatrix}^r = \mathrm{S}\ _k\begin{bmatrix} V_1 \\ V_2 \\ V_3 \\ V_4 \end{bmatrix}^i \tag{16}$$

Z_0 is the characteristic mesh line impedance, given by

$$Z_0 = \frac{h\eta_0}{\Delta l \sqrt{\epsilon_r}} \tag{17}$$

where $\eta_0 = 377\Omega$, h is the height of the planar structure, and ϵ_r its permittivity.

The node scattering matrix for a shunt node is

$$\mathbf{S} = \begin{bmatrix} -\frac{1}{2} & \frac{1}{2} & \frac{1}{2} & \frac{1}{2} \\ \frac{1}{2} & -\frac{1}{2} & \frac{1}{2} & \frac{1}{2} \\ \frac{1}{2} & \frac{1}{2} & -\frac{1}{2} & \frac{1}{2} \\ \frac{1}{2} & \frac{1}{2} & \frac{1}{2} & -\frac{1}{2} \end{bmatrix} \tag{18}$$

Lossy subregions can be modelled in TLM by connecting a lumped resistor or an infinitely long transmission line stub across each mesh node [20]. Also the modelling of nonlinear passive elements has already been treated [21,22,23]. Nonlinear active regions may be modelled by connecting nonlinear active circuit elements to the mesh nodes [24,25]

The voltage wave pulses ${}_kV^i_{\nu,m,n}$ incident on a TLM mesh node depend on the voltage wave pulses ${}_{k-1}V^r_{\nu,m,n}$ emerging from the neighboring nodes as follows:

$$\begin{aligned} {}_{k+1}V^i_{1,m,n} &= {}_k V^r_{3,m,n} \\ {}_{k+1}V^i_{2,m,n} &= {}_k V^r_{4,m,n} \\ {}_{k+1}V^i_{3,m,n} &= {}_k V^r_{1,m,n} \\ {}_{k+1}V^i_{4,m,n} &= {}_k V^r_{2,m,n} \end{aligned} \tag{19}$$

Eqs (16)-(18) and (19) describe the complete algorithm for the time discrete field evolution.

For the two-dimensional case Johns has shown the relation between the FDTD method and the TLM method [28]

$$E_z = \mathbf{p}\mathbf{q}^T + \mathbf{r} \tag{20}$$

with

$$\mathbf{q}^T = \frac{1}{2}[1\ 1\ 1\ 1] \tag{21}$$

$$\mathbf{p}^T = [1\ 1\ 1\ 1] \tag{22}$$

$$\mathbf{r} = -1 \tag{23}$$

$$_{k+1}E_z = q\mathrm{C}\left({}_kE_z + \mathrm{r}_k\mathrm{V}^i\right) \tag{24}$$

$$_{k+1}E_z = q\mathrm{Cp}\,{}_nE_z q\mathrm{CrCp}\,{}_{k-1}E_z + q\mathrm{CrCp}\,{}_{k-1}V^i \tag{25}$$

With

$$\mathrm{CrCr} = a1 \tag{26}$$

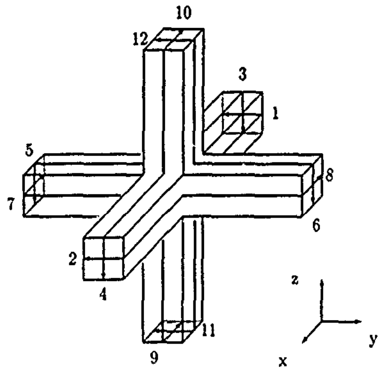

Figure 3: Three-dimensional symmetric condensed TLM node.

where a is a constant we obtain

$$_{k+1}E_z = q\mathrm{Cp}\ _kE_z q\mathrm{CrCp}\ _{k-1}E_z a_{k-1}E_z \tag{27}$$

We now have an algorithm relating $_{k+1}E_z$ to $_kE_z$ and to $_{k-1}E_z$. We have reduced the variables but increase the time depths of the algorithm

Different TLM schemes have been proposed for the three-dimensional case [16]. A symmetrical three-dimensional condensed node has been introduced by Johns [26,27]. Fig. 3 shows the symmetric condensed TLM node In the three-dimensional case we have to introduce twelve wave amplitudes The voltage wave vector is given by

$$\begin{aligned} \mathbf{V}^i &= [V_1^i V_2^i V_3^i V_4^i V_5^i V_6^i V_7^i V_8^i V_9^i V_{10}^i V_{11}^i V_{12}^i]^T \\ \mathbf{V}^r &= [V_1^r V_2^r V_3^r V_4^r V_5^r V_6^r V_7^r V_8^r V_9^r V_{10}^r V_{11}^r V_{12}^r]^T \end{aligned} \tag{28}$$

the incident wave pulses $_k\mathbf{V}^i$ at $t = k\Delta t$ and the scattered wave pulses $_{k+1}\mathbf{V}^r$ at $t = (k+1)\Delta t$ are related by

$$_{k+1}\mathbf{V}^r = \mathbf{S}\ _k\mathbf{V}^i \tag{29}$$

the scattering matrix S given by

$$\mathbf{S} = \begin{bmatrix} 0 & \mathbf{T} & \mathbf{T}^T \\ \mathbf{T}^T & 0 & \mathbf{T} \\ \mathbf{T} & \mathbf{T}^T & 0 \end{bmatrix} \tag{30}$$

with

$$\mathbf{T} = \begin{bmatrix} 0 & 0 & \frac{1}{2} & -\frac{1}{2} \\ 0 & 0 & -\frac{1}{2} & \frac{1}{2} \\ \frac{1}{2} & \frac{1}{2} & 0 & 0 \\ \frac{1}{2} & \frac{1}{2} & 0 & 0 \end{bmatrix} \tag{31}$$

We introduce the field vector $\mathbf{F}$ given by

$$\mathbf{F} = \left[\mathbf{E}^T, \frac{1}{Z_0}\mathbf{H}^T\right]^T \tag{32}$$

The wave amplitude vector $_k\mathbf{V}^i_{l,m,n}$ is related to the field vector $_k\mathbf{F}_{l,m,n}$ by

$$\mathbf{F} = \mathbf{Q}\mathbf{V}' \tag{33}$$

$$\mathbf{V}' = \frac{1}{2}\mathbf{Q}^T\mathbf{F} \tag{34}$$

with

$$\mathbf{Q}^T = \begin{bmatrix} 0 & 0 & 0 & 0 & 0 & 0 & 1 & 1 & 1 & 1 & 0 & 0 \\ 1 & 1 & 0 & 0 & 0 & 0 & 0 & 0 & 0 & 0 & 1 & 1 \\ 0 & 0 & 1 & 1 & 1 & 1 & 0 & 0 & 0 & 0 & 0 & 0 \\ 0 & 0 & 0 & 0 & -1 & 1 & 0 & 0 & 0 & 0 & 1 & -1 \\ 0 & 0 & 1 & -1 & 0 & 0 & 0 & 0 & -1 & 1 & 0 & 0 \\ -1 & 1 & 0 & 0 & 0 & 0 & 1 & -1 & 0 & 0 & 0 & 0 \end{bmatrix} \tag{35}$$

Structures to be analyzed in TLM may be segmented into substructures. This method first proposed by Kron is called diakoptics [29,30,31]. Within diakoptics the scattering of waves by boundaries is expressed via discrete Green's functions or so-called Johns matrices [17]. Discrete Green's functions may also be computed algebraically [32] The TLM method in connedtion with absorbing boundary conditions has already been applied to the analysis of a slot antenna [33]

4 Cellular Automata

John von Neumann's most extensive work in the theory of automata was the investigation of cellular automata [34]. The results of this work are contained in the manuscript "The

Theory of Automata: Construction, Reproduction, Homogeneity" [35]. John von Neumann's cellular automata are homogeneous two-dimensional arrays of square cells, each containing the same twentynine-state finite automaton. Any cell can assume at a given time the unexcitable state, one of twenty quiescent states or one of eight sensitized states. The unexcitable state represents the presence of no neuron. Quiescent cells can respond to stimuli from adjacent cells. The state of a cell at a given time is determined by a set of transition rules. The state after the transition is determined by the initial states of the cell and of its four nondiagonal neighbours. John von Neumann has shown that the twentynine states are sufficient to accomodate all logical and construction circumstances that may arise and also to establish all transition rules for moving from one state to the other. He demonstrated the logical universality of the cellular automata by showing how Turing's machine model can be reformulated in terms of cellular automata.

John von Neumann also has planned the continuous model as a further refinement. In 1969 Konrad Zuse discussed the modelling of the Maxwell's equations by cellular automata [36].

Cellular automata now meet with growing interest for modelling of physical systems [38]. The discrete system may be described in state variable form [37]. An autonomous system is described by

$$z(r, t+1) = \sum_{r' \in \lambda_1} A(r', r) z(r', t) \tag{36}$$

In vector notation this is given by

$$\mathbf{z}(t+1) = \mathbf{A}\mathbf{z}(t) \tag{37}$$

where $\mathbf{z}(t)$ is the state vector and $\mathbf{A}$ is called the transition matrix. The discrete time variable is t, and $\mathbf{r}$ is the discrete space variable.

As an example we consider the telegraphist's equation [37].

$$\begin{aligned} -L\frac{\partial i}{\partial t} &= Ri + \frac{\partial v}{\partial x} \\ -C\frac{\partial v}{\partial t} &= Gv + \frac{\partial i}{\partial x} \end{aligned} \tag{38}$$

The corressponding difference equation is given by

$$\begin{aligned} -L\Delta_t i &= Ri + \Delta_x v \\ -C\Delta_t v &= Gv + \Delta_x i \end{aligned} \tag{39}$$

Δ_t and Δ_x are given by

$$\begin{aligned} \Delta_t i(x,t) &= i(x, t+1) - i(x,t) \\ \Delta_x i(x,t) &= i(x+1, t) - i(x,t) \end{aligned} \tag{40}$$

The state vector $\mathbf{z}$ and the transition matrix $\mathbf{A}$ in eq. (37) are given by

$$\mathbf{z} = \begin{bmatrix} i(x,t) \\ v(x,t) \end{bmatrix} \tag{41}$$

and

$$\mathbf{A} = \mathbf{A}_0 + \mathbf{A}_1\Delta_x \tag{42}$$

with

$$\mathbf{A}_0 = \begin{bmatrix} -\frac{R}{L} & 0 \\ 0 & -\frac{G}{C} \end{bmatrix} \tag{43}$$

$$\mathbf{A}_1 = \begin{bmatrix} 0 & -\frac{1}{L} \\ -\frac{1}{C} & 0 \end{bmatrix} \tag{44}$$

Using the Z transformation with respect to x the variable ξ, given by

$$\mathbf{Z}\left\{\mathbf{z}(x)\right\} = \sum_{\nu=0}^{\infty} \mathbf{z}(\nu)\xi^{-\nu} \tag{45}$$

and with

$$\mathbf{Z}\left\{\Delta_x\mathbf{z}(x)\right\} = \left(\xi^{-1} - 1\right)\mathbf{Z}\left\{\mathbf{z}(x)\right\} \tag{46}$$

we obtain

$$\mathbf{z}(\xi, t+1) = \mathbf{A}\mathbf{z}(\xi, t) \tag{47}$$

with

$$\mathrm{A} = \begin{bmatrix} 1 - \frac{R}{L} & \frac{1-\xi^{-1}}{L} \\ \frac{1-\xi^{-1}}{C} & -\frac{G}{C} \end{bmatrix} \tag{48}$$

This result may be transformed into a digital circuit Fig. 4. shows the corresponding digital model of the lossy transmission line.

5 Field Modelling by Multi-Dimensional Wave Digital Filters

The numerical integration of partial differential equations using principles of multidimensional wave digital filters (MDWDFs) has been proposed by Fettweis [43,44]. The continuous-domain physical system is simulated by means of a discrete passive dynamical system. In this method in a first step the partial differential equation is modelled by a multidimensional analog circuit. This circuit is then transformed into a MDWDF equivalent circuit [45]. The advantage of this method is the robustness of the algorithm even under conditions of of rounding and truncation operations.

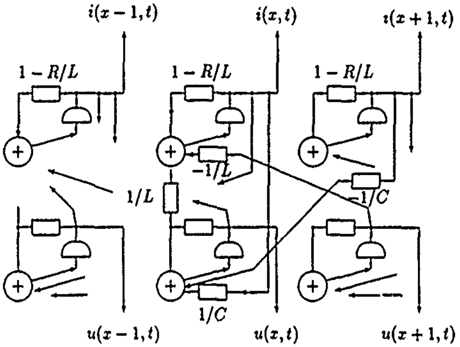

Figure 4: Digital model of the lossy transmission line.

Let us consider as an example again the two-dimensional electromagnetic field problem associated with a transverse electric field between two metal plates. We investigate the equations

$$L\frac{\partial i_1}{\partial t_3} + Ri_1 + \frac{\partial v}{\partial t_1} = u_1(t) \tag{49}$$

$$L\frac{\partial i_2}{\partial t_3} + Ri_2 + \frac{\partial v}{\partial t_2} = u_2(t) \tag{50}$$

$$\frac{\partial i_1}{\partial t_1} + \frac{\partial i_2}{\partial t_2} + \frac{\partial v}{\partial t_3} + Gv = u_3(t) \tag{51}$$

The variable t_3 corresponds to time, whereas t_1 and t_2 represent the spatial coordinates. The current density components in the upper metal plate in the directions t_1 and t_2, respectively, are given by i_1 and i_2, and v is the voltage between the metal plates. The inhomogeneous terms u_1, u_2 and u_3 represent distributed impressed sources.

In the three-dimensional complex frequency domain we obtain the algebraic equations

$$(p_3L + R)I_1 + p_1R_3I_3 = U_1 \tag{52}$$

$$(p_3L + R)I_2 + p_2R_3I_3 = U_2 \tag{53}$$

$$p_1R_3I_1 + p_2R_3I_2 + (p_3C + G)R_3^2I_3 = U_3 \tag{54}$$

where p_1, p_2 and p_3 are the complex frequencies The corresponding analog circuit representing the partial differential equations is depicted in Fig. 5 Note that the this equivalent circuit represents the complete field.

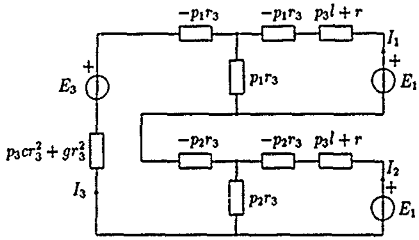

Figure 5: Multidimensional analog circuit

Introducing the differential operators

$$D_\nu = \frac{\partial}{\partial t} \qquad \text{for} \quad \nu = 1\dots3 \tag{55}$$

yields

$$(D_3L+R)I_1 + D_1R_3I_3 = U_1 \tag{56}$$
$$(D_3L+R)I_2 + D_2R_3I_3 = U_2 \tag{57}$$
$$D_1R_3I_1 + D_2R_3I_2 + (D_3C+G)R_3^2I_3 = U_3 \tag{58}$$

Using the trapezoidal rule for integration yields the replacement of the differential equations by the following difference equations:

$$v(\mathbf{t}) - v(\mathbf{t}-\mathbf{T}_\nu) = R(\mathbf{t})i(\mathbf{t}) - R(\mathbf{t}-\mathbf{T}_\nu)i(\mathbf{t}-\mathbf{T}_\nu) \tag{59}$$
$$i(\mathbf{t}) - i(\mathbf{t}-\mathbf{T}_\nu) = G(\mathbf{t})v(\mathbf{t}) - G(\mathbf{t}-\mathbf{T}_\nu)v(\mathbf{t}-\mathbf{T}_\nu) \tag{60}$$

where $\mathbf{t}$ is given by

$$\mathbf{t} = [t_1, t_2, t_3]^T \tag{61}$$

the vectors $\mathbf{T}_\nu$ are given by

$$\mathbf{T_1} = [T_1, 0, 0]^T, \quad \mathbf{T_2} = [0, T_2, 0]^T, \quad \mathbf{T_3} = [0, 0, T_3]^T, \tag{62}$$

T_3 is an arbitrary positive time increment and T_1 and T_2 are related to T_3 via

$$T_1 = T_2 = \sqrt{2}T_3/\sqrt{LC} \tag{63}$$

and $R(\mathbf{t})$ and $G(\mathbf{t})$ are given by

$$R(\mathbf{t}) = 2L(\mathbf{t})/T_\nu, \qquad G(\mathbf{t}) = 2C(\mathbf{t})/T_\nu \tag{64}$$

using the wave digital filter design rules the circuit according to Fig. 5 is converted into the wave digital filter circuit shown in Fig. 6. The methods of MDWDFs ensure that the algorithm is recursible and that the full range of robustness properties of WDFs is conserved

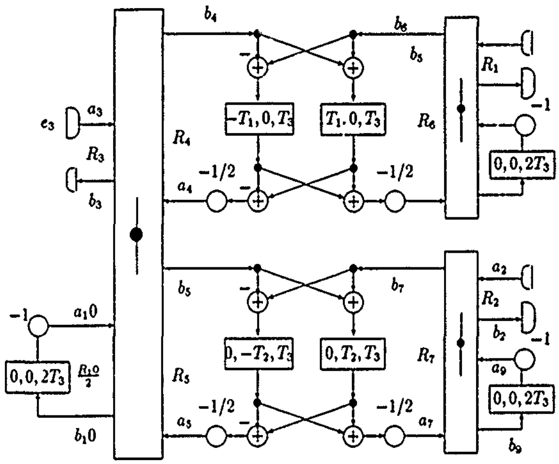

Figure 6: Wave digital filter

6 Conclusion

We have compared four different methods of discrete time domain analysis of electromagnetic fields. The methods originate from different theoretical frameworks. Whereas the FDTD method is based on mathematical considerations, TLM originates from a line model. The method of cellular automata is based on the theory of automata and systems and the method of MDWDFs uses the analogy to multidimensional circuits and wave digital filters. There are interesting analogies between these methods. Each of these methods contributes special advantages and interesting contributions to the solution of problems also relevant in the other models

This work has been supported by the Deutsche Forschungsgemeinschaft.

References

[1] T Itoh, "Numerical Techniques for Microwave and Millimeter-Wave Passive Structures," *J Wiley, New York*, 1989.

[2] R Sorrentino, "Numerical Methods for Passive Microwave and Millimeter Wave Structures," *IEEE Press, New York*, 1989

[3] E. Yamashita, "Analysis Methods for Electromagnetic Wave Problems," *Artech House, Boston*, 1990

[4] R F Harrington, "Matrix Methods for Field Problems" *Proc IEEE*, vol 55, no.2 pp 136-149, Feb 1967.

[5] R F Harrington, "Field Computation by Moment Methods", *Krieger, Malabar, Florida* 1982

[6] J.C Strikwerda, "Finite Difference Schemes and Partial Differential Equations", *Wadsworth & Brooks, Pacific Grove*, 1989.

[7] K S. Yee, "Numerical Solution of Initial Boundary Value Problems Involving Maxwell's Equations in Isotropic Media", *IEEE Trans Antennas Propagat.*, vol. AP-14,no 5, pp. 302-307,1966.

[8] D.H. Choi, W J.R Hoefer, "The Finite-Difference Time-Domain Method and its Applications to Eigenvalue Problems", *IEEE Trans Microwave Theory Tech.*, vol. MTT-34, no. 12, pp.1464-1470, 1986.

[9] D.M Sheen, S M Ali, M.D AAbouzahra, J A Kong "Application of the Three-Dimensional Finite-Difference Time-Domain Method to the Analysis of Planar Microstrip Circuits", *IEEE Trans Microwave Theory Tech.*, vol. MTT-34, no 12, pp 1464-1470, 1986.

[10] W.K Gwarek, "Analysis of Arbitrarily Shaped Two-Dimensional Microwave Circuits by Finite-Difference Time-Domain Methods", *IEEE Trans Microwave Theory Tech.*, vol. MTT-36,no 4, pp 738-744, 1988

[11] C F. Lee, R T Shin, J A Kong, "Finite Difference Method for Electromagnetic Scattering Problems", in: "Progress in Electromagnetics Research," vol 4 *Elsevier, New York*, 1991, Chapter 11, pp. 373-415.

[12] B Engquist, A. Majda, "Absorbing Boundary Conditions for the Numerical Simulation of Waves", Mathematics of Computation, Vol. 31, Nummer 139, 1977, pp. 629-651

[13] C R I. Emson, "Methods for the Solution of Open-Boundary Electromagnetic Field Problems",

[14] P.B. Johns, R L Beurle, "Numerical Solution of 2-Dimensional Scattering Problems using a Transmission-Line Matrix", *Proc. IEE*, vol.118, no 9, pp 1203-1208, Sept 1971.

[15] W J.R Hoefer, "The Transmission Line Matrix Method-Theory and Applications", *IEEE Trans Microwave Theory Tech*, vol MTT-33, no 10, pp 882-893, Oct 1985

[16] W J.R Hoefer, "The Transmission Line Matrix (TLM) Method", Chapter 8 in "Numerical Techniques for Microwave and Millimeter Wave Passive Structures", edited by T. Itoh, *John Wiley & Sons, New York*, 1989, pp 496-591

[17] W J R. Hoefer, "The Discrete Time-Domain Green"s Function or Johns Matrix-A New Powerful Concept in Transmission Line Modelling (TLM)", Int J. Numer. Modelling, vol. 2, pp. 215-255 1989

[18] E. Zauderer, "Partial Differential Equations of Applied Mathematics", New York, 1989, John Wiley & Sons, pp. 470-475.

[19] J.A Kong, "Electromagnetic Wave Theory", *J. Wiley, New York*, 1986, p. 383.

[20] S. Akhtarzad, "Analysis of Lossy Microstrip Structures and Microstrip Resonators by the TLM Method", Ph.D dissertation, *University of Nottingham, England*, July 1975.

[21] P.B Johns, M. O'Brien, "Use of the Transmission Line Modelling (t.l m.) Method to solve Nonlinear Lumped Networks", The Radio and Electronic Engineer, vol. 50, No.1/2, pp. 59-70, Jan./Febr 1980

[22] S.A. Kosmopoulos, W.J.R. Hoefer, A. Gagnon "Non-Linear TLM Modelling of High-Frequency Varactor Multipliers and Halvers", Intl. Journal of Infrared and Millimeter Waves, Vol 10, No 3, pp. 343-352, Mar. 1989.

[23] R A. Voelker, R J. Lomax, "A Finite-Difference Transmission Line Matrix Method Incorporating a Nonlinear Device Model", IEEE Trans Microwave Theory Tech , vol. MTT-38,no 3, pp 302-312, 1990

[24] P Russer, P P M So, W. J. R. Hoefer, "Modeling of Nonlinear Active Regions in TLM", IEEE Microwave and Guided Wave Letters, vol 1, No. 1, pp. 10-13, Jan 1991

[25] W J. R. Hoefer, B. Isele, P. Russer, P. P. M. So, "Modeling of Nonlinear Active Devices in TLM", to be published at the International Conference on Computation in Electromagnetics, London, 25-27 Nov. 1991.

[26] P B. Johns, "New Symmetrical Condensed Node for Three-dimensional Solution Use of Electromagnetic Wave Problenms by TLM," Electron Lett., vol.22, pp 162-164, Jan. 1986

[27] P.B Johns, "Numerical Results for the Symmetrical Condensed TLM Nodes", IEEE Trans Microwave Theory Tech., vol MTT-35,no 4, pp 378-382, 1989

[28] P B Johns, "On the Relationship Between TLM and Finite-Difference Methods for Maxwell's Equations," IEEE Trans Microwave Theory Tech., vol. MTT-35,no 1, pp 60-61, 1989.

[29] G. Kron, "Equivalent Circuit of the Field Equations of Maxwell-I", Proc I.R E , vol 32, pp 360-367, 1944.

[30] P b Johns, S Akhtarzad, "The Use of Time-Domain Diakoptics in Time Discrete Models of Fields", Int J Numer Methods Eng , vol 17, pp 1-14, 1981

[31] Eswarappa, "New Developments in the Transmission Line Matrix and the Finite Element Methods for Numerical Modeling of Microwave- and Millimeter- Wave Structure", Ph D.Dissertation, University of Ottawa, Canada 1990

[32] P. Russer, M Krumpholz, "The Hilbert Space Formulation of the TLM Method," paper presented within this Workshop.

[33] F Ndagijimana, P Saguet, M.Bouthinon, "Application of the TLM-Method to Slot Antenna Analysis", Proc of the 20th European Microwave Conference, 1990, Vol.2, pp. 1495 - 1500.

[34] W Aspray, "John von Neumann and the Origins of Modern Computing", *MIT Press, Cambridge, Masssachusetts*, 1990

[35] J.v Neumann, "The Theory of Self-Reproducing Automata," in Burks "Essays on Cellular Automata," *University of Illinois Press*, Urbana 1970

[36] K Zuse, "Rechnender Raum," in. "Schriften zur Datenverarbeitung, Band 1", *Vieweg, Braunschweig*, 1969.

[37] G. Wunsch, "Zellulare Systeme - Mathematische Theorie kausaler Felder," *Akademie-Verlag Berlin*, 1977.

[38] T. Toffoli, "Cellular Automata Machines", *MIT Press, Cambridge, Masssachusetts*, 1987

[39] R. Wait, A R Mitchell, "Finite Element Analysis and Applications", Chichester, 1985, John Wiley & Sons

[40] P.P Silvester, R.L Ferrari, "Finite Elements for Electrical Engineers", Cambridge, 1983, 1990 Cambridge University Press

[41] A.C Cangellaris, C -C. Lin, K K Mei, "Point-Matched Time-Domain Finite-Element Methods for Electromagnetic Radiation and Scattering", IEEE Trans. Antennas Propagat., vol AP-35, pp. 1160-1173, Oct. 1987

[42] T. Toffoli, "Cellular Automata Machines", MIT Press, Cambridge, Massachusetts, 1987.

[43] A Fettweis, G. Nitsche, "Numerical Integration of Partial Differential Equations Using Principles of Multidimensional Wave Digital Filters," "Proc IEEE Int Symp. Circuits and Systems, New Orleans, May 1990, pp. 954-957

[44] A Fettweis, G. Nitsche, "Numerical Integration of Partial Differential Equations Using Principles of Multidimensional Wave Digital Filters," *Journal of VLSI Signal Processing*, vol. 3, pp 7-24, 1991

[45] A Fettweis, "Wave Digital Filters Theory and Practice", *Proc IEEE*, vol 74, pp. 270-327, Feb 1986

RADIATION AND SCATTERING OF TRANSIENT ELECTROMAGNETIC FIELDS

by

Leopold B. Felsen
Dept. of Electrical Engineering/Weber Research Institute
Polytechnic University
Farmingdale, NY 11735, USA

ABSTRACT

"Ultrawideband" (UWB) and "Very Short Pulse" (SP) provide alternative designations for the same class of transient electromagnetic wave phenomena. However, UWB relates these phenomena to the frequency domain whereas SP relates the same phenomena to the time domain (TD). By generating SP-TD data through UWB frequency synthesis, the evolution of the TD signal with increasing bandwidth can be tracked systematically to its highly localized UWB form. Localized pulse-like features (observables) in data suggest that modeling and interpretation in terms of a TD "observable-based parametrization" (OBP) is physically more appropriate. Implementing a TD-OBP requires new thinking and concepts directly in the time domain. A systematic OBP strategy for learning to "think TD" via identification of TD wave objects is proposed and illustrated by examples involving SP excitation of layered media, strip gratings and aperture-coupled cavities. Of special interest is the TD evolution of the strongly dispersive leaky modes, Floquet modes and cavity modes, and their role in synthesizing the SP response.

PROCEEDINGS
OF THE SECOND

INTERNATIONAL
CONFERENCE
ON

ELECTROMAGNETICS IN AEROSPACE APPLICATIONS

SEPTEMBER 17-20, 1991 - POLITECNICO DI TORINO, ITALY

VERY SHORT PULSE SCATTERING-
TIME DOMAIN OBSERVABLE-BASED PARAMETRIZATION

Leopold B. Felsen

Department of Electrical Engineering/Weber Research Institute
Polytechnic University, Farmingdale, N.Y. 11735

Abstract: Concerning radar scattering from targets and other environments, there has been a recent trend toward wide and even ultrawide bandwidths (UWB) in order to enlarge the available data base and information retrieval options. In the ultrawideband (very short pulse) regime, analysis and synthesis via the frequency domain becomes not only computationally intensive but it also incorporates the wrong physics for interpreting the "observables" (time-resolved spikes and dips, as well as other nonharmonic manifestations) in the time domain (TD) data. It is therefore suggestive to explore alternative data processing schemes tied to the TD observables by observable-based parametrization (OBP). The result is a new analysis and synthesis strategy, built directly around self-consistent combinations of TD basis elements and wave functions, instead of the conventional procedure based on time-harmonic constituents. These concepts are explored here and illustrated by examples

1. Introduction and summary

While all signals, whether controlled by man or caused by natural events, are transients in nature, the analysis and synthesis of transient-source-excited waves and the interaction of these waves with environmental features has generally not been performed directly in the time domain but has been structured around time-harmonic constituents. This approach has been favored because propagation environments generally respond selectively to different components of the signal spectrum (they are dispersive), thereby rendering operation at single frequencies or over narrow bands of frequencies more easily controllable. Yet, it has been recognized that a data base for extracting certain types of information -- in particular, in reference to environment interrogation and classification -- becomes more effective by operating over wider frequency bands. Continuing along these lines to successively broader frequency spectra eventually yields input signals confined to short time intervals, in contrast to the long-duration quasi-steady-state wavetrains with narrow frequency bands. Monitoring these wideband time domain (TD) events in terms of their constituent frequency components becomes not only cumbersome from the point of view of data processing but also obscures the understanding of the concomitant time-limited physical wavefields with their typical narrow spikes and dips; the frequency domain interpretation of such waveforms has to be based on intricate constructive and destructive interference between harmonic wavetrains at various frequencies. This suggests that serious attention should be given to approaching TD events induced by short pulses (SP) *directly* in the time domain. From this perspective, the basic synthesizing events are *short-time wave bursts* instead of *long-time oscillations*, with the complementary relation between them furnished by the Fourier transform. The direct TD approach requires new physical concepts, new signal processing techniques, new instrumentation, etc.

Direct UWB-TD thinking and operation offers potentially attractive possibilities for communications, remote sensing, target detection and identification (including the presence of clutter), penetration into structures, and a host of other applications in electromagnetics that have traditionally been addressed by thinking and operating in the frequency domain. In the present context, UWB implies pulse durations so short as to permit resolution of relevant *local* features in the interrogated environment by monitoring *separated* scattered arrivals. The pros and cons associated with the direct TD approach, especially the need for direct TD source-shaping, receiving and data-processing instrumentation, are being actively debated within the scientific and engineering community. While there are strong opinions voiced from both ends of the spectrum (figuratively and literally), there appears to be general agreement that much more has to be understood about *direct-TD* wave processes and phenomenology, direct TD data analysis and synthesis, and other direct TD ramifications, before an objective assessment can be made.

This paper presents a strategy for systematic analytic modeling *directly in the time domain*. While Fourier synthesis from the frequency domain may be the most reliable, though circuitous, route for furnishing *initially* the outcome of an analytical or numerical experiment, this is to be followed by *direct TD interpretation* and *parametrization* of the *results*, thereby permitting their subsequent *quantitative reconstruction* in terms of TD wave analysis, synthesis and data processing. Implementation of the strategy proceeds as follows.

a. Select, analytically tractable canonical (prototype) problems that highlight various fundamental wave phenomena under SP plane wave, dipole, beam-type, or distributed aperture excitations. Such phenomena include diffraction, multiple interaction, structural and/or material dispersion, exterior-interior cavity coupling, guiding and leakage, etc.

b. Generate rigorous TD reference solutions by any convenient technique, but preferably one that decomposes the problem into basis elements in a (space-time)-(wavenumber-frequency) *phase space: wave-matched pre- and post-signal processing*

c. Identify "observable" features in the TD data: spikes, dips, quasi-periodicities, etc.

d. Try to identify, via the phase space processing in b., those SP-TD wave phenomena responsible for the observables; this may involve time resolution and time windows; localized multiple interactions; TD "resonant" effects, and their relation to phenomena in various frequency windows; etc. If successful, this procedure furnishes a *TD observable-based parametrization (OBP)*. For example, if the results in b. are generated by the conventional (frequency domain) route of performing spatial wavenumber synthesis over *time-harmonic* basis elements *before temporal wavenumber* (frequency) synthesis, a direct TD algorithm *reverses* that sequence and expresses the TD fields as spatial wavenumber distributions of *TD* basis elements. Being observable-based, such a parametrization is expected to have the correct "TD physics". This should then be *robust under weak* *perturbation away from the canonical conditions*, and thereby accommodate a *class* of *noncanonical* problems instead of a single prototype. It is also potentially more efficient for computation in appropriate parameter regimes. Finally, OBP forms the basis for *parametric inversion* of data in the time domain.

The analytical tools employed in the implementation of OBP include [1-13].

1. The spectral theory of transients (STT), in which source-excited pulsed transient fields are expressed *directly in the time domain* by *spatial* spectral superposition of *transient* basis fields.

2. The *hybrid wavefront-resonance* algorithm, which constructs time-dependent fields scattered by targets or inhomogeneous media in terms of *self-consistent combinations of progressing (wavefront) and oscillating (resonance)* basis fields. This has systematized the fundamental distinction between the early time and late time response, and has thereby clarified the limitations associated with the singularity expansion method

3. The *phase-space* beam algorithm for *self-consistent* decomposition and subsequent recombination of time-harmonic or transient fields into windowed *beam-type basis fields* on a configuration-wavenumber phase space lattice or in a phase space continuum. The beam-type fields are "good propagators" and are tracked conveniently through complex propagation and scattering encounters.

4. The *complex source point* (CSP) method for modeling of *pulsed beam type* inputs, and the scattering of these pulsed beams by environments.

The OBP modeling strategy described above has been applied to a variety of propagation and scattering environments in electromagnetics and underwater acoustics [12-29]. These applications have been primarily in the frequency domain, covering broad frequency intervals. Transient SP scattering by UWB synthesis, and subsequent direct TD-OPB, is presently being implemented for various environmental conditions. SP plane wave scattering from a slit coupled cavity has already been implemented [30]. Other examples include SP excitation of

a. single and multiple strip targets
b. periodic and quasi periodic arrays of strips without and with a reflecting plane backing.
c. planar and cylindrically layered dielectrics

These latter examples permit investigation of the TD buildup of multiple interactions and of dispersive effects associated with periodic structures and guided modes; understanding this phenomenology is expected to be useful for subsequent studies of SP scattering by clutter and by targets in clutter. Preliminary results are presented here.

2. Synthesis options for TD dyadic Green's Functions

A. Plane layered dielectric media

1. Formal aspects

Dyadic Green's functions for plane stratified dielectrics (which may tend to perfect conductors in the limit of infinite permittivity) have been well explored in the open literature [31]. The dyadic Green's functions may be derived from suitably chosen scalar potential functions, which thereby play a fundamental role in field synthesis. With z and $\rho = (x,y)$ denoting the coordinates perpendicular and parallel to the layer interfaces, respectively, the potential solutions may be constructed by spectral (Fourier) decomposition into the transverse wavenumber domain $\underline{k}_t = (k_x,k_y)$ and the temporal wavenumber (frequency) domain ω, solving the z-dependent problem in the $(\underline{k}_t,\omega)$ domain by invoking the boundary conditions across layer interfaces and the initial conditions at the source location $\underline{r}' = (x',y',z')$, and thereafter performing spectral synthesis. This leads to the following generic form for the potential function f at the space-time observation point $(\underline{r},t)$,

$$f(\underline{r},t;\underline{r}',t') = \frac{1}{2\pi}\iiint_{-\infty}^{\infty} d\omega\, dk_x dk_y\, F(\underline{r},t;\underline{r}',t';\omega,\underline{k}_t) \qquad (1)$$

where the wave object F, defined in the (space-time)-(wavenumber-frequency) phase space, has the composition

$$F = N(z,z';\omega,\underline{k}_t)[D(\omega,\underline{k}_t)]^{-1}\exp[i\underline{k}_t\cdot(\rho-\rho')-i\omega(t-t')], \qquad (1a)$$

and the denominator D is written conveniently as

$$D(\omega,\underline{k}_t) = 1 - R_+(\omega,\underline{k}_t)R_-(\omega,\underline{k}_t). \qquad (1b)$$

Here, R_+ and R_- are spectral domain reflection coefficients seen looking along the (+z) and (-z) directions, respectively, from the source plane $z = z'$. For the most versatile treatment of the spectral integrals in (1), it is useful to separate (1/D) self-consistently into hybrid "ray-mode" constituents

$$D^{-1} = \sum_{n=N_1}^{N_2} (R_+R_-)^n + [1-(R_+R_-)^{N_1} + (R_+R_-)^{N_2+1}]D^{-1},$$

$$|R_+R_-| < 1. \qquad (2)$$

Obtained by partial power series expansion, each term in the series portion respresents n-times reflected waves which can be manipulated into generalized ray fields after synthesis, whereas the remainder, with its resonant denominator, can be manipulated into guided mode fields. Note that the amplitude of the modal term depends self-consistently on the indexes N_1 and N_2 of the excised rays, with $N_1 = 0$, $N_2 = \infty$ furnishing a pure ray field series, and intact retention of D^{-1} furnishing a pure mode field series.

For greatest flexibility in subsequent reduction of the formal spectral integrals in (1), with (2), it is useful to treat the real potential f as an analytic signal f_+ defined in the lower half of the complex t plane,

$$f_+(\underline{r},t;\underline{r}';t') = \frac{1}{\pi}\int_0^{\infty} d\omega F(\underline{r},t;\underline{r}',t';\omega,\underline{k}_t)e^{-i\omega t}, \mathrm{Im}\, t \le 0 \qquad (3)$$

$$\Gamma(..t,..\omega) = \int_{-\infty}^{\infty} f_+(..t)\, e^{i\omega t}\, dt; \; f(.,t) = \mathrm{Re}\, f_+(..t) \qquad (3a)$$

In the reduction, the most significant options are associated with whether the ω-inversion is performed *after* or *before* the $\underline{k}_t$ inversion. The former is the *conventional* route, going from the full solution in the frequency domain to the time domain, while the latter route is *nonconventional* and utilizes *transient plane waves* in the point source synthesis. Exercising these alternatives together with the decomposition in (2), and performing contour deformations in the complex spectral planes to steepest descent paths (SDP) through saddle points of the integrands, one may arrive at *exact* hybrid ray-mode formulations comprised of

$$f_+ = \sum_{n=N_1}^{N_2} (\text{generalized ray fields})_n + \sum_{q(N_{1,2})} (\text{modified mode fields})_q$$

$$+ \text{(Ray-mode remainder)}_{N_{1,2}} \qquad (4)$$

Each n-term in the first series contains an SDP integral with a "ray phase"; its asymptotic evaluation by the saddle point method yields a space-time ray field (wavefront). Each q-term in the second series arises from a residue at the poles of D^{-1} encountered during the SDP contour deformation, while the last term in (4) is a hybrid spectral integral remainder along the N_1 and N_2 SDP's, having a ray (i.e., saddle point) phase but a mode-type amplitude. Both the second and third terms in (4) are derived from the second term in (2). Details of these reductions may be found in [32].

The conventional and nonconventional routes in performing the spectral synthesis lead to the following alternative treatments of the dispersion equation that defines the modal contributions in (4):

$$\text{a)}\, D(\omega,\underline{k}_{tp})=0 \Rightarrow \underline{k}_{tp}(\omega);\ \text{b)}\, D(\omega_m,\underline{k}_t)=0 \Rightarrow \omega_m(\underline{k}_t) \qquad (5)$$

Here, q=p identifies the conventional frequency dependent spatial wavenumber poles $\underline{k}_{tp}(\omega)$, whereas q=m identifies the nonconventional wavenumber dependent frequency poles $\omega_m(\underline{k}_t)$. The corresponding modal phases and amplitudes may be inferred from the spectral integrands in (1a), with (2), evaluated at $(\omega,\underline{k}_{tp}(\omega))$ and $(\omega_m(\underline{k}_t),\underline{k}_t)$, respectively.

2. Mode asymptotics

The spectral integrals, which remain in the complex ω and the complex $\underline{k}_t$ planes for the options in (5a) and (5b), respectively, can be evaluated asymptotically by the saddle point method. The respective saddle point conditions $\omega = \omega_s$ and $\underline{k}_t = \underline{k}_{ts}$ are specified by

$$\text{a)}\, d\Phi_p(\omega)/d\omega\,|_{\omega_s} = 0;\quad \text{b)}\, \nabla_{\underline{k}_t}\Phi_m(\underline{k}_t)\,|_{\underline{k}_{ts}} = 0 \qquad (6)$$

where $\nabla_{\underline{k}_t}$ denotes the gradient operator in the $\underline{k}_t$ spectral domain. This implies that conditions (5) and (6) must be satisfied *simultaneously* to yield the final space-time modal spectral wavenumbers $\omega_s(\underline{r},t;\underline{r}',t')$ and $\underline{k}_{ts}(\underline{r},t;\underline{r}',t')$; these *final* values are independent of the manner (conventional or nonconventional) by which they were derived. The simultaneous requirements above can be schematized by graphical construction which locates on the four-dimensional dispersion surface $D(\omega,\underline{k})=0$ those points $(\omega_s,\underline{k}_s)$ that have a surface normal $\underline{n}$ parallel to the four-dimensional space-time ray vector $(\underline{r}-\underline{r}', t-t')$, with the orientations of the coordinate axes in the spectral and configurational domains arranged as in Fig. 1 [33]. Here, $\underline{k} = (\underline{k}_t, k_z(\underline{k}_t))$ is the three-dimensional wavevector. While $(\omega_s,\underline{k}_s)$ are generally complex, good approximations for the phases of weakly complex modes can be obtained by plotting the real parts $(\omega_{sr},\underline{k}_{sr})$ as in Fig. 1.

Consideration from here on will be restricted to a single dielectric layer on a perfectly conducting ground plane, with the source point $(\underline{r}',t') = (0,0,z',0)$ inside, and the observation point $(\underline{r},t)$ located outside, the layer (Fig. 2). The relevant mode fields are now the leaky modes because the trapped modes have external evanescent fields. The saddle point conditions in (6), which yield identical results for modes q=p or m, are explicitly

$$t - \underbrace{\frac{n_1 L_1}{c}}_{\text{ray}} - \underbrace{\frac{L_2}{v_g}}_{\text{mode}} - \underbrace{\frac{L_3}{c}}_{\text{ray}} = 0,\ v_g = \partial\omega/\partial k_t \qquad (7)$$

This relation can be schematized by the space-time dependent self-consistent ray-mode trajectories in Fig. 2, with v_g representing the modal *group* speed. The modal phase evaluated at (ω_s,k_{ts}) becomes

$$\Phi_q(\underline{r},\underline{r}';t,t') = \omega_s(\underline{r},t;\underline{r}')\left(\frac{n_1 L_1}{c} + \frac{L_2}{v_p} + \frac{L_3}{c} - t\right) \qquad (8)$$

where $v_p = \omega_s/k_{ts}$ is the modal *phase* speed.

3. Numerical results

Numerical results for the configuration in Fig. 2 have been generated for an input pulse $f(t)$ derived from the analytic delta function $\delta_+(\tau) = (i\pi\tau)^{-1}$, $\tau = t - it_i$, $\mathrm{Im}\,\tau<0$. The potential field at $(\underline{r},t)$ has been synthesized a) via direct summation of multiple reflected wavefronts (first term in (4) with $N_1 = 0$, $N_2 = N$) and b) via leaky mode summation (second term in (4) with the full spectral integrand in (1a)) over those modes whose frequencies ω_s lie within the frequency window of the pulse spectrum $F(\omega)$. Because the multiple reflected wavefront fields in a) are nondispersive, they can be evaluated in simple form; the wavefront series is truncated directly by the n-delayed arrival times that fit into the time interval of observation, and indirectly by the decrease, at each air-dielectric reflection, of the field amplitude. The results are shown in Figs. 3, and are explained in the figure captions. Of special interest is the synthesis of the wavefront driven SP observables by successive addition of the strongly dispersive leaky modes. This illustrates the role of dispersion under SP conditions and the virtue of OBP in the fully synthesized data.

The above analytic summary and numerical samples have been extracted from a full manuscript being prepared for publication [32].

Acknowledgement

The long-term research summarized and referenced in this paper has been supported by the Office of Naval Research, the Army Research Office, and the Joint Services Electronics Program.

References

[1] E. Heyman and L.B. Felsen, "Creeping waves and resonances in transient scattering by smooth convex objects," *IEEE Trans. Ant. Propagat.* AP-31, (1983), pp. 426-437.

[2] The Hague, Netherlands, Series E: *Applied Sciences*, No. 86, (1984), pp. 269-284.

[3] E. Heyman and L.B. Felsen, "A wavefront interpretation of the singularity expansion method," *IEEE Trans. Ant. Propagat.*, AP-33, (1985), pp. 706-718.

[4] E. Heyman and L.B. Felsen, "Non-dispersive closed form approximations for transient propagation and scattering of ray fields," *Wave Motion*, Vol. 7, (1985), pp. 335-358.

[5] E. Heyman and L.B. Felsen, "Weakly dispersive spectral theory of transients: I-formulation and interpretation," *IEEE Trans. Ant. Propagat.*, AP-35, (1987), pp. 80-86.

[6] E. Heyman and L.B. Felsen, "Weakly dispersive spectral theory of transients: II-evaluation of the spectral integral," *IEEE Trans. Ant. Propagat.*, AP-35, (1987), pp. 574-580.

[7] E. Heyman and L.B. Felsen, "Propagation pulsed beam solutions by complex source parameter substitution," *IEEE Trans. Ant. Propagat.*, AP-34, (1986), pp. 1062-1065.

[8] L.B. Felsen and E. Heyman, "Discretized beam methods for focused radiation from distributed apertures," *Proceedings of the SPIE Symposium, Microwave and Particle Beam Sources and Propagation*, 873, (1988), pp. 320-328.

[9] E. Heyman and L.B. Felsen, "Complex source pulsed beam fields," *J. Opt. Soc. Am.* A6, (1089), pp. 806-81⁻.

[10] B.Z. Steinberg, E. Heyman and L.B. Felsen, "Phase space beam summation for time-harmonic radiation from large apertures," *J. Opt. Soc. Am.*, A8, (1991), pg. 59.

[11] B.Z. Steinberg, E. Heyman and L.B. Felsen, "Phase space beam summation for time-dependent radiation from large apertures: continuous parametrization," to be published in *J. Opt. Soc. Am.*, A.

[12] L.B. Felsen, "Progressing and oscillatory waves for hybrid synthesis of source excitated propagation and diffraction," *IEEE Trans. on Antennas and Propagation*, AP-32, (1984), pp. 775-796.

[13] E. Niver, A. Kamel and L.B. Felsen, "Modes to replace transitional asymptotic ray fields in a vertically inhomogeneous earth model," *Geophys J.R. Astron. Soc.*, 80, (1985), pp. 280-312.

[14] L.B. Felsen, "Novel ways for tracking rays," *J. Opt. Soc. Am.* A2, (1985) pp. 954-963.

[15] I.T. Lu and L.B. Felsen, "Ray, mode and hybrid options for transient source excited propagation in an elastic layer," *Geophys. J. Roy. Astron. Soc.* 86, (1986), pp. 177-201.

[16] I.T. Lu and L.B. Felsen, "Ray, Mode and Hybrid Options for Source Excited Propagation in an Elastic Plate," *J. Acoust. Soc. Am.* 78, (1985), pp. 701-714.

[17] H. Shirai and L.B. Felsen, "Wavefront and resonance analysis of scattering by a perfectly conducting flat strip," *IEEE Trans. on Ant. and Propagat.*, AP-34, (1986), pp. 1196-1207.

[18] L.B. Felsen, "Target strength: some recent theoretical developments," *IEEE Journal of Ocean Engineering*, OE-12, (1987) pp. 443-452.

[19] H. Shirai and L.B. Felsen, "Rays and modes for plane wave coupling into a large open-ended circular waveguide," *Wave Motion* 9, (1987) pp. 461-482.

[20] T. Ishihara and L.B. Felsen, "Hybrid (ray)-(parabolic equation) analysis of propagation in ocean acoustic guiding environments," *J. Acoust. Soc. Am.* 83, (1988) pp. 950-960.

[21] E. Heyman, G. Friedlander and L.B. Felsen, "Ray-mode analysis of complex resonances of an open cavity," *IEEE Proceedings, Special Issue on Radar Cross Sections of Complex Objects*, 77, (1989) pp. 780-787.

[22] L.B. Felsen and I.T. Lu, "Ray treatment of wave propagation on thin-walled curved elastic plates with truncations," *J. Acoust. Soc. Am.* 86, (1989) pp. 360-374.

[23] I.T. Lu, L.B. Felsen and J.M. Klosner, "Beam-to-mode conversion in an aluminum plate for ultrasonic NDE applications," *ASME J. of Engineering Materials and Technology*, 112, (1990) pp. 236-240.

[24] I.T. Lu, L.B. Felsen and J.M. Klosner, "Observables due to beam-to-mode conversion of a high-frequency gaussian p-wave input in an aluminum plate in vacuum," *J. Acoust. Soc. Am.* 87, (1990) 42-53.

[25] L.B. Felsen, J.M. Ho and I.T. Lu, "Three-dimensional green's function for fluid-loaded thin elastic cylindrical shell: alternative representations and ray-acoustic forms," *J. Acoust. Soc. Am.* 87, (1990) pp. 554-569.

[26] J.M. Ho and L.B. Felsen, "Nonconventional and ray-acoustic reductions traveling wave formulations for source-excited fluid-loaded thin elastic spherical shells," *J. Acoust. Soc. Am.* 88, (1990) pp. 2389-2414.

[27] L.B. Felsen, "Observable-based wave modeling: wave objects, spectra and signal processing," to be published in proceedings of the symposium on Huygens' principle: theory and applications, *North Holland Publ. Co.*, pp. 1690-1990, 1991.

[28] L.B. Felsen and G. Vecchi, "Wave scattering from slit-coupled cylindrical cavities with interior loading: I-formulation by ray-mode parametrization," to be published in *IEEE Transactions on Antennas and Propag.*

[29] L.B. Felsen and G. Vecchi, "Wave scattering from slit-coupled cylindrical cavities with interior loading: II-resonant mode expansion," to be published in *IEEE Transactions on Antennas and Propag.*

[30] G Vecchi and L.B. Felsen, "Transient plane wave scattering from a circular cylinder backed by a slit-coupled coaxial cavity," to be published in *Directions in Electromagnetic Wave Modeling*, H. Bertoni and L.B. Felsen (eds.), Plenum Press, New York, 1991.

[31] N.K. Uzunoglu, N.G. Alexopoulos and J.G. Fikioris, "Radiation properties of microstrip dipoles," IEEE Trans. Antennas Propag., Vol. AP-27, No. 6, pp. 853-585, Nov. 1979.

[32] L.B. Felsen and F. Niu, manuscript in preparation.

[33] L.B. Felsen and N. Marcuvitz, *Radiation and Scattering of Waves*, Prentice Hall, New Jersey, 1973. Sec. 1.6.

Fig. 1. Leaky mode dispersion surface for plane layered dielectric, and graphical construction for determination of the real modal wavenumber $\underline{k}_r(\underline{r},t)$ and frequency $\omega_r(\underline{r},t)$ defined in (6). The subscripts have been omitted, and $\underline{k}_t \equiv \underline{k}_\rho$.

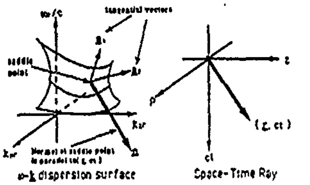

Fig. 2. Horizontal-electric-dipole-excited dielectric layer with relative permittivity $\varepsilon_1 = n_1^2$ and relative permeability μ_1, backed by a perfectly conducting (PEC) ground plane, with observer located in the outside vacuum. Schematization of self-consistent ray-mode trajectories that establish the time-domain asymptotic leaky mode field, as specified in (7). Both the incident ray field and the detaching leaky ray field to the observer are phase matched to the leaky mode longitudinal wavenumber; this matching condition determines the space-time dependent respective ray angles $\Theta_{1i}(\underline{r},t)$ and $\Theta_i(\underline{r},t)$.

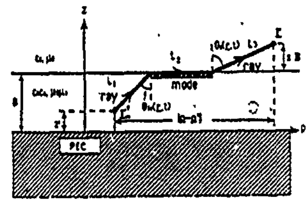

Fig. 3. Numerical results for TE contribution to E_x field component, normalized to incident pulse amplitude E_o. Physical configuration as in Fig 2, with problem parameters listed on each figure.

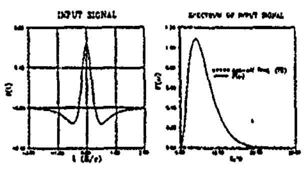

a) input pulse [analytic Rayleigh wavelet $f_+(\tau) = i t_1^2 \cdot (\pi \tau^2)^{-1}$] and its frequency spectrum [$F(\omega) = (\omega t_1)^2 \cdot \exp(-\omega t_1)$, $t_1 = 0.5\,B/c$]. $f(t) = \mathrm{Re}\, f_+(\tau)$. The circles on the $k_o B \equiv \omega B/c$ axis identify the cutoff frequencies ω_{cm} of the leaky modes. Only the first 12 modes $(0 \le m \le 11)$ are covered by the pulse spectrum, with m=3 excited most strongly.

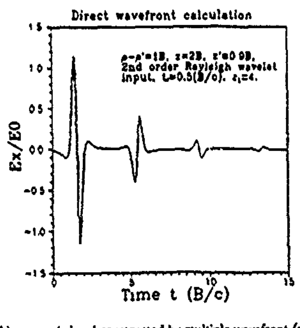

b) received signal constructed by multiple wavefront (ray field) tracking; multiple reflections are clearly resolved, with phase reversal after each reflection at the PEC.

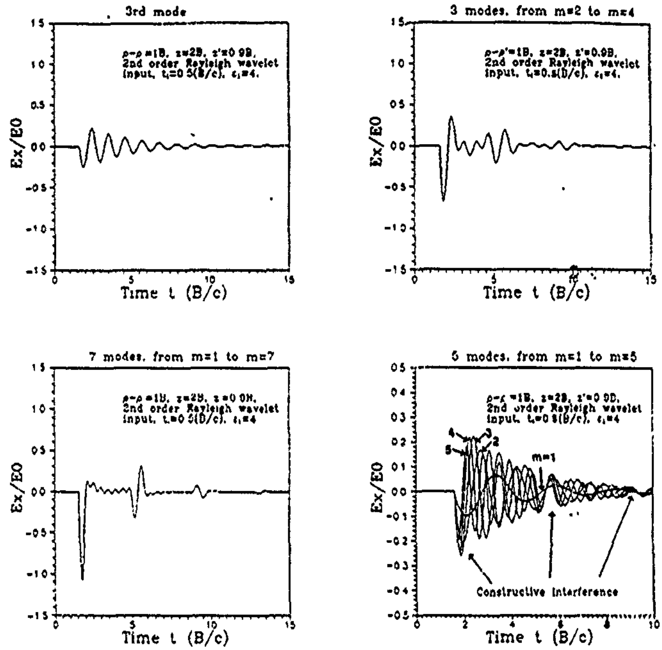

c) buildup of received signal by modal superposition: mode m=3 (most strongly excited); modes $2\leq m\leq 4$; modes $1\leq m<7$; modes $1\leq m\leq 5$, with details of constructive and destructive interference. Mode sum $0\leq m\leq 11$ completely reconstructs the field in b). Note the delayed turn-on times at the observer; these are compatible with the earliest phase matched propagation paths identified in Fig. 2. The abrupt start should not be taken literally; it arises from nonuniform asymptotics.

Finite-Difference Time Domain Modelling of Electromagnetic Fields

Ingo Wolff, Duisburg University

For the design of planar microwave integrated circuits up to 1985 mainly analysis techniques in the frequency domain have been used With the requirements for new and flexible tools in the design of planar circuits e g with closely coupled elements and three-dimensional discontinuitioc liko oirbridgco, alternative techniques must be studied. One of these techniques is the finite-difference time domain analysis (FDTD) which in principle is known since 30 years. Yee already in 1966 proposed this technique for the analysis of electromagnetic boundary value problems [1]

During a long time the FDTD technique only was used to quantitatively demonstrate electromagnetic field solution in the time domain Only the introduotion of aosorbing walls made this technique to a powerful tool for the solution of real problems.

The FDTD is a numerical method for the solution of electromagnetic field problems which has a large numerical, but a low analytical expense. Despite the large numerical expense it is believed to be one of the most efficient techniques, because basically it stores only the field distribution at one moment in memory instead of working with a large equation system matrix. The field solution for each other time then is determined from Maxwell's equations and is calculated using a time stepping procedure based on the finite-difference method in time domain. Available algorithm, called the "leapfrog algorithm" fits very well on modern computer architectures, so that the data required to describe a three-dimensional field distribution can be handled in a reasonable time. Therefore it can efficiently be implemented on vector or parallel computers as well Sufficiently accurate results can be received by using a single precision floating point expression requiring only four bytes. It is a further advantage that the transient analysis delivers a broad band frequenoy response in one single computation run.

In this talk it shall be demonstrated that the FDTD technique can be applied to real microwave circuit design problems It will be shown that this technique enables to model arbitrarily shaped planar structures with multiple coupled discontinuities and planar lines and three-dimensional circuit structures Several applications to realistic problems of modern monolithic integrated microwave circuit design problems will be demonstrated In the future the application of FDTD method surely is a powerful analysis technique for nonlinear microwave integrated circuit design by combining physical semiconductor models which work in the time domain with the FDTD description of the passive circuit elements.

[1] K S Yee, "Numerical solution of initial boundary value problems involving Maxwell's equations in isotropic media", *IEEE Trans Antennas Propagat*, Vol 14, 1966, pp. 302-307

FINITE DIFFERENCE TIME DOMAIN SIMULATION OF ELECTROMAGNETIC FIELDS AND MICROWAVE CIRCUITS

Ingo Wolff

Department of Electrical Engineering and
Sonderforschungsbereich 254,
Duisburg University, D-4100 Duisburg

FINITE DIFFERENCE TIME DOMAIN ANALYSIS OF PLANAR MICROWAVE CIRCUITS

1) Introduction
2) The FDTD algorithm
3) Nonequidistant discretization
4) The excitation of the electromagnetic field
5) Absorbing walls and matched sources
6) Realized applications
7) Error discussion
8) Future developments

THE FINITE DIFFERENCE TIME DOMAIN METHOD

- Simulation of wave propagation phenomena based on time dependent Maxwell's equations
- Eigenvalue analysis of resonant structures and transient analysis possible
- One-, two- and real three-dimensional electromagnetic wave problems can be solved
- Applied method: finite difference discretization of time and space

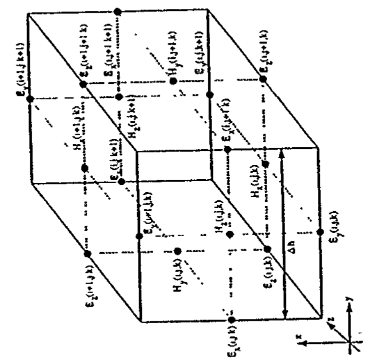

THE LEAPFROG ALGORITHM

THE LEAPFROG ALGORITHM

$$E_x^{n+1}(i,j,k) = E_x^{n}(i,j,k) + \frac{\Delta t}{\varepsilon \Delta h} \left(H_z^{n+1/2}(i,j,k) - H_z^{n+1/2}(i,j-1,k) - H_y^{n+1/2}(i,j,k) + H_y^{n+1/2}(i,j,k-1) \right)$$

$$E_y^{n+1}(i,j,k) = E_y^{n}(i,j,k) + \frac{\Delta t}{\varepsilon \Delta h} \left(H_x^{n+1/2}(i,j,k) - H_x^{n+1/2}(i,j,k-1) - H_z^{n+1/2}(i,j,k) + H_z^{n+1/2}(i-1,j,k) \right)$$

$$E_z^{n+1}(i,j,k) = E_z^{n}(i,j,k) + \frac{\Delta t}{\varepsilon \Delta h} \left(H_y^{n+1/2}(i,j,k) - H_y^{n+1/2}(i-1,j,k) - H_x^{n+1/2}(i,j,k) + H_x^{n+1/2}(i,j-1,k) \right)$$

$$H_x^{n+1/2}(i,j,k) = H_x^{n-1/2}(i,j,k) - \frac{\Delta t}{\mu \Delta h} \left(E_z^{n}(i,j+1,k) - E_z^{n}(i,j,k) - E_y^{n}(i,j,k+1) + E_y^{n}(i,j,k) \right)$$

$$H_y^{n+1/2}(i,j,k) = H_y^{n-1/2}(i,j,k) - \frac{\Delta t}{\mu \Delta h} \left(E_x^{n}(i,j,k+1) - E_x^{n}(i,j,k) - E_z^{n}(i+1,j,k) + E_z^{n}(i,j,k) \right)$$

$$H_z^{n+1/2}(i,j,k) = H_z^{n-1/2}(i,j,k) - \frac{\Delta t}{\mu \Delta h} \left(E_y^{n}(i+1,j,k) - E_y^{n}(i,j,k) - E_x^{n}(i,j+1,k) + E_x^{n}(i,j,k) \right)$$

THE LEAPFROG ALGORITHM

- Difference equations of second order accuracy
- Stability condition.

$$v_{ph}\, \Delta t \leq \frac{1}{\sqrt{\frac{1}{\Delta x^2} + \frac{1}{\Delta y^2} + \frac{1}{\Delta z^2}}} \; .$$

- Fits very well with modern computer architectures (vector and parallel computers)
- Requires 6NML memory places

THE EXCITATION OF THE ELECTROMAGNETIC FIELD

a) Define the electromagnetic field within the total space at starting time t_0

b) Define a harmonic field oscillation on the boundary of the structure

c) Define a pulse excitation with finite length in space and time for transient analysis

d) Define matched sources for feeding planar circuits

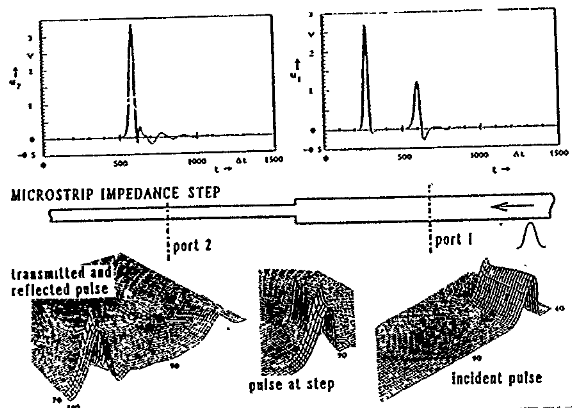

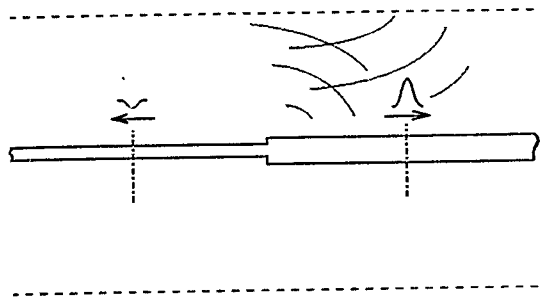

Disturbance of the investigated pulse due to reflections.

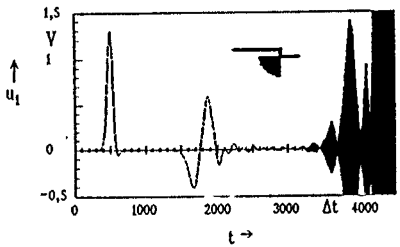

:ability problem.

Matched Sources

- an absorbing boundary is switched on after pulse excitation
- with matched sources the calculation domain does not depend on the excited pulse

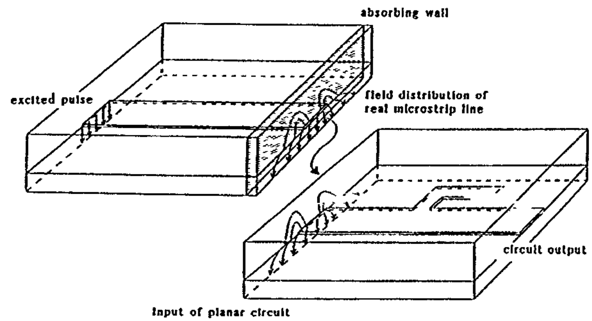

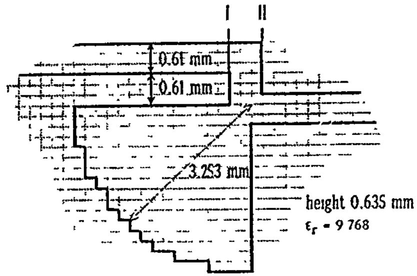

The radial stub

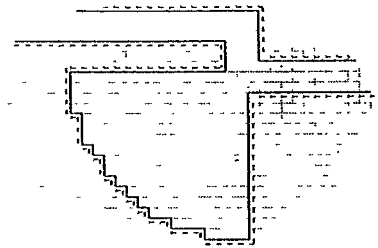

The Coarseness Error

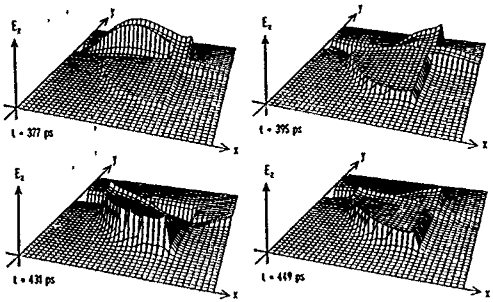

Time dependent E-field perpendicular to the substrate under the metallization

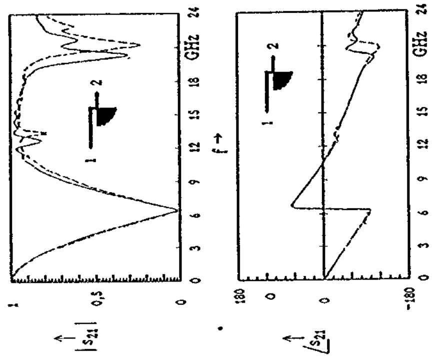

Calculated (—) and measured (---) S-parameters of the radial stub. Al_2O_3, ε_r = 9.768 (measured), height = .635 mm, width = .61 mm, gap = .61 mm, radius = 3 253 mm

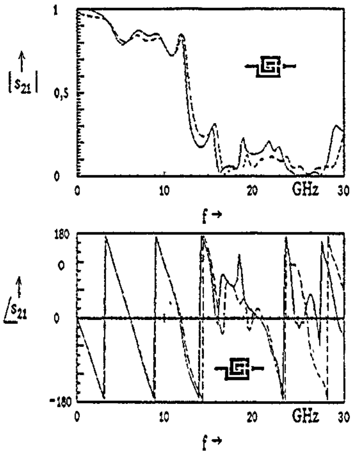

Calculated (—) and measured (– – –) S-parameters of the spiral inductor

Errors

- single mode propagation for S-parameter determination
- truncation error
- imperfect absorbing boundaries
- velocity error
- coarseness error

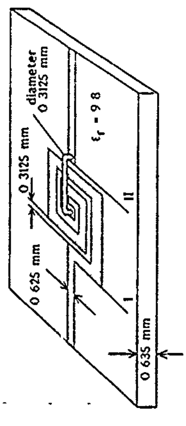

The spiral inductor.

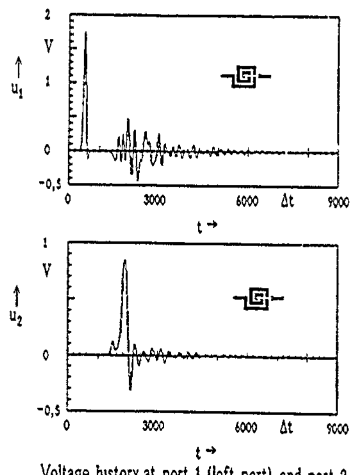

Voltage history at port 1 (left port) and port 2 (right port) of the spiral inductor. Al_2O_3, $\varepsilon_r = 9.8$, height = .635 mm, width = .625 mm, gap = .3125 mm, air-bridge diameter = 3125 mm.

An. ysis of Nonlinear Microwavc Circuits by Segmentation

- Division of circuit into several segments $\Rightarrow$ Independent modelling.
- Definition of reference planes between segments.
- Description in terms of scattering parameters.
- Nonlinear devices are connected to the segments' ports.
- Simulation by Harmonic Balance (HB).

Part of a Circuit and Corresponding Equivalent Circuit

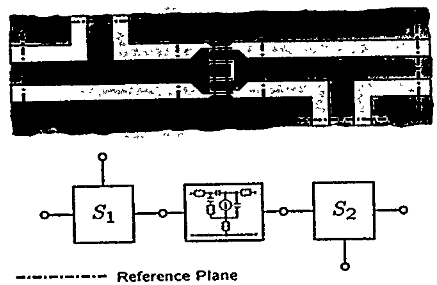

Advantages

- Modular approach.
- Preservation of HB analysis options, including
  - Multitone excitation analysis.
  - Multiple analysis.
  - Noise analysis.

Disadvantages

- Scattering parameters based on common field distribution in reference plane $\Rightarrow$ Restricted locations for nonlinear devices.

LUFET Structure [TOKUMITSU et al]

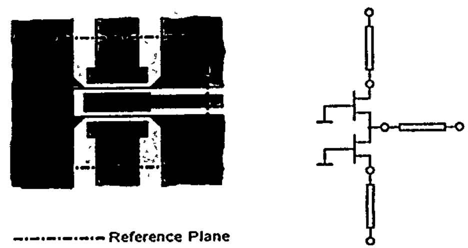

Analysis of Nonlinear Microwave Circuits in Time Domain

- Simulation of passive structures.
- True 3D-simulation possible.
- Enhancement to nonlinear elements by field dependent variation of material parameters.

Advantages

- Few restrictions in nonlinear device location.
- Simulation resembles physical process.

Disadvantages

- Multiple analyses.
- Multitone excitations.
- Noise analysis.

The Compression Approach

Basic Procedure

- Decomposition into a linear part and several nonlinear devices.
- Description of linear part ⇒ Compression Matrix.
- Nonlinear devices ⇒ CAD-Models.
- Definition of "inner" ports ⇒ Less restrictions in placement of nonlinear devices.
- Overall nonlinear simulation by HB.

Definition of Inner Ports

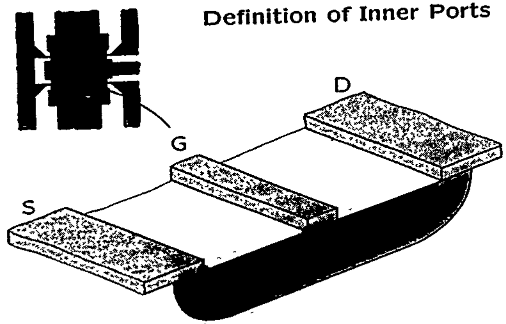

Definition of Inner Ports

- Assume applicability of Kirchhoff's laws.
- Path for voltage integration and current flow.
- Interface between embedding linear part and nonlinear devices ⇒ **No assumption on field distribution in port area.**

Determination of the Compression Matrix

- No reference planes at inner ports ⇒ Decomposition into physical waves difficult.
- Field theoretical methods: Excitation via lines.
- Indirect excitation of inner ports by varying terminations (Open, Short).
- Determination of "virtual" waves.

$$\Rightarrow \mathbf{S_C} = \mathbf{B}\mathbf{A}^{-1}$$

where $\mathbf{B} = (\mathbf{b}_1\mathbf{b}_2\cdots\mathbf{b}_p)$, $\quad \mathbf{A} = (\mathbf{a}_1\mathbf{a}_2\cdots\mathbf{a}_p)$.

Scattering parameters

MNA requires

$$\mathbf{Au} + \mathbf{Bi} = \mathbf{c}, \qquad (1)$$

u and **i** vector of voltages and currents, resp.
With scattering parameters

$$(\mathbf{I} - \mathbf{S}')\mathbf{u} - (\mathbf{I} + \mathbf{S}')\mathbf{Zi} = 0, \qquad (2)$$

$$\mathbf{S}' = (s'_{ij}), \quad s'_{ij} = s_{ij}\sqrt{\frac{Z_i}{Z_j}}, \quad \mathbf{Z} = \mathbf{diag}(Z_i).$$

LUFET Structure [TOKUMITSU et al]

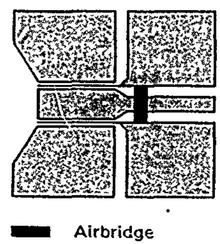

$\varepsilon_r = 12.9$
Gate width $= 200\mu m$
$Z_{CPW} = 50\Omega$
$Z_{Slotline} = 70\Omega$
Area $= 500\mu m \times 500\mu m$
$h \gg s_{Slotline}$
$\Delta x = 10\mu m$

Equivalent Circuits

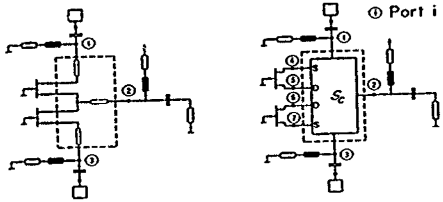

Segmentation Compression

Coupling Gain

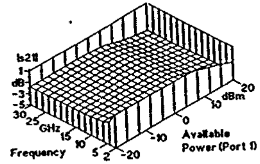

Segmentation

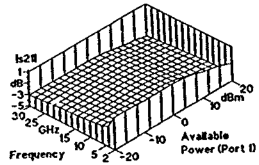

Compression

Input Isolation

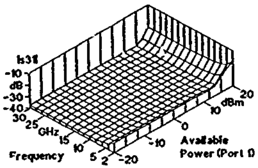

Segmentation

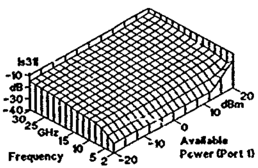

Compression

Compression Matrix

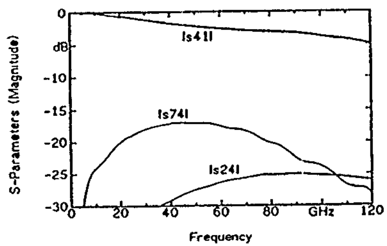

	SM	TD/NL	CA
• Narrow Struct.	−	+	+
• NLD-Locations	−	+	+
Multitone Anal.	+	−	+
Noise Anal.	+	−	+
Multiple Anal.	+	−	+
Software Requir.	+	+	−

SM Segmentation Method
TD/NL Time-Domain / Nonlinear
CA Compression Approach

Conclusion

- Combination of well-known methods.
- Comprehensive analysis.
- Suited for integrated design tools.

TLM Modelling of Electromagnetic Fields

Wolfgang J. R. Hoefer

Address: Laboratory for Electromagnetics and Microwaves,
Dept of Electrical Engineering, Univ. of Ottawa,
Ottawa, Ontario, Canada, K1N 6N5.

ABSTRACT

In this workshop paper the principal features of TLM analysis of electromagnetic fields will be summarized, and research trends in this area will be discussed. Time domain modeling in general, and TLM modeling in particular, is focusing on the realization of a new generation of time domain simulation tools which link geometry, layout, physical and processing parameters of a microwave or high speed digital circuit with its system specifications and the desired time and frequency performance, including electromagnetic susceptibility and emissions. Such CAD systems will most likely employ dedicated parallel processors configured in a 3D array. Furthermore, the specific nature of discrete time domain algorithms affords optimization and synthesis procedures which differ radically from those employed in traditional frequency domain CAD tools.

1 PROPERTIES OF TIME DOMAIN FIELD MODELS

1.1 Time-Stepping Algorithms

Most time domain field models describe only the local properties of the propagation space. The most current forms are based either on a discretization of Maxwell's Equations (Finite Difference - Time Domain or FD-TD formulation) or on the description of space by a discrete spatial network (Transmission Line Matrix or TLM formulation). Fig. 1 shows the basic 2D TLM impulse scattering process which can be considered as a computer implementation of Huygens' principle. Finite Element formulations in the time domain are also possible but have not been used extensively so far.

FD-TD and TLM methods employ similar but different formulations. While FD-TD is expressed in terms of total electric and magnetic field components, TLM uses incident and reflected wave quantities in a spatial network. As a general rule, both formulations are equivalent; for each TLM scheme there exists an equivalent FD-TD formulation. Fig. 2 shows two such pairs. Figs. 2a and b show Johns' distributed TLM node [1] and Yee's unit FD-TD cell. [2]. Figs. 2c and d compare Johns' condensed TLM node [3] and the equivalent FD-TD scheme derived by Chen et al. [4]. Fig. 3 shows the dispersion characteristics of the discretization schemes in Fig. 2 as derived by Nielsen and Hoefer [5]. For low frequencies the dispersion surfaces form a unit sphere in all cases. However, at higher frequencies the dispersion characteristics of the condensed TLM node and Chen's FD-TD scheme (Fig. 3b) are far superior to the other two (Fig. 3a).

Clearly, the equivalent TLM and FD-TD schemes possess identical dispersion and error characteristics They can also be derived formally one from the other. Furthermore, optimized codes for equivalent schemes require a similar computer memory and execution time. Nevertheless, they have their respective advantages and disadvantages when implementing boundaries, dispersive constitutive parameters, and nonlinear devices. In the final analysis, the choice between TLM or FD-TD is based more on personal preferences and familiarity with one or the other method rather than on objective criteria. In the following, the salient features of time domain simulators will thus be described in terms of TLM formalism with the understanding that there exists, or could be found, an equivalent FD-TD formulation unless indicated otherwise.

1.2 Requirements for Time Domain Field Analysis

The principal advantages of modeling electromagnetic fields in the time domain are well known. However, in order to exploit them in a practical application, dispersive and nonlinear properties, moving boundaries, and sophisticated signal processing procedures must be implemented, which include forward and inverse Fourier transform, convolution, and absorbing boundaries. Another important requirement for practical applicability is a graphic user interface for 3D geometry editing, parameter extraction and display, as well as dynamic visualization of fields, charges and currents.

The feasibility of these features has been demonstrated both in TLM and FD-TD environments [6]-[8]. However, the computational requirements for modeling complex structures with such methods are still extremely severe. Therefore, research efforts are being focused on the development of accelerating techniques, the most important of which will be discussed below.

2 ACCELERATING TECHNIQUES IN TLM MODELLING

In the following, the most important accelerating techniques will be briefly described. The first exploits the localised nature of the time domain algorithms through parallel processing, the second is based on the numerical processing of the time domain output signal using the Prony-Pisarenko Method, and the third involves the reduction of the so-called coarseness error by improving the properties of the discrete TLM mesh in the vicinity of sharp corners and edges.

2.1 Parallel Processing

The principle of causality ensures that any change in the state of a TLM node affects only its immediate neighbours at the next computational step. This allows the implementation of TLM in a form quite different from the program on a serial machine. Since in a parallel computer each processor has its own memory, it is practical to assign to each of them an impulse scattering matrix and a set of boundary conditions. The impulse scattering matrix incorporates the local properties of the computational space such as permittivity, permeability, conductivity, and mesh size in the three co-ordinate directions. The boundary conditions specify whether there are boundaries between a node and its neighbours, or whether the nodes are connected together. This parallel implementation greatly facilitates variable mesh grading, conformal boundary modeling, and the simulation of highly inhomogeneous materials and complicated geometries.

Fig. 4 compares, on a logarithmic scale, the improvements made over the last year in computing speed using various programming techniques [9] and parallelisation. The original matriz formulation by Johns [3] requires 144 multiplications and 126 additions and subtractions per scattering per node. Through manipulation of the highly symmetrical impulse scattering matrix, Tong and Fujino [9] have reduced the scattering to six multiplications, 36 additions/subtractions and 12 divisions by four, increasing computing speed over six times. Programming in Assembler rather than C++ accelerates the process again four times. Finally, parallel processing increases speed by more than two orders of magnitude over the fastest serial version implemented on a 386 computer in C++ language. The combined measures effectively reduce computation times from hours to seconds.

This comparison strongly suggests that future implementations of time domain simulators for CAD purposes will be based on dedicated parallel processors or supercomputers that emulate parallel processing.

2.2 Signal Processing

The fast Fourier Transform (FFT) is the most frequently used signal processing method for extracting the spectral characteristics of a structure from a time domain simulation. For efficient computations it is of prime importance to reduce the number of time samples required to extract a meaningful frequency response. To achieve this goal, processing of the time response using the Prony-Pisarenko method has been applied successfully. [10].

In this approach the discrete time domain output signal is treated as a deterministic signal drowned in noise. (Fig. 5). The signal is then approximated by a superposition of damped exponential functions (Prony's method), and the noise is minimized using Pisarenko's model. This signal processing technique reduces the number of required time samples by typically one order of magnitude.

2.3 Reduction of Coarseness Error

One of the principal sources of error in the TLM analysis of structures with sharp edges and corners is the so-called coarseness error. It is due to the insufficient resolution of the edge field by the discrete TLM network. The error is particularly severe when boundaries and their corners are placed halfway between nodes as shown in Fig. 6. It is clearly seen that the nodes situated diagonally in front of an edge are not interacting directly with the boundary but receive information about its presence only across their neighbours who have one branch connected to it. The network is thus not sufficiently "stiff" at the edge, and results obtained are always shifted towards lower frequencies. The classical remedy for this problem is to use a finer mesh in the vicinity of the edge, but this introduces additional complications and computational requirements. On the other hand, the dispersion characteristics of the condensed 3D TLM node (see Fig. 3b) are so good that the velocity error is practically negligible even for rather coarse meshes. A much better and more efficient way is thus to modify the corner node such that it can interact directly with the corner through an additional stub as shown in Fig. 7 for the 2D case. Since this stub is longer than the other branches by a factor $\sqrt{2}$ it is simply assumed to have a correspondingly larger propagation velocity. In the 3D case up to three stubs must be added depending on the nature of the corner. The effect of this corner correction is demonstrated in Fig. 8 which shows typical results for the first resonant frequency of a cavity containing a sharp edge as a function of the mesh parameter Δl. The parameter p is proportional to the fraction of power carried by the fifth branch of the corner node and is equal to half the characteristic admittance of the corner branch when normalized to the link line admittance (see Fig 7). For $p = 0$ (no corner correction) the coarseness error increases almost linearly with increasing Δl, while for $p = 0.1$ the frequency remains accurate even for a very coarse mesh.

3 BOUNDARIES IN ARBITRARY POSITIONS

3.1 Accurate Dimensioning and Curved Boundaries

The accurate modeling of waveguide components, discontinuities and junctions requires a precision in the positioning of boundaries that is identical to, or better than the manufacturing tolerances. If boundaries can only be introduced either across nodes or halfway between nodes, then the mesh parameter Δl would have to be very small indeed, leading to unacceptable computational requirements. Similar considerations apply when curved boundaries with very small radii of curvature must be modeled. It is therefore important to provide for arbitrary positioning of boundaries. The basis for this feature has been described already in 1973 by Johns [11].

Fig. 9 shows the concept of arbitrary wall positioning in two-dimensional TLM. The boundary branch which has a length different from $\Delta l/2$ is simply replaced by an equivalent branch of length $\Delta l/2$ having the same input admittance. This ensures synchronism, but requires a different characteristic admittance for the boundary branch and hence, a modification of the impulse scattering matrix of the boundary node. (see [11]). The effect of such boundary tuning is shown in Fig. 10 which indicates that the length of the boundary branch can be continuously tuned over a range of more than one mesh parameter length Δl without appreciable error. This important technique removes the restriction that dimensions of TLM models can only be integer multiples of the mesh parameter.

An alternative method which avoids the modification of the S-Matrix of the boundary nodes is to replace the extension of a boundary beyond its standard position by an equivalent reactance. The differential equation of that reactance is discretized, resulting in a recursive formula for the impulse reflected by the boundary. This method is preferrable for a serial type computer implementation while the former is more appropriate for a parallel version.

3.2 Moving Boundaries and Time Domain Optimization

Since it usually takes considerable time to build up a quasi-stationnary field in a structure of high Q-factor, optimization based on a new complete analysis after every modification is extremely time consuming. Instead, techniques for continuously varying the boundary position and other characteristics of a structure during a TLM simulation will be developed. Two different methods will be investigated. One is to modify the scattering matrix of nodes situated close to a boundary, the other is to generate the impulses reflected by moving boundaries using recursive algorithms. In order to implement automatic optimal tuning these measures will be coupled with appropriate optimization strategies. Furthermore, if optimization criteria are to be formulated in the frequency domain, a sliding Fourier transform window will be introduced as well in order to extract the time-varying frequency domain characteristics from the evolving time domain response.

4 NUMERICAL SYNTHESIS BY REVERSE TLM

It has been shown recently by Sorrentino et al. [12] that the TLM process can be reversed without modification of the algorithm, yielding the source distribution from the resulting field by going backwards in time. Direct numerical electromagnetic synthesis is completely unchartet territory as yet, and the exact procedure and its implementation are not very clear. The desired characteristic of a structure or component is usually given for a limited frequency range and for the dominant mode of propagation. This information is insufficient to synthesise the exact topology of the structure. Therefore, the missing information must be generated and added by the designer. Implementation will most likely be an alternate sequence of analyses and syntheses which will converge much faster than repeated analysis and optimization in traditional CAD.

5 CONCLUSION

Computer time and memory required to model realistic electromagnetic structures are still obstacles when it comes to practical applications of time domain modelling techniques. Therefore, considerable research efforts are concentrating on ways to reduce the computation count significantly. In this workshop paper we describe three different ways to achieve this, namely parallel processing, Prony-Pisarenko signal processing, and coarseness error compensation at sharp corners and edges. All these methods can be combined to accelerate TLM simulations by several orders of magnitude. Since the computation count for TLM analyses increases faster than the fourth power of the linear mesh density, these accelerating features enhance our ability to model complex structures to a much greater extend than the mere memory size and speed of the computer. Procedures for fine tuning of wall positions have also been described.

Future time domain CAD systems will most likely employ dedicated parallel processors configured in a 3D array. Furthermore, the specific nature of discrete time domain algorithms requires optimization and synthesis procedures different from those employed in traditional frequency domain CAD tools. These include the implementation of moving boundaries for geometrical tuning during a simulation as well as numerical synthesis through reversal of the TLM process in time. It is conceivable that at the present rate of progress in time domain modeling these procedures will equal or surpass the capabilities of frequency domain CAD tools in the next decade.

REFERENCES

[1] S. Akhtarzad and P.B. Johns, "Solution of Maxwell's Equations in Three Space Dimensions and Time by the T.L.M. Method of Analysis," Proc. IEE, vol. 122, no. 12, pp. 1344-1348, Dec. 1975.

[2] K.S. Yee, "Numerical Solution of Initial Boundary Value Problems involving Maxwell's Equations in Isotropic Media," IEEE Trans. Antennas Propagation, vol. AP-14, no. 5, pp. 302-307, May 1966.

[3] P.B. Johns, "A Symmetrical Condensed Node for the TLM Method," IEEE Trans. Microwave Theory Tech., vol. MTT-35, no. 4, pp. 370-377, April 1987.

[4] Z. Chen, W.J.R. Hoefer and M. Ney, "A new Finite-Difference Time-Domain Formulation equivalent to the TLM Symmetrical Condensed Node," in 1991 IEEE Intl. Microwave Symp. Dig., pp. 361-364, Boston, Mass., June 11-13, 1991.

[5] J. Nielsen, W.J.R. Hoefer, "A Complete Dispersion Analysis of the Condensed Node TLM Mesh," in 4th Biennial IEEE Conference on Electromagnetic Field Computation Dig., Toronto, Ont., Oct. 22-24, 1990.

[6] P.P.M. So, W J.R. Hoefer, "3D-TLM Time Domain Electromagnetic Wave Simulator for Microwave Circuit Modeling," in 1991 IEEE Intl. Microwave Symp. Dig., pp. 631-634, Boston, Mass., June 11-13, 1991.

[7] P.P.M. So, Eswarappa, W.J.R. Hoefer, "A Two-dimensional TLM Microwave Field Simulator using New Concepts and Procedures," IEEE Trans. Microwave Theory Techniques, vol. MTT-37, no. 12, pp. 1877-1884, Dec. 1989.

[8] M.A. Morgan, Editor, "Finite Element and Finite Difference Methods in Electromagnetic Scattering," PIER 2 Progress in Electromagnetics Research, Elsevier, 1990.

[9] C.E. Tong, Y. Fujino, "An Efficient Algorithm for Transmission Line Matrix Analysis of Electromagnetic Problems using the Symmetrical Condensed Node," IEEE Trans. Microwave Theory Techniques, vol. MTT-39, no. 8, pp. 1420-1424, Aug. 1991.

[10] J.L. Dubard, D. Pompei, J. Le Roux, A. Papiernik, "Characterization of Microstrip Antennas using the TLM Simulation Associated with a Prony-Pisarenko Method," Intl. Journal of Numerical Modelling, vol. 3, no. 4, pp. 269-285, Dec. 1990.

[11] P.B. Johns, "Transient Analysis of Waveguides with Curved Boundaries," Electronics Letters, vol. 9, no. 21, 18th Oct. 1973.

[12] R. Sorrentino, P.P.M. So, W.J.R. Hoefer, "Numerical Microwave Synthesis by Inversion of the TLM Process", in 21st European Microwave Conference Dig., Stuttgart, Germany, 9 - 12 Sept. 1991.

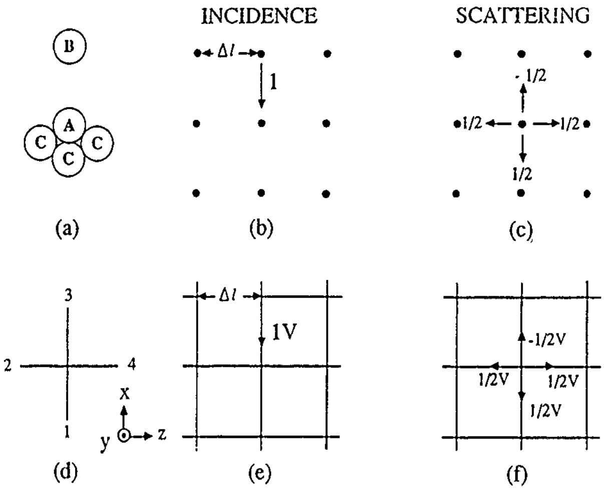

Fig. 1 Huygens's model of light propagation (a) and its formalised version in discretized two-dimensional space (b and c), together with its equivalent transmission line model (d,e, and f).

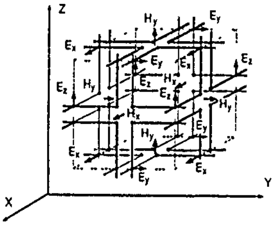

Fig 2a Johns' distributed 3D TLM node [1]

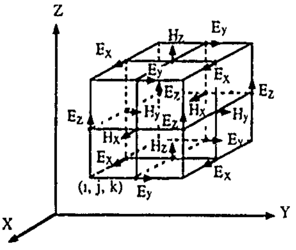

Fig 2b Yee's Finite Difference - Time Domain grid [2]

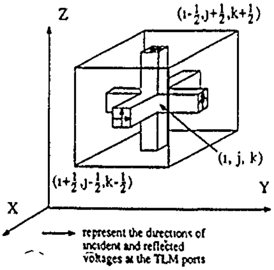

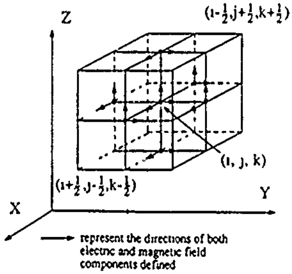

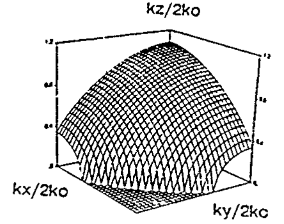

(a)

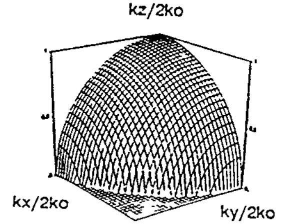

(b)

Fig. 3 Plots of the dispersion surfaces for the schemes shown in Fig 2
(a) Expanded TLM node and Yee's FD-TD scheme;
(b) Condensed TLM node and Chen's FD-TD scheme
(Normalized frequency $2 \pi \Delta l/\lambda = 0.7$ Stability factor for the FD-TD schemes $s = 0.5$. The surfaces are unit spheres when $2 \pi \Delta l/\lambda = 0$)

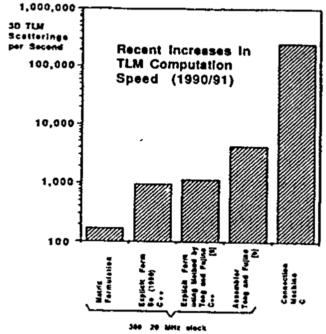

Fig 4

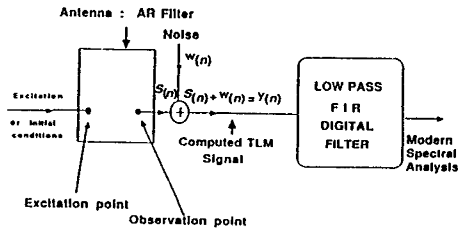

Fig 5

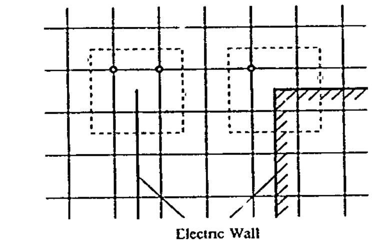

Fig 6 Corner nodes in 2D TLM mesh are not interacting directly with the boundaries, thus causing large coarseness error

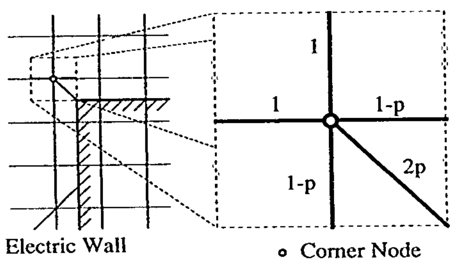

Fig. 7 Compensation of coarseness error by adding a fifth branch to the corner node

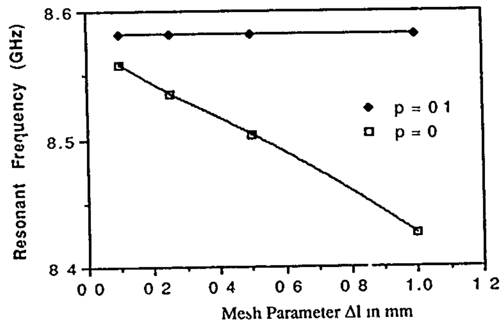

Fig. 8 Effect of the fifth branch of a corner node on the accuracy of TLM simulations of structures with sharp edges or corners.

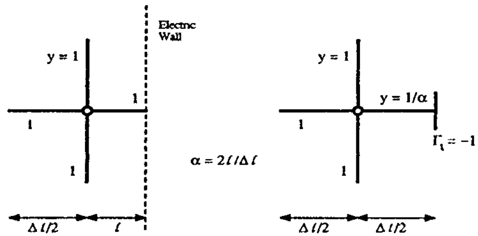

Fig 9 Modification of boundary node for arbitrary position of boundary

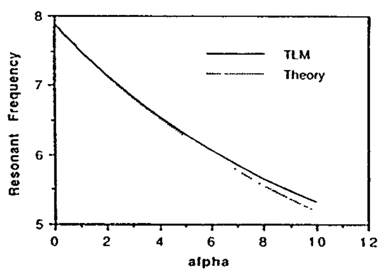

Fig 10 Resonant frequency of a quarter wave resonator terminated by a tunable electric wall as a function of relative position α

RUHR-UNIVERSITÄT BOCHUM
Fakultät für Elektrotechnik
Lehrstuhl für Nachrichtentechnik

"Multi-Dimensional Wave Digital Filters"
Alfred Fettweis.

Essential idea Consider the actual passive physical system (i e the one described by the given system of PDEs) Simulate this system by means of a discrete passive dynamical system

This amounts to replacing the system of PDEs by an appropriate system of difference equations in the same independent physical variables (e g spatial variables, time) as those occuring in the original PDEs, or in independent variables obtained from the former by simple transformations

90/1/1a

Questions 1 How can we properly define a discrete passive dynamical system?

2 How can the desired simulation be achieved?

3 How can this be done in such a way that

31 full robustness is guaranteed, i e, that the errors due to discretization in space and time (linear effects!) as well as those due to discretization in value (nonlinear effects!) are fully kept under control?

32 massive parallelism is available, interconnections only local?

Solution Use principles of multidimensional (MD) wave digital filters (WDFs)

Some specific aspects follow

90/1/1b

1 Physical sys ms are usually passive (contractive) due to conservation of energy Thus, the simulation should preserve this natural passivity

2 Passive simulation is greatly facilitated if one starts from original system of PDEs (partial differential equations), thus not from global PDE obtained by eliminating a certain number of dependent variables (e g all of them except 1 or 2)

Observe A global PDE cannot characterize the passivity of a system, as is also the case of a global ordinary differential equation in the 1-D (one-dimensional) case

The same holds true for transfer functions

89/3/47
90/1/2

3 Physical systems are by nature massively parallel and only locally interconnected (action at proximity versus action at a distance)

The simulation should preserve this massive parallelism and the exclusively local nature of the interconnections

4 Simulation should be done preferably by trapezoidal rule

This ensures best possible approximation in space and time

In the constant case, it amounts to the best possible approximation in the multidimensional (MD) frequency domain (say, in spatio-temporal frequency domain)

(Note spatial frequency = wave number)

89/3/48
90/1/?

5 by using wave quantities (short waves) instead of the original quantities (voltages, currents, electromagnetic field quantities, pressure, velocity etc) a recursible, thus explicitly computable passive MD (multidimensional) simulation becomes feasible Thus in particular MD-WDF principle (WDF = wave digital filter)

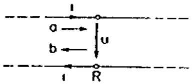

u = voltage, i = current

R = port resistance

a,b = waves

Voltage waves $a = u + Ri$, $b = u - Ri$

power waves $a = (u + Ri)/2\sqrt{R}$, $b = (u - Ri)/2\sqrt{R}$

a = "flowing to the right", b = "flowing to the left"

89/3/49
90/1/4

Note Description by waves and scattering matrix is of fundamental, universal physical importance

input quantities ⟶ reflected and transmitted quantities,

cause ⟶ effect

Closely related to this ensuring explicit computability by use of waves

Note voltage waves preferred but not always possible

6 Due to simulation by passive MD-WDF circuits (multidimensional wave digital filter circuits), numerical instabilities that otherwise could occur due to discretization in space and time (linear discretization) can fully be excluded

89/3/50
90/1/5

7 In particular passivity and even incremental passiv[ity] can fully be ensured by simple means if the highly nonlinear effects are taken into account that are due to the unavoidable rounding / truncation operations and to overflow of the available number range

This way, the complete catalog of all requirements can be satisfied that are known so far for ensuring that the behaviour of the system in the presence of rounding / truncation errors and overflows differs as little as possible from the one that would be obtained in the case of exact computations

In short Full robustness achievable

89/3/51
90/1/6

8 Due to the direct discrete simulation while preserving massive parallelism, arbitrary variations of the characteristic parameters in space and time as well as arbitrary boundary conditions can easily be taken into account

9 Approach is easily applicable for time-dependent problems, e g for problems of hyperbolic type

10 Application to problems of elliptic type possible e g by relaxation determine equilibrium state obtained from dynamic problem

11 Problems of parabolic type can be treated by adding a term ensuring finite propagation speed

Note distinction hyperbolic, elliptic, parabolic in usual mathematical sense not that important

89/3/52
90/1/7

12 Al· ·native types of multigrid methods are appl· ·le (e.g sucessive increase of grid density in order to increase accuracy in equilibrium problems)

13 Application of multirate principle of digital signal processing should be possible for taking into account changing grid densities (Interpolation, decimation zero stuffing, dropping of sampling points)

14 Simplifications are possible for determining steady-state solutions

15 Usual digital filters are linear Thus application simplest in the case of linear problems. However can be extended in principle to nonlinear problems

89/3/53
90/1/8

16 Approach is suitable as basis for building specialized computers with massive parallel processing that are conceived for numerically solving specific classes of systems of partial differential equations (PDEs) Such computers would consist of large number of similar and similarly programmable individual processors These need only carry out additions/subtractions and multiplications, at least for linear PDEs Then, individual processors = digital signal processors,

possibly even of simplified type and with reduced wordlength requirements for coefficients and signal parameters

89/3/54
90/1/9

Approach coordinate transformation $\underline{t} \longrightarrow \underline{t}'$

Original coordinates $\underline{t} = (t_1, \quad , t_k)^T$, $t_k = t$ = time.

New coordinates $\underline{t}' = (t_1, \quad , t_k')^T$, $\underline{t} = \underline{V}^{-1}\underline{H}\,\underline{t}'$

$\underline{V} = \mathrm{diag}\,(1, \quad , 1, v)$, v = positive constant

$\underline{H}$ = k x k matrix, preferably orthogonal.

t_k should be main diagonal of $\underline{t}'$-system of coordinates, i e, all entries of last column of $\underline{H}$ should be equal to a same positive constant, say $d > 0$

$D_x = \dfrac{\partial}{\partial t_x}$, $D_x' = \dfrac{\partial}{\partial t_x'}$, $x = 1$ to k,

$\underline{D} = (D_1, \quad , D_k)^T$, $\underline{D}' = (D_1, \quad , D_k')^T$, $\underline{D}' = \underline{H}^T\underline{V}^{-1}\underline{D}$.

Can apply e g uniform sampling in $\underline{t}$ $T_x' = T'$ = basic shift

From this, can derive other attractive sampling patterns

90/1/30
90/37

Suitable choices for rotation / transformation matrix $\underline{H}$

For k = 2 $\quad \underline{H} = \dfrac{1}{\sqrt{2}} \begin{pmatrix} 1 & -1 \\ 1 & 1 \end{pmatrix}$

For k = 3 $\quad \underline{H} = \begin{pmatrix} 1/\sqrt{2} & -1/\sqrt{2} & 0 \\ 1/\sqrt{6} & 1/\sqrt{6} & -\sqrt{2/3} \\ 1/\sqrt{3} & 1/\sqrt{3} & 1/\sqrt{3} \end{pmatrix}$

$$= \mathrm{diag}\left(\frac{1}{\sqrt{2}}, \frac{1}{\sqrt{6}}, \frac{1}{\sqrt{3}}\right) \begin{pmatrix} 1 & -1 & 0 \\ 1 & 1 & -2 \\ 1 & 1 & 1 \end{pmatrix}$$

For k = 4 $\quad \underline{H} = \mathrm{diag}\left(\dfrac{1}{\sqrt{2}}, \dfrac{1}{\sqrt{6}}, \dfrac{1}{\sqrt{12}}, \dfrac{1}{2}\right) \cdot \begin{pmatrix} 1 & -1 & 0 & 0 \\ 1 & 1 & -2 & 0 \\ 1 & 1 & 1 & -3 \\ 1 & 1 & 1 & 1 \end{pmatrix}$

90/1/31

Simple possibility feasible for $k = 2^m$, $m \in \mathbb{N}$

Use Hadamard matrix, always orthogonal

Choose symmetric type, i e with $\underline{H} = \underline{H}^T = \underline{H}^{-1}$

$$k=2 \qquad \underline{H} = \frac{1}{\sqrt{2}} \begin{pmatrix} -1 & 1 \\ 1 & 1 \end{pmatrix}$$

$$k=4 \qquad \underline{H} = \frac{1}{2} \begin{pmatrix} 1 & -1 & -1 & 1 \\ -1 & 1 & -1 & 1 \\ -1 & -1 & 1 & 1 \\ 1 & 1 & 1 & 1 \end{pmatrix}$$

Note Hadamard matrices also exist for many cases where k = multiple of 4

90/1/32

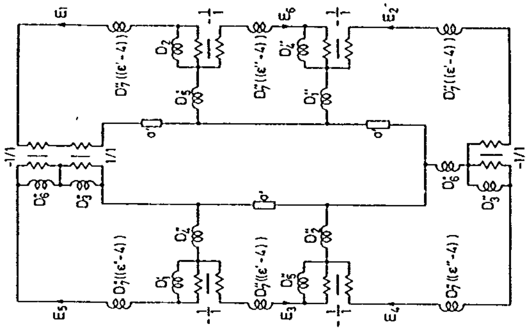

Fig 10 Circuit representing Maxwell's equations after coordinate rotation by means of an Hadamard matrix

90/1/22

Applying Hadamard rotation to Maxwell's equations

$D_7''(\varepsilon' E_1) + (D_5'' - D_2'')\,E_6 + (D_3'' - D_6'')\,E_5 + \sigma' E_1 = 0$

$D_7''(\varepsilon' E_2) + (D_6'' - D_3'')\,E_4 + (D_1'' - D_4'')\,E_6 + \sigma' E_1 = 0$

$D_7''(\varepsilon' E_3) + (D_4'' - D_1'')\,E_5 + (D_2'' - D_5'')\,E_4 + \sigma' E_3 = 0$

$D_7''(\varepsilon'' E_4) + (D_2'' - D_5'')\,E_3 + (D_6'' - D_3'')\,E_2 = 0$

$D_7''(\varepsilon'' E_5) + (D_3'' - D_6'')\,E_1 + (D_4'' - D_1'')\,E_3 = 0$

$D_7''(\varepsilon'' E_6) + (D_1'' - D_4'')\,E_2 + (D_5'' - D_2'')\,E_1 = 0$

where $\varepsilon' = 2r_0 v\varepsilon$, $\varepsilon'' = 2v\mu/r_0$, $\sigma' = 2\sigma r_0$, $r_0 = \text{const} > 0$

$D_1'' = D_1 + D_4$, $D_2'' = D_2' + D_4'$, $D_3'' = D_3 + D_4'$, $E_{3+i} = r_0 H_i$, $i = 1$ to 3,

$D_4'' = D_2' + D_3$, $D_5'' = D_1' + D_3$, $D_6'' = D_1' + D_2$, $D_7'' = D_1' + D_2' + D_3' + D_4'$

Leads to structure with nonnegative elements if

$v \ge 2/\sqrt{\varepsilon_{min}\mu_{min}}$ and, e g, $r_0 = \sqrt{\mu_{min}/\varepsilon_{min}}$

90/1/42

Generalized trapezoidal rule (nonconstant parameters)

Let be T_{10}, T_{20}, T_{30} constants ≥ 0, $\underline{T}_0 = (T_{10}, T_{20}, T_{30})^T$

Differential relation (given, using $D_\chi = \frac{\partial}{\partial t_\chi}$, $\chi = 1$ to k)

$$u = \frac{1}{2}\,(T_{10} D_1 + T_{20} D_2 + T_{30} D_3)\,(Ri), \qquad R = R(\underline{t})$$

This will be approximated by

$$u = \Delta(\underline{T}_0)\,\{Ri\},$$

i e, by

$$u(\underline{t}) + u(\underline{t} - \underline{T}_0) = R(\underline{t})\,i(\underline{t}) - R(\underline{t} - \underline{T}_0)\,i(\underline{t} - \underline{T}_0)$$

This equivalent to applying the conventional trapezoidal rule in direction determined by $\underline{T}_0$

Define (voltage) waves $a = u + Ri$, $b = u - Ri$,

Find $b(\underline{t}) = -a(\underline{t} - \underline{T}_0)$

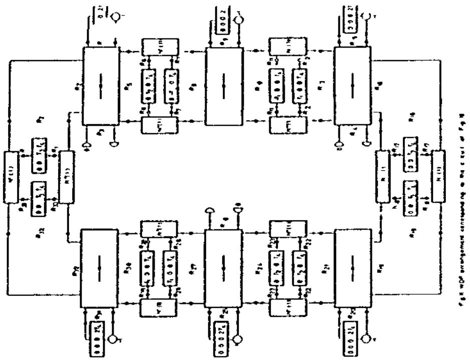

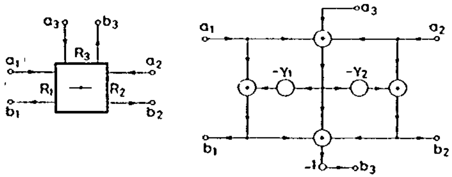

Three-port series adaptor and a corresponding signal-flow diagram (port 3 = dependent port)

$Y_1 = 2R_1/(R_1+R_2+R_3)$, $\quad Y_2 = 2R_2/(R_1+R_2+R_3)$

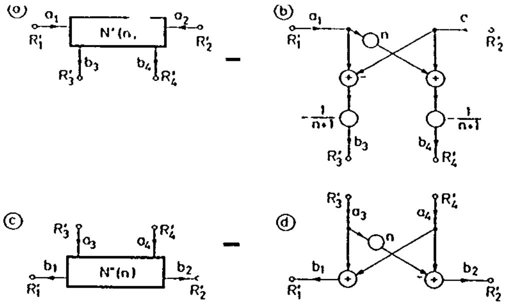

Fig 4 ⓐ and ⓒ Two adaptors as appearing in Fig 3 for n=1 and n=2
ⓑ and ⓓ Corresponding signal-flow diagrams

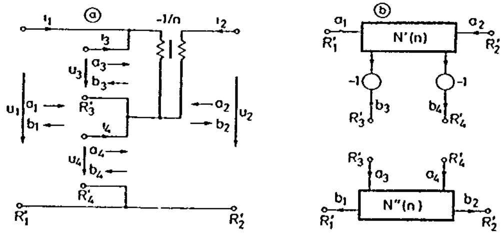

Fig 5 ⓐ a 4-port occuring in circuits such as that of Fig 2
ⓑ Corresponding signal-flow (wave-flow) representation

40/1/18a

Boundary conditions

Can easily take into account

- arbitrary boundary conditions,
- arbitrarily shaped boundaries

This is a result of fact that parameters involved

1 may vary arbitrarily from point to point,

2 multiplier coefficients remain bounded even if
port resistances of adaptors go to 0 or ∞

In particular, may thus consider, for arbitrary shapes,

- hard boundaries (resistivity = 0 or ∞),
- reflection-free boundaries

90/1/26

For deriving, from continuous-domain MD circuit, the corresponding discrete-domain MD circuit, apply substitution:

1. If simple sampling is carried out in original coordinates, $\underline{t}$:

D_1'', $D_4'' \rightarrow \frac{2}{T}\Delta(\pm T, 0, 0, T_4)\{\cdot\}$, T = spatial shift

D_2'', $D_5'' \rightarrow \frac{2}{T}\Delta(0, \pm T, 0, T_4)\{\cdot\}$, T_4 = time shift

D_3'', $D_6'' \rightarrow \frac{2}{T}\Delta(0, 0, \pm T, T_4)\{\cdot\}$, $T_4 = T/v$

$$D_7''((\varepsilon'-4)\cdot) = D_4\left(\left(\frac{\varepsilon'-4}{v}\right)\cdot\right) \rightarrow \begin{cases} \Delta(0,0,0,T_4)\left\{\frac{2(\varepsilon'-4)}{T}\cdot\right\} & \text{for canonic sampling;} \\ \Delta(0,0,0,2T_4)\left\{\frac{\varepsilon'-4}{v}\cdot\right\} & \text{for offset sampling.} \end{cases}$$

Similarly for $D_7''((\varepsilon''-4)\cdot) = D_4((\varepsilon''-4)\cdot)$.

2. More efficient (densest ball packing!), but less easy, if simple sampling is carried out in rotated coordinates, $\underline{t}'$.

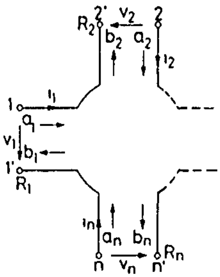

<u>Series connection</u> of n ports (numbered $v = 1$ to n).

R_v = port resistance

$v_1 + v_2 + \cdots + v_n = 0$

$i_1 = i_2 = \cdots = i_n$

$a_v = v_v + R_v i_v$, $b_v = v_v - R_v i_v$

Thus, have $3n$ equations in $4n$ variables

Eliminate all v_v, i_v. Solve for the b_v:

$b_v = a_v - \gamma_v(a_1 + a_2 + \cdots + a_n)$, $\gamma_v = 2R_v/(R_1 + R_2 + \cdots + R_n)$

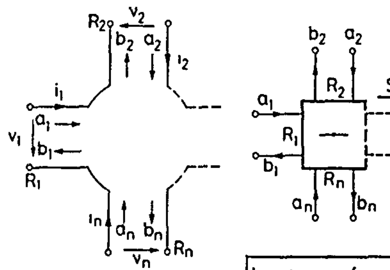

<u>Series adaptor,</u>

with n ports

$\nu = 1$ to n

$$\boxed{b_\nu = a_\nu - \gamma_\nu (a_1 + a_2 + \cdots + a_n)}$$

$\gamma_\nu = 2R_\nu/(R_1 + R_2 + \cdots + R_n)$, $\gamma_1 + \gamma_2 + \cdots + \gamma_n = 2$

Can choose one port as <u>dependent</u> port,

e.g. $\nu = 1$: $\gamma_1 = 2 - \gamma_2 - \gamma_3 - \cdots - \gamma_n$. Thus, need

$n-1$ multipliers (not n^2) = number degrees of freedom.

Recent Developments of in Numerical Integration of Differential Equations

Wolfgang Mathis
University of Wuppertal

Abstract

Numerical Integration of differential equation is a standard discipline in numerical mathematics and basically for simulating dynamical systems in all areas of engineering. In dependence of the kind of modelling dynamical systems will be described by ordinary or partial differential equations. In this paper we restrict us mainly to the former case. The most general type of ordinary differential equation has the implicit form

$$F(x, \dot{x}, t) = 0, \tag{1}$$

and is called *differential-algebraic equation* (DAE). By means of a suitable transformation the explicit dependence of t can be dropped If F is solvable for $\dot{x}$ globally we obtain

$$\dot{x} = f(x); \tag{2}$$

we refer this type as ODE Because these equations possess a manifold of solutions rather than a unique solution additional conditions must be prescribed to x. If x is determined at one time t_0 this situation is called initial valued problem (IVP) whereas conditions in different time points are called boundary valued problem (BVP).

In order to simulate a dynamical system we start with a system description of type (1) or (2). In dependence of our interests we formulate a IVP or a BVP. For calculating the solution $x(t)$ we associate a convenient difference equation to (1) or (2). It is obviously to replace the derivative $\dot{x}$ by a difference approximation with a step-size h and to construct a discrete sequence of $x(t_n)$. The quality of such approximations will be characterized by consistency, convergency and stability. The theory of numerical integration of ODE (1) and the art of its implementation are available. In this paper we are interested mainly but not only in multistep methods. In most applications, e g. mechanics and electrical engineering, most dynamical systems are represented by DAE's in a natural manner. For this reason we discuss the main aspects of to the theory and implementations of numerical integration methods for DAE's and remark that the essential results are developed during the last ten years.

Furthermore we will discuss the problem of step-size control and switching between different integration algorithms (order control) from a control theoretical point of view; this part includes also some results worked out in our corresponding project. We illustrate this material by means of some examples from circuit simulation.

The final section contains something about the problem of rounding errors. This is an essential subject because the development of algorithms (operations) and the characterization of their properties will be discussed in the real numbers $\mathbb{R}$ and in other sets, e g. $\mathbb{C}$, $\mathbb{R}^n, \mathbb{R}^{n \times n}$, which are constructed in a 'vertical manner'. In classical numerics we choose a suitable finite set (e.g. floating point numbers F) of $\mathbb{R}$ and associated operations and construct the 'higher' sets and operations in a 'vertical manner'm, too Therefore it is not clear that the *numerical algorithm* (implemented in F) works in the manner as the algorithm in $\mathbb{R}$. To circumvent this problem it seems to be useful to apply a well-defined arithmetic (Kulisch-arithmetic) and well-adapted algorithms. This approach is close related to the wave-digital filter method of Fettweis.

Bergische Universität - GH Wuppertal

Rechnergestützter Schaltungsentwurf

RSE

Recent Developments in Numerical Integration of Differential Equations

Wolfgang Mathis

University of Wuppertal

Content

1 Description Equations for Circuit Simulation
2. Some Basic Concepts in ODE's
3 DE's from ODE's
- Some Construction Principles of DE's from ODE's
- Basic Properties of DE's from ODE's
4. Stability Properties of DE's from Special ODE's
- A Universal Linear Test ODE
- Step Size Control and 'Stiffness'
- 'Stiff' ODE's
5 Remarks to Implementating ODE-Solver
6 Revised 'Description Equations for '
7 DAE's are not ODE's
8 Numerical Solution of DAE's
9 Summary and Outlook

1. Description Equations for Circuits Simulation

- Step 1 Modeling of the Circuit ⇒ Network

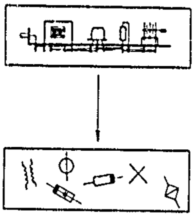

- Step 2: Description the Networks ⇒ Network Equations

Fundamental Relationships
- Kirchhoffian Equations
- Dynamical and Nondynamical Konstitutive Relations

Example

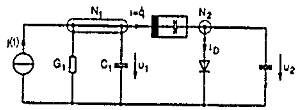

Kirchhoffian Equations + Konstitutive Relations

$$N_1 \quad G_1u_1 + C_1u_1' + q' - j(t) = 0 \qquad (1)$$

$$N_2 \quad \underbrace{i_S(e^{bu_2} - 1)}_{i_D} + C_2u_2' - q' = 0 \qquad (2)$$

Nonlinear Capacitor (Charge Voltage Relation)

$$q = C_3a(1 + bu_C^2) \qquad (3')$$

$$\Rightarrow q' = C_3 \underbrace{ab}_{=\lambda} 2u_C \; u_C' \qquad (3'')$$

$$\Longrightarrow \quad q' = 2C_3\lambda(u_1 - u_2)(u_1' - u_2') \qquad (4)$$

Explicit Reformulation (State Space Equations)

$$u_1' = -\frac{2C_3}{g(u_1 - u_2)}\left\{-(G_1u_1 - j(t))\frac{C_1}{2C_3} + K\left(i_S(e^{bu_2} - 1) + (G_1u_1 - j(t))\right)(u_2 - \right.$$

$$u_2' = -\frac{2C_3}{g(u_1 - u_2)}\left\{-i_S(e^{bu_2} - 1)\frac{C_1}{C_3} + \lambda\left(i_S(e^{bu_2} - 1) + (G_1u_1 - j(t))\right)(u_2 - u_1\right.$$

$$q = -\frac{2C_3}{g(u_1 - u_2)}\lambda\left\{-i_S(e^{bu_2} - 1)C_1 + (G_1u_1 - j(t))C_2\right\}(u_2 - u_1)$$

where

$$g(u_1 - u_2) = -(C_1 + C_2)\left(\frac{C_1C_2}{C_1 + C_2} + 2C_3\lambda(u_1 - u_2)\right)$$

- **Type of Network Equations**

$$x' = f(x, t)$$

Explicit Ordinary Differential Equations (ODE's)

2 Some Basic Concepts in ODE's

- **'Autonomization'**, $x_{n+1} = t$

$$\begin{pmatrix} x' \\ x'_{n+1} \end{pmatrix} = \begin{pmatrix} f(x, x_{n+1}) \\ 0 \end{pmatrix}$$

and with

$$\hat{x} = \begin{pmatrix} x \\ x_{n+1} \end{pmatrix} \quad \Longrightarrow \quad \dot{\hat{x}} = \hat{f}(\hat{x})$$

- **Kinds of Problems in ODE's.**
  - **Initial value Problem**

$$\dot{x} = f(x) \quad \oplus \quad x(t_0) = x_0$$

  ⟶ local uniqueness and existence theorems
  - **Boundary-value Problem**

$$\dot{x} = f(x) \quad \oplus \quad r(x(t_1), x(t_2)) = 0$$

  ⟶ global uniqueness and existence theorem

- **Restriction in this Paper:**

Initial value Problems

- **Local Theorems for ODE's**
  - **Existence (→ Cauchy Peano)**
  f continuous ⟶ $x(t)$ locally exists
  Constructive Method: Cauchy Euler Method
  - **Uniqueness (→ Picard)**
  f Lipschitz continuous ⟶ $x(t)$ locally unique
  Constructive Method: Picard Iteration

  Remark
  f is Lipschitz-continuous in $D \subset \mathbb{R}^n$, if $L \in \mathbb{R}_+$ exists and

$$\|f(x) - f(y)\| \leq L\|x - y\|$$

  is satisfied for all $x, y \in D$

- **Types of Solutions of ODE's**

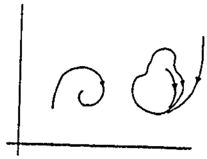

- **Restriction in this Paper:**

Transient Solutions of ODE's

Calculation of Solutions of ODE's

- **(Linear) Engineers Interpretation of Solving ODE's**
  Representation of the 'General Solution' of an ODE
  by means of Elementary Functions
  ⟶ A General Solution contains 'global' Information
- **In the case of nonlinear ODE's:**
  A 'General Solution' is (very often) not available
  ⟶ Calculation of approximative solutions
- **Types of Approximation Methods:**
  - Analytical Methods
  - Numerical Methods

- **Restriction in this Paper**

Numerical for ODE's

- **Main Property of a Computer.** Finite Memory
  ⟶ Approximated Representation of Mathematical Objects

- **General Approach for Solving ODE's**

ODE's ⟶ Difference Equations (DE)

3 DE's from ODE's

- **Representation of Functions:**
  continuous time f ⟶ discrete time $\{x_n\}_{n=0}^{N}$, $\{x'_n\}_{n=0}^{N}$
  where $x(t_n) \approx x_n$ on the grid $\{t_0, \ldots, t_n\}$

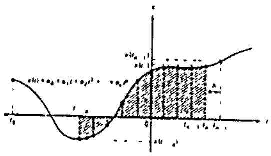

- **Therefore**

ODE's ⟶ DE

- **Exact Replacement ODE → DE**

  Example

$$x' + 2x = 1 \qquad \& \qquad x(0) = 1 \tag{1}$$

  If $\{t_0, \ldots, t_n, t_{n+1}, \ldots, t_N\}$ is a grid

  - Integration form $t_n \to t_{n+1}$ ($\Delta t = t_{n+1} - t_n$)

$$x_{n+1} - x_n = \int_{t_n}^{t_{n+1}} (1 - 2x(\tau))\, d\tau = \Delta t - 2\int_{t_n}^{t_{n+1}} x(\tau)\, d\tau \tag{2}$$

  - Analytical Solution of (1) in $[t_n, t_{n+1}]$

$$x(t) = \frac{1}{2}\left(1 - e^{-2(t-t_n)}\right) + x_n e^{-2(t-t_n)} \tag{3}$$

  - Substitution of (3) in the integral of (2) ⟶ DE

$$x_{n+1} - e^{-2\Delta t} x_n = \frac{1}{2}\left(1 - e^{-2\Delta t}\right)$$

- **Approximative DE, if $\Delta t \ll 1$**

  With $e^{-2\Delta t} = 1 - 2\Delta t + O(\Delta t^2)$ we have

$$x_{n+1} - (1 - 2\Delta t + O(\Delta t^2))x_n = \frac{1}{2}(1 - 1 + 2\Delta t + O(\Delta t^2))$$

$$\Longleftrightarrow \quad \underbrace{x_{n+1} = x_n + \Delta t(1 - 2x_n)}_{\text{Euler Method}} + O(\Delta t^2)$$

- **Type of the DE:**
  - $h = \Delta t = \text{const}$ for all n

    ⟶ linear DE with constant coefficients
  - Δt varies for n

    ⟶ linear DE with varying coefficients

3 1 Some Construction Principles of DE's from ODE's

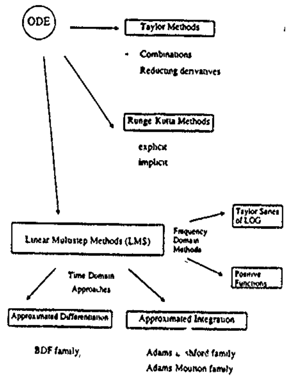

- **Restriction in this Paper:**

  Linear Multistep Methods

Restriction to the 1-dimensional case

Let $\{t_0, \ldots, t_n, t_{n+1}, \ldots, t_N\}$ a grid on $I \subset I\!R$

- **Taylor Methods**
  - Expansion of $x(t)$ at t_n

$$x_{n+1} = x_n + \Delta t\, x_n' + \frac{\Delta t^2}{2} x_n'' + \ldots \tag{1}$$

  With $x_n' = f(x_n)$

$$\longrightarrow x_{n+1} = x_n + \Delta t\, f(x_n)) \tag{2}$$

  Explicit Euler Method

  - Expansion of $x(t)$ at t_{n+1}

$$x_n = x_{n+1} - \Delta t\, x_{n+1}' + \frac{\Delta t^2}{2} x_{n+1}'' + \ldots \tag{3}$$

  With $x_{n+1}' = f(x_{n+1})$

$$\longrightarrow x_{n+1} = x_n + \Delta t\, f(x_{n+1})) \tag{4}$$

  Implicit Euler Method

- Combinations of Taylor Methods
  - Subtraction of (2) and (4)

$$x_{n+1} = x_n + \frac{\Delta t}{2}(f(x_n) + f(x_{n+1})) + O(\Delta t^3) \tag{5}$$

  Crank Nicolson Method ('One Step Trapezoidal Rule')

  Remark This Method is of second order accuracy!

  (Because of $x_{n+1}'' = x_n'' + \Delta t x_n''' + \ldots$)

  - Writing (1) at times t_{n-1}, t_n

$$x_{n-1} = x_n - \Delta t\, x_n' + \frac{\Delta t^2}{2} x_n'' + \ldots$$

  Subtraction from (1)

$$x_{n+1} = x_n + 2\Delta t\, f(x_n) + O(\Delta t^3)$$

  Explicit Second Order Nyström Method ('Midpoint Rule')

- **Reduction of Derivatives in Taylor Series**

  With

$$x_n'' = \frac{x_n' - x_{n-1}'}{\Delta t} + O(\Delta t)$$

  and with (1) we obtain

$$x_{n+1} = x_n + \Delta t\, x_n' + \frac{\Delta t^2}{2}\left(\frac{x_n' - x_{n-1}'}{\Delta t}\right) + \frac{\Delta t^3}{6} x_n''' + \ldots$$

$$\Longleftrightarrow \quad x_{n+1} = x_n \frac{\Delta t}{2}(3x_n' - x_{n-1}') + O(\Delta t^3)$$

  With $x_n' = f(x_n)$ and $x_{n-1}' = f(x_{n-1})$

$$x_{n+1} = x_n + \frac{\Delta t}{2}(3f(x_n) - f(x_{n-1}))$$

  An (Explicit) Adams Bashford Method

  Remark This is a two-step method

- **Approximated Integral Methods**

$$x'(t) = f(x(t)) \qquad \text{for } t \in [t_n, t_{n+1}]$$

is equivalent (in some sense) with

$$x(t_{n+1}) = x(t_n) + \int_{t_n}^{t_{n+1}} x'(\tau)\,d\tau = \int_{t_n}^{t_{n+1}} f(x(\tau))\,d\tau$$

- **Replacement**

$$F(t) = f(x(t)) \quad \longrightarrow \quad \mathcal{P}^k(t) \quad \text{Polynomial Function}$$

- **Integration of $\mathcal{P}^k$ is easy**

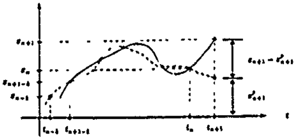

- Representation of $\mathcal{P}^k$ by means of different Basis
  - Taylor Interpolation
  - Lagrange Interpolation
  - Newton Interpolation (divided differences)
  - Modified Divided Differences (Krogh)

3.2 Basic Properties of DE from ODE

- **Difference Operator of Linear Multistep Methods**

$$\mathcal{L}_h(x(t)) = \sum_{j=0}^{k} \alpha_j x(t - jh) - h \sum_{j=0}^{k} \beta_j x'(t - jh)$$

Denotations

- h Step Size
- k Number of Steps

Characterization of $\mathcal{L}_h$ by Polynomials

$$\rho(z) = \sum_{j=0}^{k} \alpha_{k-j} z^j$$

$$\sigma(z) = \sum_{j=0}^{k} \beta_{k-j} z^j$$

- **Order of $\mathcal{L}_h$**

If $x(t)$ analytically (e.g. a polynomial)

$$\longrightarrow \quad \mathcal{L}_h(x(t)) = \sum_{j=0}^{\infty} C_j x^{(j)}(t) h^j$$

$\mathcal{L}_h$ is of order p, if

$$C_0 = C_1 = \ldots = C_p = 0 \qquad \text{and} \qquad C_{p+1} \neq 0$$

- **Linear Multistep Methods associated to $\mathcal{L}_h$**

$$\sum_{j=0}^{k} \alpha_j x_{n-j} - h \sum_{j=0}^{k} \beta_j f(x_{n-j}) = 0$$

where $x_{n-k}, \ldots, x_n$ are the approximative values of $x(t_{n-k}), \ldots, x(t_n)$

Denotations

- $\beta_k = 0$ explicit LMS Method
- $\beta_k \neq 0$ implicit LMS Method

- **Definition of the Local Truncation Error (LTE) of LMS**

  ($\mathcal{L}_h$ of order p and $x(t)$ a solution of the ODE)

$$\mathcal{L}_h(x(t_n)) = \Big(\sum_{j=0}^{k} \alpha_j x(t_{n-j}) - h \sum_{j=0}^{k} \beta_j f(x(t_{n-j}))\Big) = -C_{p+1} h^{p+1} x^{p+1}(t_n) + \mathcal{O}(h^{p+2})$$

Denotations

$-C_{p+1} h^{p+1} x^{p+1}(t_n) + \mathcal{O}(h^{p+2})$ Local Truncation Error (LTE)

$-C_{p+1} h^{p+1} x^{p+1}(t_n)$ Principal Local Truncation Error

C_{p+1} Error Constant

$e_n = x(t_n) - x_n$ Global Error

Asymptotic Properties

- **Consistency**

$$\text{DE} \xrightarrow{h \to 0} \text{ODE}$$

- **Convergence**

$$\text{Solution(DE)} \xrightarrow{h \to 0} \text{Solution(ODE)}$$

- **Sources of Errors in Computations:**
  - Computer Arithmetic $\longrightarrow$ Rounding Errors
  - Replacement of the exact DE $\longrightarrow$ Truncation Errors
  - Replacement of an ODE by higher order DE $\longrightarrow$ extraneous solutions

- **An Example for Extraneous Solutions:**

Apply second order Adams Bashford

$$x_{n+1} = x_n + \frac{h}{2}(3f(x_n) - f(x_{n-1}))$$

(h=const.) to the linear ODE

$$x' = f(x) = -x$$

$$\Longrightarrow \quad x_{n+1} = x_n + \frac{h}{2}(3x_n - x_{n-1})$$

Solving this DE by means of the characteristic equation

$$s^2 - s\left(1 - \frac{3}{2}h\right) - \frac{h}{2} = 0$$

Roots $s_{(+)} = 1 - h, \quad s_{(-)} = -h/2$

Interpretation

- $s_{(+)}$ physical solution
  (approx. the ODE-solution $\exp(-h) = 1 - h + (1/2)h^2 + \ldots$)
- $s_{(-)}$ numerical mode

Condition for a decreasing numerical mode

$$|s_{(-)}| = |h/2| < 1$$

- (Asymptotic) Stability Property of Dahlquist
  Bounded initial values $\longrightarrow$ Bounded Solution(DE)
  (h sufficient small)
- Theorem of Lax&Richtmeyer and Henrici
  Consistency $\oplus$ stability $\Longleftrightarrow$ Convergence
- Classification of LMS by means of ρ and σ
  - Consistency
    $$\rho(1) = 0 \qquad \rho'(1) = \sigma(1)$$
  - Stability
    - All zeros of $\rho(z)$ lie in the closed unit disc
    - while those on the boundary of the disc are simple

4. Stability Properties of DE's from Special ODE's

4.1 A Universal Test ODE

- Till now only asymptotic properties are discussed:
  that is, $h \to 0$
- Very interesting for practical applications:
  finite step size, that is, $h \neq 0$ ($h \not\to 0$)
- Linear test ODE (1-dimensional case)
  $$z' = f(z) = -\lambda z$$
  $$\overset{\text{LMS}}{\Longrightarrow} \qquad \sum_{j=1}^{k} \alpha_j z_{n-j} - (h\lambda) \sum_{j=1}^{k} \beta_j z_{n-j} = 0 \qquad (*)$$
- LMS (*) is absolut stabil at $h\lambda$, if
  $$\rho(z) - (h\lambda)\sigma(z) = 0$$
  has roots $|z_i| < 1$ $i = 1, \ldots, k$
  Denotation:
  $$S = \{h\lambda \in \mathbb{C} \mid \text{LMS method is absolut stabil for } h\lambda\}$$
  is called Stability Region
- Stability region of the test ODE $z' = -\lambda z$,
  solution $z(h) = e^{s} z_0$ where $s = \lambda h$
  $$\Longrightarrow \qquad S_{an} = \{s \in \mathbb{C} \mid \mathrm{R}\{s\} \leq 0\} = \mathbb{C}^-$$
- Stability region of a DE from the test ODE:
  approx. solution $z_1 = R(s) z_0 \approx e^{s} z_0$
  $$\Longrightarrow \qquad S_{nu} = \{s \in \mathbb{C} \mid |R(s)| \leq 1\}$$

- Ideal Condition
  $$S_{nu} = \mathbb{C}$$
  Example: Crank Nicolson Method

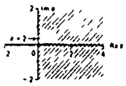

- Dahlquist's A Stability
  Analytical decreasing solutions(ODE) $\longrightarrow$ decreasing solutions(DE)
  $$\Longrightarrow \quad S_{nu} \supseteq \mathbb{C}^-$$
  Example: Implicit Euler Method

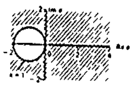

- Unfortunately: A Stability restricts Accuracy
  Theorem (Dahlquist)
  Explicit LMS methods cannot be A stabil
  Implicit LMS methods with order $p \geq 3$ cannot be A stabil

4.2 Step Size Control and 'Stiffness'

- Accuracy determines the Step Size
  Example:
  $$z' = -\lambda z, \qquad \lambda \in \mathbb{R}$$
  - Analytical Solution $z(t) = A e^{-\lambda t}$ (*)
  - Using explicit Euler method
    $$\begin{aligned} z_{n+1} &= z_n + h f(z_n) \\ \Longrightarrow \qquad &= z_n - h\lambda z_n \\ &= (1 - h\lambda) z_n \end{aligned}$$
  - Principal LTE (using (*))
    $$LTE = \frac{h^2}{2} z''(t_n) \approx \frac{h^2}{2} \lambda^2 A \quad (t_n \ll 1)$$
  - Error Control Approach
    $$|LTE| \approx |\frac{h^2}{2} \lambda^2 A| = \epsilon$$
    ϵ Tolerance
    $$\Longrightarrow \qquad h = \left(\frac{2\epsilon}{\lambda^2 A}\right)^{1/2}$$
    $\longrightarrow$ ϵ small $\longrightarrow$ h small

- Stability determines h for 'Stiff' ODE's

Example

$$x' = -\lambda(x - p(t)) - p'(t), \quad x(0) = x_0$$

- Solution $x(t) = (x_0 - p(0))e^{-\lambda t} + p(t)$
- Accuracy Principal LTE for explicit Euler methods

  $t \ll 1$ Initial Transient

$$h\left(\frac{2\varepsilon}{x''(t)}\right) = \left(\frac{2\varepsilon}{(x_0 - p(0))\lambda^2}\right)^{1/2}$$

$$\longrightarrow \quad \text{h small}$$

  $t \gg 1$ Slow variations with p

$$h\left(\frac{2\varepsilon}{|p''(t)|}\right), \ |p''(t)| \ \text{small}$$

$$\longrightarrow \quad \text{h large}$$

- Stability Studying the global error $\varepsilon_n = x(t_n) - x_n$

$$\varepsilon_{n+1} = (1 + h\lambda)\varepsilon + LTE_n$$

  ε_n is amplified unless

$$-2 < h\lambda < 0$$

Stability restricts h!

- These time intervals of ODE's are called 'stiff'

4 3 'Stiff' ODE

- An ODE is said to be stiff on $[0, T]$, if there exist's a component of a solution that varies large compared to $1/T$
- For linear time invariant ODE's $\mathbf{x}' = A\mathbf{x}$

  This ODE's are 'stiff', if

$$\max_i |\lambda_i(A)| \gg \min_i |\lambda_i(A)|$$

- Remark The last definition is invalid for linear time variant ODE's

  Example:

$$\mathbf{x}' = \begin{pmatrix} -1 - 9\cos^2 6t + 6\sin 12t & 12\cos^2 6t + 9/2\sin 12t \\ -12\sin^2 6t + 9/2\sin 12t & -1 - 9\sin^2 6t - 6\sin 12t \end{pmatrix}\mathbf{x}$$

  Eigenvalues 1 and 10 (constant!)

  Exact Solution

$$\mathbf{x}(t) = C_1 e^{2t}\begin{pmatrix} \cos 6t + 2\sin 6t \\ 2\cos 6t - \sin 6t \end{pmatrix} + C_2 e^{-13t}\begin{pmatrix} \sin 6t - 2\cos 6t \\ 2\sin 6t + \cos 6t \end{pmatrix}$$

  Interpretation $\exp(-t)$ and $\exp(-10t)$ are not included

- The initial transient is not 'stiff', because $|h\lambda|$ is small

  Example Van der Pol Equation

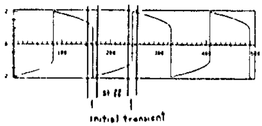

- Design Approaches for 'nonstiff' and 'stiff' ODE's
  - Global Error Equation

$$\varepsilon_{n+1} = S_n \varepsilon_n + LTE_n$$

  - Design goal in nonstiff' cases

    LTE_n small as possible
  - Design goal in stiff cases

    S_n small as possible

    Price LTE_n not minimal

Different Stability Concepts for Stiffness

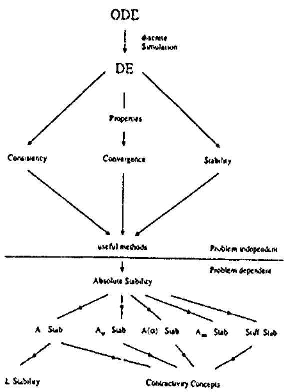

Further Characterizations of 'Stiffness'

- Large Step Size h
  - ⟶ Implicit methods
  - ⟶ Solving nonlinear equations (nonlinear ODE's)
  - ⟶ Because of $|h\lambda| > 1$ simple iteration methods are not succesful
    (Sandberg&Shichman, 1968)
- Stiffness requires Newton type Methods
  - 'good' starting point for Newton type methods is needed
- Predictor method determines starting point
- Predictor Corrector difference provides a reasonable LTE estimation

5 Remarks to the Implementation of ODE-Solvers

Problems for implementing a LMS family

- Suitable Polynomial Representation
- Efficient Step Size Control
- Efficient Order Control
  - Very Useful Concepts from Control Theory
    An Example: Ring Modulator

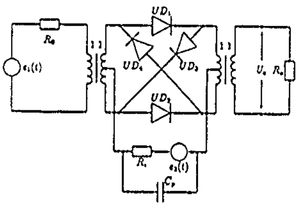

Classical Step Size Control

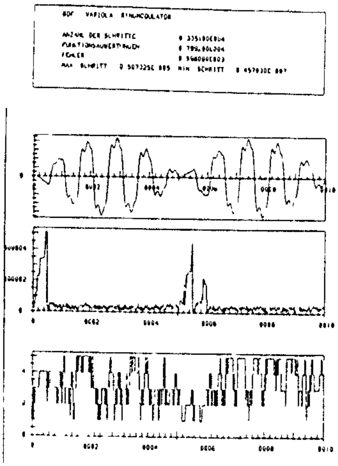

Step Size Control with PI Controller:

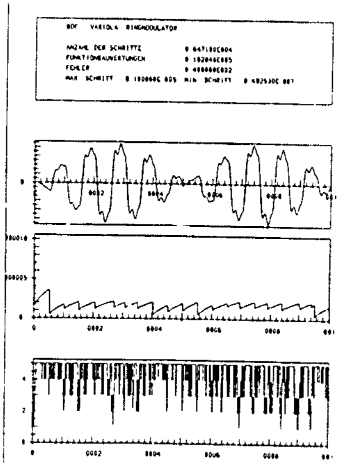

Further Remarks to Implementations

- Stiffness Detection
- Efficient Nonlinear Solver (Newton type Methods)

6 Revised 'Description Equation for ..'

- Explicit ODE's are not naturally for Circuit Simulation
  - See Example in Section 1: implicit ODE directly obtained
- Types of Differential/Algebraic Equations (DAE)
  - Implicit ODE (or DAE)

$$F(x, x', t) = 0$$

  - Semi explicit DAE

$$x' = f(x, y)$$
$$0 = g(x, y)$$

- Electrical Networks are described by a mixture of
  - Algebraic equations
    (Kirchhoffian equations, linear and nonlinear resistive equations, source characterization)
  - Differential equations
    (linear and nonlinear capacitor and inductor characterizations)

Describing Networks by Semi explicit DAE's

Example

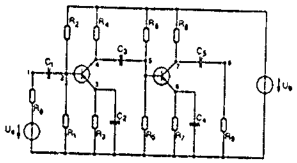

$$\frac{U_e(t)}{R_0} - \frac{u_1}{R_0} + C_1\frac{d(u_2 - u_1)}{dt} = 0$$
$$\frac{U_b}{R_2} - u_2\left(\frac{1}{R_1} + \frac{1}{R_2}\right) + C_1\frac{d(u_1 - u_2)}{dt} + (\alpha - 1)f(u_2 - u_3) = 0$$
$$f(u_2 - u_3) - \frac{u_3}{R_3} - C_2\frac{du_3}{dt} = 0$$
$$\frac{U_b}{R_4} - \frac{u_4}{R_4} \quad C_3\frac{d(u_4 - u\ )}{dt} - \alpha f(u_2 - u_3) = 0$$
$$\frac{U_b}{R_6} - u_5\left(\frac{1}{R_5} + \frac{1}{R_6}\right) + C_3\frac{d(u_4 - u_5)}{dt} + (\alpha - 1)f(u_5 - u_6) = 0$$
$$f(u_5 - u_6) - \frac{u_6}{R_7} - C_4\frac{du_6}{dt} = 0$$
$$\frac{U_b}{R_8} - \frac{u_7}{R_8} - C_5\frac{d(u_7 - u_8)}{dt} - \alpha f(u_5 - u_6) = 0$$
$$\frac{u_8}{R_9} - C_5\frac{d(u_7 - u_8)}{dt} = 0$$

where $f(u) = \beta\left(e^{\frac{u}{u_F}} - 1\right)$

Input signal

$$U_e(t) = 0.1 \sin(200\pi t)$$

Parameters

$$U_b = 6 \quad (\text{power supply})$$
$$u_F = 0.026 \quad \alpha = 0.99, \quad \beta = 10^{-6},$$
$$R_0 = 1000 \quad R_k = 9000 \text{ for } k = 1, \ldots, 9,$$
$$C_k = k \cdot 10^{-6} \text{ for } k = 1, \ldots, 5$$

- Interpretable as semi explicit Differential/Algebraic Equation

7. DAE's are not ODE's

- Titel form Linda Petzold's paper in 1982
- **Analytical Aspects**
  - Semi explicit DAE as ODE on manifolds

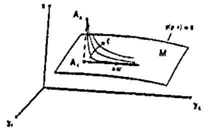

- Consistent initial conditions
  Satisfy the DAE ($\leftrightarrow$ on the manifold)
- Solution manifold differs from ODE's
- **Classification by 'Index' Concepts**

1) Local Index: Linear DAE with constant Coefficients

Example $Bx' = x - g$

$$\begin{pmatrix} 0 & 0 & 0 \\ 1 & 0 & 0 \\ 0 & 1 & 0 \end{pmatrix} \begin{pmatrix} x_1' \\ x_2' \\ x_3' \end{pmatrix} = \begin{pmatrix} x_1 \\ x_2 \\ x_3 \end{pmatrix} - \begin{pmatrix} g(t) \\ 0 \\ 0 \end{pmatrix} \qquad (*)$$

The integer k with

$$N^{k-1} \neq 0, \quad N^k = 0$$

is called local index

$\Longrightarrow$ (*) has the local index=3

2) Global Index

Minimal number of times that a DAE must be differentiated with respect to t in order to determine y' as a continuous function of y and t

Example. Semi explicit DAE

$$x' = f(x,y) \qquad (1)$$
$$0 = g(x,y) \qquad (2)$$

$$(2) \Longrightarrow \quad g_x x' + g_y y' = 0 \qquad (3)$$

Subst (1) in (3)

$$y' = -g_y^{-1} g_x f$$

Condition g_y local invertable

$\Longrightarrow$ global index = 1

3) Index Reduction

Example

$$y' = f(x,y) \qquad (4)$$
$$0 = g(y) \qquad (5)$$

$$(5) \Longrightarrow \quad 0 = g_y y' = g_y f(y,x) = F(x,y) \qquad (6)$$

If $F(x,y)$ is local invertable to x

$\Longrightarrow$ (4) $\oplus$ (6) is index = 1

$\Longrightarrow$ (4) $\oplus$ (5) is index = 2

- **Numerical Aspects**

Solving (*) with implicit Euler method

$$\begin{pmatrix} 0 & 0 & 0 \\ 1 & 0 & 0 \\ 0 & 1 & 0 \end{pmatrix} \begin{pmatrix} x_1' \\ x_2' \\ x_3' \end{pmatrix} = \begin{pmatrix} x_1 \\ x_2 \\ x_3 \end{pmatrix} - \begin{pmatrix} g(t) \\ 0 \\ 0 \end{pmatrix}$$

$$x_{1n} = g(t_n)$$
$$x_{2n} = \frac{x_{1n} - x_{1n-1}}{h_n}$$
$$x_{3n} = \frac{x_{2n} - x_{2n-1}}{h_n}$$

Let x_{10} x_{20} x_{30} be inconsistent (fulfills (*))

x_{1n} is correct for all n
- x_{2n} is incorrect for the first step (then correct)
- x_{3n} is incorrect for the first two steps (then correct)

Condition h_n is constant

If h_n is nonconstant then

$$x_{3n} = \frac{\frac{g(t_{n+1}) - g(t_n)}{h_{n+1}} - \frac{g(t_n) - g(t_{n-1})}{h_n}}{h_{n+1}}$$

instead of

$$x_{3n} = \frac{\frac{g(t_{n+1}) - g(t_n)}{h_{n+1}} - \frac{g(t_n) - g(t_{n-1})}{h_n}}{\frac{h_{n+1} + h_n}{2}}$$

The error behaves like $O(h_n^{-1})$

$\longrightarrow$ divergence for small h_n!

8. Numerical Solutions of DAE's

Numerical Integration Methods available:

- **Linear time-invariant DAE's:**
  - Constant Step Size
  - Local Index < 2
  - Special DAE's with Local Index 3
  - Ideas for index-detection
- **Linear time-variant DAE's**
  - Global Index 1
  - Global Index 2 → Stability Problems
  - Global Index 3 → almost in every Case. Stability Problems
- **Nonlinear DAE's**
  - Global Index 1 (Implementation nontrivial)
  - Global Index 2 – Semi-explicit DAE's
  - Global Index 3 – Special Semi-explicit DAE's

Problems: Iteration matrix ill-conditioned, Error test difficult

9. Summary and Outlook

Problems in ODE and DAE Numerics

- Discontinuous right-hand sides of ODE
- Oscillatory Solutions
- Theory of variable step size and order methods
- Adaptive control of step size and order
- Robust DAE-solver with Index Detection
- Global Error Control
- Contractive Methods
- Other Classes of Stiff ODE- and DAE-Solver
  - Implicit Runge-Kutta Family
  - Semi-implicit Extrapolation Methods
  - Rosenbrock-Wanner Methods

Cellular Automata: Applications and Implementation

Lothar Thiele
Lehrstuhl fur Mikroelektronik
Universität des Saarlandes
D 6600 Saarbrucken

Definition of CA

Discrete in space: CA consist of a discrete lattice of sites

Discrete in time: CA evolve in discrete time steps

Discrete states: Each state takes on a finite set of possible values

Homogeneous: All cells are identical and are arranged in a regular way

Synchronous: All cell values are updated in synchrony

Deterministic: Each cell is updated according to a fixed deterministic rule

Spatially local: The rule depends only on the values of a local neighborhood

Temporally local. The rule depends only on values for a fixed number of preceding steps

Formal Definition

$$\forall I \quad I \in \mathbf{I} \quad a(I,t) = \phi(\{a(I-d,t-1) \quad d \in \mathcal{D}\})$$

I site index

$\mathbf{I}$ index domain of CA

ϕ arbitrary function $\phi \quad S^{|\mathcal{D}|} \rightarrow S$

$\mathcal{D}$ neighborhood, e g $\mathcal{D} = \{J \quad J \in Z^n \wedge \|I\|_\infty \leq r\}$

S set of states, i e $a(I,t) \in S$

Σ set of configurations, i e $\Sigma = S^{|\mathbf{I}|}$

Φ global mapping, i e $\Phi \quad \Sigma \rightarrow \Sigma$

Ω^t set of configurations generated after t iterated applications of ϕ, i e $\Omega^t \in \Sigma$, $\Omega^{t-1} = \phi\Omega^t = \phi^{t+1}\Omega$

Related Models

Partial differential equations: space, time and site values are continuous

Finite difference equations: site values are continuous

Particle models: particles have continuous positions and velocities

Neural network models. connection patterns are arbitrary, site values are continuous, updates are asynchronous

Cellular neural networks: site values are continuous

Iterative arrays: different purpose than CA

Array processors: sites can store extensive information

Applications of CA

(iputation Theory

- self reproduction (J v Neumann 1949, Conway 1970)
- formal language (S Wolfram 1984)
- classification (S Wolfram 1984/1985)

Biological Modeling

- self reproduction (J v Neumann 1949)
- evolution (S Ulam 1948)
- models of memory (M Minsky 1969)

Physical Modeling

- calculating spaces (K Zuse 1940)
- hydrodynamics (J Hardi 1973, U Frisch 1986)
- growth mechanisms (J D Gunton 1983)
- attern recognition (K Preston 1984)
- spin models (M Creutz 1980)
- wave models (H Chen 1988)

J B Salem, S Wolfram Thermodynamics and Hydrodynamics with Cellular Automata In Theory and Applications of Cellular Automata World Scientific, 1987

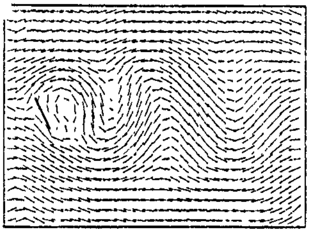

Flow past an obstacle (from Salem and Wolfram)

Physical Modeling

Motivation

- phenomena are often described by (nonlinear) (partial) differential equations, two different approaches to simulation.
  1. difference equation on a macroscopic scale
     - discretization in time and space
  2. microscopic, discretized mode'
     - large number of similar components with local interactions
- functional homogeneity reflects space and time invariance, locality reflects finite speed of information
- cellular automata are simple to program and amenable to parallel processing
- studies of collective phenomena possible (turbulence, chaos, fractality,)

Fluid Dynamics

(Hardy Pazzis Pomeau 1972, Frisch Haslacher Pomeau 1986)

- fluid incompressible, absence of external forces Navier-Stokes Equation (NSE)

$$\frac{\partial V}{\partial t} + V\,\Delta V = -\frac{1}{\rho}\nabla p + v\,\nabla^2 V$$

V velocity

ρ (constant) density

v viscosity

- fictitious microscopic model
  - as simple as possible dynamics (not necessarily following Hamiltonian equations for interacting particles)
  - reproduces NSE on r croscopic level
- particles and their scattering are modeled by reversible CA rules

J B Salem, S Wolfram Thermodynamics and Hydrodynamics with Cellular Automata In Theory and Applications of Cellular Automata World Scientific, 1987

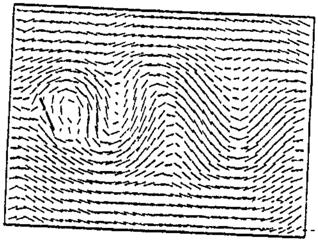

Flow past an obstacle (from Salem and Wolfram)

Lattice Gas

- Particles move on a lattice and satisfy certain symmetry requirements Moving and scattering by reversible rules
- Derivation of macroscopic behavior
  - molecular level motion is reversible
  - kinetic level nonequilibrium statistical mechanics
  - macroscopic level continuum approximation
- Wave equations:
  - for small perturbations from equilibrium: linear elastic properties of lattice gas
  - propagation of a disturbation is governed by wave equation
  - study of wave interference, reflection, diffraction, refraction

T Toffoli, N Margolus Cellular Automata Machines MIT Press 1987

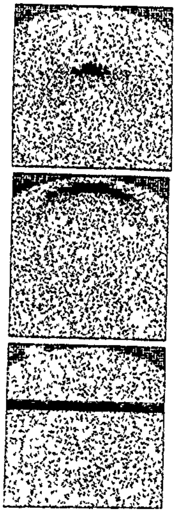

A plane pulse traveling towards a concave mirror (a) is shown right after the reflection (b) and approaching the focal point (c)

T Toffoli N Margolus Cellular Automata Machines MIT Press 1987

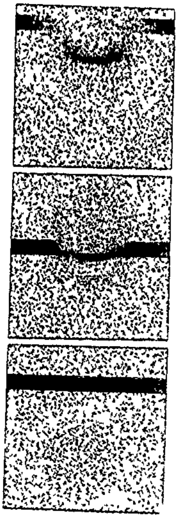

Refraction and reflection patterns produced by a spherical lens

Modeling of Wave Equations

(H Chen 1988)

- Linear wave propagation

$$\frac{\partial^2 u(x,t)}{\partial t^2} = C^2\ \nabla^2 u(x,t)$$

- Invariants

energy $\quad H = \int \left\{ \left(\frac{\partial u}{\partial t}\right)^2 + C^2(\nabla u)^2 \right\} dx$

momentum $\quad P = 2\int \left\{ \left(\frac{\partial u}{\partial t}\right)\nabla u - u\nabla\left(\frac{\partial u}{\partial t}\right) \right\} dx$

- Concept
  - two kinds of photons propagating on a lattice $\sigma = \xi$, $\sigma = -\xi$
  - $N_a^\sigma(x,t)$: number of photons with quantum σ at a particular site x and time t moving with velocity $\hat{c}_a$

$$u(x,t) = \sum_{a,\sigma} \sigma\ N_a^\sigma(x,t)$$

- Hyugens principle any spatial point can be thought of as a new wave source with intensity

$$\tilde{u}(x,t) = \frac{1}{m} u(x,t)$$

- decay rate of source

$$g(x,t+1) = g(x,t) + \sum_{a,\sigma} \sigma\left(N_a^\sigma(x,t) - N_a^\sigma(x + \hat{c}_a, t)\right)$$

$$\tilde{u}(x,t+1) = \tilde{u}(x,t) - g(x,t+1)$$

- continuous linear wave equation is recovered after making an ensemble averaging
- result can be converted to a finite difference equation

H Chen, S Chen, G Doolen, Y C Lee Simple Lattice Gas Models for Waves Complex Systems 2 (1988) 259-267

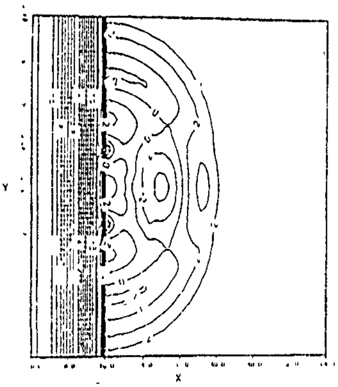

Spatial interference pattern of the wave amplitude in a two-dimensional wave lattice gas double slit experiment at a given instant

Implementation of Cellular Systems

(S Y Kung, P Dewilde, E Deprettere S Merker)

Specification

- Cellular automata

$$(\| I \quad I \in \mathbf{I} \quad a(I,t) = \phi(\{a(I-d, t-1) \quad d \in \mathcal{D}\}))$$

- Cellular Systems

$$\begin{aligned}
(\| I \quad & I \in \mathbf{I} \\
& a_1(I) = \phi_1(\{a_1(I-d) \quad d \in \mathcal{D}_{11}\}, \ldots, \\
& \qquad \{a_V(I-d) \quad d \in \mathcal{D}_{V1}\}) \; \| \\
& \\
& a_V(I) = \phi_1(\{a_1(I-d) \quad d \in \mathcal{D}_{1V}\}, \ldots, \\
& \qquad \{a_V(I-d) \quad d \in \mathcal{D}_{V1}\}) \\
)
\end{aligned}$$

Example

Dependence graph

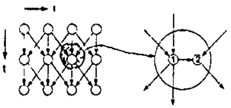

Program

$$
\begin{aligned}
&(\| \, i, t \quad 0 \le i \le 2 \wedge t \ge 0 \\
&\qquad a_1(i,t) = \phi_1(a_2(i-1,t-1), a_1(i,t-1)) \; \| \\
&\qquad a_2(i,t) = \phi_2(a_1(i,t), a_1(i+1,t-1)) \\
&)
\end{aligned}
$$

Reduced dependence graph

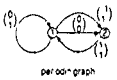

Target Architecture

- dedicated hardware (CAM-6, CAM-8 (Toffoli))
- coarse grain parallel systems (MIMD, Transputer)
- fine grain parallel systems (SIMD, Connection Machine)

Mapping criteria

- communication ⟷ computation
- consideration of pipelined arithmetic units
- consideration of finite resources
- suited for automatic compilation

Applications

- neural networks
- iterative arrays
- cellular automata
- solution of PDE
- systolic arrays

F Bagnoli, A Francescato A Cellular Automata Machine
In Springer Proceedings in Physics 46 (1990) 312–318

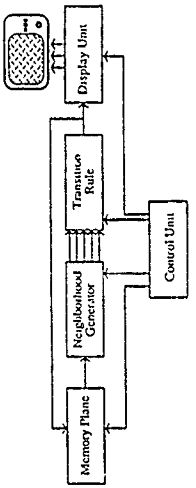

Scheme of the architecture of CAM 6 like machines

F Bagnoli, A Francescato A Cellular Automata Machine
In Springer Proceedings in Physics 46 (1990) 312–318

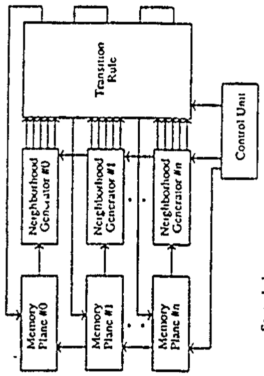

Several planes are processed together

Implementations

nfiguration:

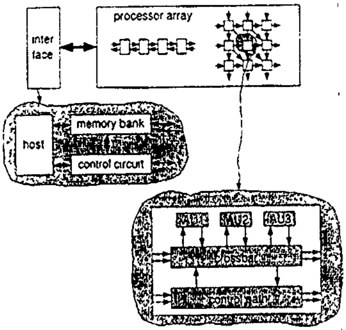

Mapping Problems

Partitioning (limited resources)

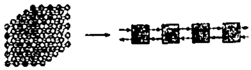

Synchronization (control path)

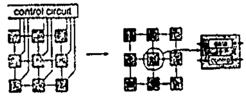

Scheduling (pipelined arithmetic units)

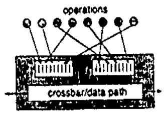

Specification of embedding (software)

Partitioning

Projection.

- reduce dimension of DG by 1
- affine projection of DG

ultiprojection·

- reduce dimension of DG arbitrarily
- loop control or flow control
- match I/O rate and computation rate

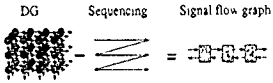

Passive Clustering·

- make inefficient array efficient
- make use of pipelined units

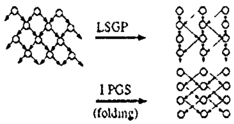

Partitioning

Active Clustering.

- match given number of cells
- match given dimension of array
- combine multiprojection and passive clustering

Local Sequential / Global Parallel (LSGP):

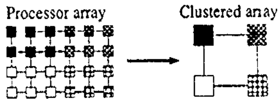

Local Parallel / Global Sequential (LPGS)·

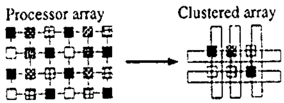

Hierarchical Transformations

- tiling of iteration space using tiling matrix P

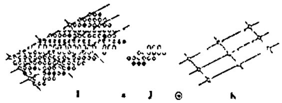

- introduction of terminals

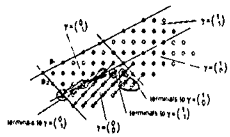

- program transformation

<u>always</u>

$$\langle \| \; I \quad I \in \mathbf{I} \quad x[I] = \mathcal{F}\{x[I-d]\} \rangle$$

<u>always</u>

$$\langle \| \; J, K, \gamma \quad J \in \mathbf{J} \wedge K \in \mathbf{K} \wedge \gamma \in \Gamma$$
$$x[J, K] = \mathcal{F}\{x[J - d - P\gamma \;\; K + P\gamma]\}$$
$$\text{if } J - d - P\gamma \in \mathbf{J} \rangle$$

Hierarchical Representation of Algorithms

- Each node represents a program containing functions defined in lower hierarchical levels

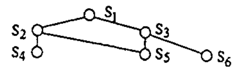

- There are two *basic program schemas*
  a Straight line code (set of assignment statements, nonregular dependence graph)

  b Regular algorithm (regular dependence graph)

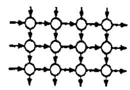

Hierarchical Compilation Strategy

- sequence of provable correct program transformations
- specification of parameterizable basic transformations
- optimization

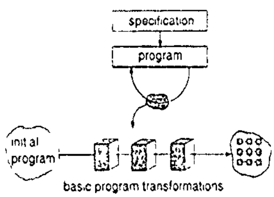

Mathematical Tools

- operations on index sets
- tiling of iteration spaces
- integer linear algebra
- linear and integer linear programming
- geometry of numbers
- combinatorial algorithms on periodic graphs

Compiler For Cellular Systems

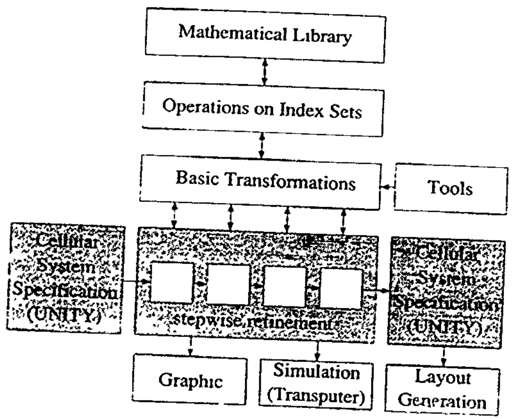

International Workshop of the German IEEE MTT/AP Joint Chapter
and the German IEEE CAS Chapter
on
Discrete Time Domain Modelling of Electromagnetic Fields and Networks

October 24 25 1991

Technical University Munich

Cellular Automata

G Wunsch

TH Dresden

Dynamisches System (T, X, Ξ)

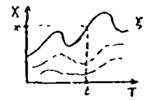

$\} \, \Xi$

T Zeitbereich
X Phasenraum (Alphabet)

$\xi \; T \to X$ Signal, $\xi(t) = x$
$\Xi \subset X^T$ Prozeß, $\xi \in \Xi$, Realisierung
$T \subset R$

Spezielle Grundmengen T, X

- $T = \mathbb{R}, \mathbb{Z}, \mathbb{N}$,
- $X = \mathbb{R}, \mathbb{Z}, A$ (endliche Menge)
  $= X_1 \times X_2$ input-output System
  $= \boxed{X^R, \; R = \mathbb{Z}^2, X = A}$ Zellularer Automat ($T = \mathbb{Z}$)
  $R = \mathbb{R}^3$, $X = \mathbb{R}$ Physik ($T = \mathbb{R}$)

Felder

$\boxed{\Phi \; R \to X}$, Feld $\Phi \in X^R$

$R = \mathbb{Z}^2$
$\Phi(i,j) = a \in A$

Zell Autom $\Phi \; \mathbb{Z}^2 \to A$ Diskretes Feld, Konfiguration
Physik $\Phi \; \mathbb{R}^3 \to \mathbb{R}$ Kontinuierl Feld

Markov-System $(T, Z, \mathcal{Z})$

$\mathcal{Z} \subset Z^T$, $\zeta \; T \to Z$ $\quad \zeta(t) = z$

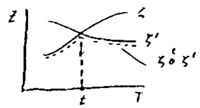

Def Markov-Prozeß

$$\boxed{\zeta, \zeta' \in \mathcal{Z} \;\wedge\; \zeta(t) = \zeta'(t) \Rightarrow \zeta \overset{t}{\circ} \zeta' \in \mathcal{Z}}$$

$\Updownarrow$ zeitinvariant determiniert

$\boxed{(T, Z, F)}$ $\quad F \;\; T \times Z \to Z$, $F(\tau, z) = z'$

Markov-Struktur.

Halbgruppe $(F(\tau, \cdot), \circ)$

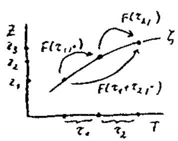

$$\left| \begin{array}{l} F(\tau_2, \cdot) \circ F(\tau_1, \cdot) = F(\tau_1 + \tau_2, \cdot) \\ F(0, \;) = Id \quad \text{(neutr Elem)} \end{array} \right.$$

Felder: $\quad \zeta \;\; T \to Z^R$, $\zeta(t) = \psi \quad (z \to \psi)$,
$(Z \to Z^R)$ $\qquad \psi \;\; R \to Z$ $\quad$ Markov-Feld

Zell Autom $\quad \zeta \;\; \mathbb{Z} \to A^{\mathbb{Z}^2}$, $\zeta(t) = \psi$
(diskr Zeit) $\qquad \psi \;\; \mathbb{Z}^2 \to A \quad (\mathbb{Z} \to A)$

Zustandsdarstellung

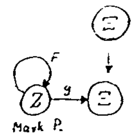

$x = \xi(t)$, $\xi \in \Xi$

$\downarrow$ $(\mathcal{Z} \subset Z^T$, Markov-Prozeß$)$

$$\left| \begin{array}{l} z' = F(\tau, z) \\ x = g(z) \end{array} \right| \quad \text{Überführungsfkt}$$

$z' = \zeta(t + \tau)$, $z = \zeta(t)$
$x = \xi(t)$

$z = [\xi] \in \Xi/_{\sim}$ $\quad$ Zustand (Konstr aus Ξ !)

Sonderfälle

$| z' = F(\tau, z) \,\|$

diskr Zeit $\quad \tau = n \in \mathbb{Z}$ $\qquad\qquad$ $\tau \in \mathbb{R}$ $\quad$ stetige Zeit

$\boxed{z' = f(z)}$ $\; (= F(1, z))$ $\qquad\qquad$ $\boxed{\dot{z} = f(z)}$ $\; \left(= \left.\frac{\partial F(\tau, z)}{\partial \tau}\right|_{\tau = 0} \right)$

$\downarrow$ Feld

$\psi' = f(\psi)$ $\quad \left| \begin{array}{ll} \psi \;\; R \to Z & \text{Raumzustand} \\ \psi(r) = z & \text{Ortszustand} \end{array} \right.$

$\downarrow$ zell Autom

$\psi \;\; \mathbb{Z}^2 \to Z \; (= A)$
$\psi(i, j) = z$

IV

input-output-System

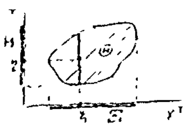

• Ausgangspunkt

Binäre Prozeß $\Theta \subset (Y \times Y)^T$

$\Leftrightarrow \Theta \subset Y^T \times Y^T$

$\Leftrightarrow \boxed{\Theta \subset \Xi \times H}$ $\quad \Xi \subset X^T, H \subset Y^T$

■ $\Theta \subset \Xi \times H$ Bin Proz

$\downarrow$ (Klassenb in Θ)

■ $Z \subset Z_1 \times Z_2$ Bin Markov-P (Zustandsgl)

$\downarrow$ (Sonderfall)

■ input-output-Gl

$$\boxed{\begin{aligned} z' &= F(z, z, \xi) \\ y &= g(z) \end{aligned}}$$

(Moore-Modell)

Wechselwirkung $\Xi \rightleftarrows H$

$\downarrow$

Wechselwirk $Z_1 \rightleftarrows Z_2$

$\downarrow$

Gerichtete Wirk $\Xi \to H$

Felder

$(\Phi) \longrightarrow (\Psi) \longrightarrow (\Gamma)$

$\xi(t) = \Phi \quad F \to X$, Eingabefeld
$z = \zeta(t) = \Psi \quad R \to Z$, Zustandsfeld
$y = \eta(t) = \Gamma \quad R \to Y$, Ausgabefeld

3.2 Feldprozesse

3.2.1 Grundbegriffe (Markov-Felder)

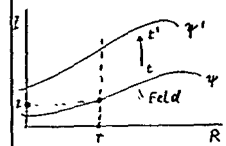

Spezialisierung (!):

allg. $Z \subset Z^T$

a) $Z \to Z_1 \times Z_2 \times \cdots \times Z_n$, Z^n $(n \in \mathbb{N})$
n-äre Prozesse

b) $Z \to Z^R$, R Raumbereich

Feldprozeß:

$\boxed{Z \subset (Z^R)^T}$, T: Zeitbereich

$\zeta : T \to Z^R$: Feldtrajektorie

$\zeta(t) = \Psi : R \to Z$ $\quad$ Feld z Z t

$\Psi(r) = z$ $\quad$ Feldwert in r z Z. t

Alternative Schreibweisen:

$$\Psi(r) = \zeta(t)(r) = \begin{cases} \zeta_r(t) \\ \psi(r, t) \end{cases}$$

Klassifizierung (wie im allg. Fall), außerdem nach R.

T \ R	$\mathbb{Z}^n$	$\mathbb{R}^n$
$\mathbb{Z}$	Z endlich: Automatennetz	
$\mathbb{R}$	$Z = \mathbb{R}$ Neuronennetz	$Z = \mathbb{R}^3$ physikalische Felder

Bem. Analoge Begriffe für beliebige (nichtmarkovsche) Felder

3.2.2 Zeitinvariante u. determinierte Markov-Felder

allgemein: $z' = F(\tau, z)$ $\longrightarrow$ Felder $(z \to \psi)$ $\psi' = F(\tau, \psi)$

$F(\tau,\cdot)$: Globaler Überführungsoperator $(\psi \xrightarrow{\tau} \psi')$

$F(\tau,\cdot)$ Halbgruppe $F(\tau_1+\tau_2,\cdot) = F(\tau_1,\cdot) \circ F(\tau_2,\cdot)$

• Am Ort r:

$$\psi'(r) = F(\tau,\psi)(r) = f(r,\tau,\psi)$$

$f(r,\tau,\cdot)$ Lokaler Überführungsoperator

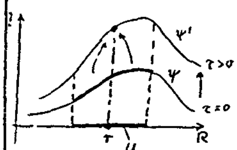

Grundeigenschaften

a) $f(r,\tau_1+\tau_2,\cdot) = f(r,\tau_2,\cdot) \circ F(\tau_1,\cdot)$

b) „Wirkungsausbreitung" erfolgt „mit endlicher „Geschwindigkeit"

$$\boxed{\psi'(r) = \underbrace{f(r,\tau,\psi)}_{\tilde f(r,\tau,\psi|U)} = f(r,\tau,\psi,\lambda)}$$

$\lambda(r,\tau) \subset R$

$U = \lambda(r,\tau)$ Umgebung von r z. Z. τ

λ: Kopplungsfunktion (Raum-Zeit-Struktur)

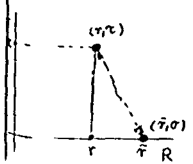

λ beschreibt Kopplung zwischen der Raum-Zeitpunkten (Weltpunkten) (r,τ) und $(\tilde r, 0)$

3.2.3 Koppl gsfunktion λ

$$\lambda : R \times T \to \mathcal{P}(R) \quad , \quad \lambda(r,\tau) = U \subset R$$

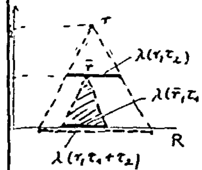

Aus Halbgruppeneigenschaft von $F(\tau,\cdot)$ folgt:

$$\boxed{\lambda(\cdot,\tau_1+\tau_2) = \lambda(\cdot,\tau_1) \circ \lambda(\cdot,\tau_2)}$$

oder

$$\boxed{\lambda(r,\tau_1+\tau_2) = \bigcup_{\tilde r \in \lambda(r,\tau_2)} \lambda(\tilde r,\tau_1)}$$

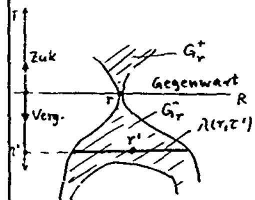

Vergangenheit von r

$$G_r^- = \{(r',\tau') \mid r' \in \lambda(r,\tau')\}, \ \tau'<0$$

Zukunft von r

$$G_r^+ = \{(r',\tau') \mid r' \in \lambda(r,\tau)\}, \ \tau'>0$$

Spezielle Kopplungen: $(R \subset \mathbb{R}^n)$

1) Regulärer Raum: $\lambda(r,\tau_1+\tau_2) \supset \lambda(r,\tau_1) \supset \lambda(r,0) \supset \{r\}$

2) Homogener Raum: $\lambda(r_0+r,\tau) = r_0 + \lambda(r,\tau)$

3) Isotroper Raum: $r' \in \lambda(r,\tau) \Leftrightarrow |r'-r| \leq \varkappa(\tau)$

$\varkappa(\tau) > 0$: Wirkungsradius

3.2.4 Feldzustandsgleichungen

- Feld (allg.) $\Xi \subset (X^R)^T$, $\xi(t) = \Phi \; R \to X$
- Markov-Feld $Z \subset (Z^R)^T$, $\zeta(t) = \psi \; R \to Z$

Globaler Zustand von Ξ z.Z. t

Zustandsgleichungen, global

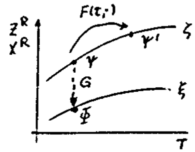

$$\boxed{\begin{aligned}\psi' &= F(\tau,\psi)\\ \Phi &= G(\psi)\end{aligned}} \qquad \psi' = \zeta(\tau),\; \psi = \zeta(0)$$

$F(\tau,\cdot)$ Überführungsoperator, global

G Ergebnisoperator, global

$F(\tau,\;)$ τ-parametrisierte Halbgruppe bez. Komposition $\circ$

Zustandsgleichungen, lokal

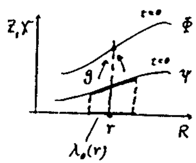

$$\boxed{\begin{aligned}\psi'(r) &= f(r,\tau,\psi,\lambda)\\ \Phi(r) &= g(r,\psi,\lambda_o)\end{aligned}} \qquad \psi(r) = z : \text{lokaler Zustand}$$

λ Zustandskopplung

$\lambda(r,\tau) = U \subset R$

λ_o Ausgabekopplung

$\lambda_o(r) = U_o \subset R$

$g(r,\psi,\lambda_o) \Leftrightarrow g(r,\psi|\lambda_o(r))$

$f(r,\tau,\cdot,\lambda)$: Überführungsoperator, lokal ; $f(\cdot,\tau,\cdot,\lambda) = F(\tau,\cdot,\lambda)$

$g(r,\cdot,\lambda_o)$: Ergebnisoperator, lokal

$f(r,\cdot,\cdot,\lambda)$: Zellfunktion ($R = \mathbb{Z}^n$)

Klassifizierung nach $\{T, R, Z, X$

3.3 Automatennetz (zellularer Automat)

3.3.1 Grundgleichungen

Vorauss.: $\boxed{T = \mathbb{Z},\; R = \mathbb{Z}^2,\; Z \text{ endlich}}$, regularer Raum

Zustandsgleichungen (Vereinfachungen):

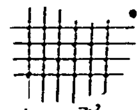

Array $\mathbb{Z}^2$

- global: $\psi' = F(n,\psi)$

$$= [\underbrace{F(1,\cdot)}_{F(\cdot)} \circ F(1,\cdot) \circ \cdots \circ F(1,\cdot)]\,\psi$$

$$= F^n(\cdot)\,\psi = F^n(\psi) \qquad (F^1 = F)$$

$\boxed{\psi' = F(\psi)}$ $(n=1)$

- Lokal: $\psi'(r) = [\underbrace{f(r,1,\cdot,\lambda)}_{f(r,\cdot,\lambda)} \circ \overbrace{\underbrace{f(\cdot,1,\cdot,\lambda)}_{F(1,\cdot,\lambda)}}^{f(\cdot,\cdot,\lambda)} \circ \cdots\,]\,\psi$

$\boxed{\psi'(r) = f(r,\psi,\lambda)}$ $(n=1)$

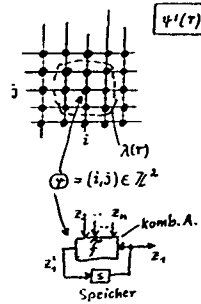

Zellautomat in r

Spezielle Kopplungsfkt.:

$\boxed{\lambda = \mu \circ \lambda^*}$

- $\lambda^* : r \mapsto (r_1, \ldots, r_n) \in \mathbb{R}^n$, $n = \text{card}\,\lambda(r)$

$(\lambda_1^*(r), \ldots, \lambda_n^*(r)) = \lambda^*(r)$

- $(\mu \circ \lambda^*)(r) = \mu(\lambda^*(r))$

$= \mu(r_1, \ldots, r_n) = \{r_1, \ldots, r_n\}$

$$\Rightarrow \left\| \begin{aligned} \psi'(r) &= \bar f(r, \psi|\lambda(r))\\ \underbrace{\quad}_{z_1'} &= \tilde f(r, \underbrace{\psi(r_1)}_{z_1}, \ldots, \underbrace{\psi(r_n)}_{z_n}) \end{aligned} \right. \qquad (r_1 = r$$

$\| \; f(r,\cdot,\lambda) = \tilde f(r,\cdots)$ $\quad (\tilde f = \tilde f_{\lambda^*})$

Zellfunktion des Automaten

3 3 2 Sonderfall

~ Hällt!

Vorauss 1 homogener Raum $\lambda^*(r) = r + \lambda^*(0)$

$\lambda^*(0) = \lambda^0$ Kopplungsmuster

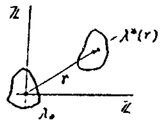

2 Identische Zellfunktionen

$$f(r, \psi, \lambda^*) = f(\sigma, \sigma^r \psi, \lambda^*)$$

$$\Rightarrow \quad \psi'(r) = \tilde{f}(\sigma, (\psi^n \circ \lambda^0)(r)) = f_0(\psi^n(\lambda^0))(r)$$

$\Rightarrow$ Faktorisierung von $F(\psi)$: Zusammenhang zwischen globaler u. lokaler Beschreibung ($F \leftrightarrow f_0$)

lokal. $\psi'(r) = (f_0 \circ \psi^n \circ \lambda^0)(r)$

global: $\psi' = \boxed{F(\psi) = f_0 \circ \psi^n \circ \lambda^0}$

$$\begin{tikzcd} R \arrow[r, "\lambda^0"] \arrow[d, "F(\psi)"'] & R^n \arrow[d, "\psi^n"] \\ Z & Z^n \arrow[l, "f_0"'] \end{tikzcd}$$

- $\lambda^0(r) = \underbrace{(\overbrace{r+\lambda_1^*(0)}^{\bar{r}_1}, \dots, \overbrace{r+\lambda_n^*(0)}^{\bar{r}_n})}_{\lambda^*(0) = \lambda^0}$
  $= (\bar{r}_1, \dots, \bar{r}_n) \in R^n$
- $\psi^n(\bar{r}_1, \dots, \bar{r}_n) = (\underbrace{\psi(\bar{r}_1)}_{z_1}, \quad \underbrace{\psi(\bar{r}_n)}_{z_n}) \in Z^n$
- $f_0(z_1, \dots, z_n) = z_1' \in Z$

3 4 Analognetze (input-output)

~ H & U.

3 4 1 Grundgleichungen

Vorauss.: $\boxed{T = \mathbb{R},\ R = \mathbb{Z}^2,\ Z = \mathbb{R}}$, regulärer Raum

Gesteuerter Prozeß:

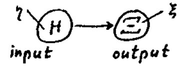

$\eta \quad T \to Y^R, \ \eta(t): R \to Y$

Beschreibung (Zustandsdarstellung):

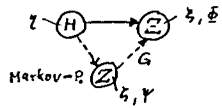

$\boxed{\begin{aligned} \psi' &= F(\tau, \psi, \eta) \\ \Phi &= G(\psi) \end{aligned}}$ $\eta | T^\tau$ global

$\downarrow$

$\boxed{\begin{aligned} \psi'(r) &= f(r, \tau, \psi, \eta, \lambda, \bar{\lambda}) \\ \Phi(r) &= g(r, \psi, \lambda_0) \end{aligned}}$ lokal

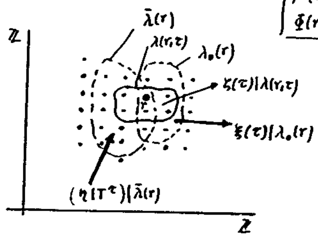

$\bar{\lambda}$: Eingabekopplun.
$\bar{\lambda}(r) \subset R$

- $\zeta(t) = \psi: R \to Z$ Zustand
- $\xi(t) = \Phi: R \to Y$ Ausgabe

$\left. \begin{array}{l} \eta: T \to Y^R \\ \eta(t): R \to Y \end{array} \right\}$ Eingabe

3 4 2 Glatte Systeme

mllöll

Vorauss:

1 $\frac{d}{d\tau} \underbrace{\psi'(r)}_{\zeta_r(\tau)} \Big|_{\tau=0}$ exist.

2 $\lambda(r,\tau) = r + \lambda(0,\tau)$
$\bar\lambda(r) = r + \bar\lambda(0)$
$\lambda_0(r) = r + \lambda_0(0)$

3 $\lambda(r,0) \supset \{r\}$ (echt)

$\Rightarrow \psi'(r) = \zeta_r(\tau) = f(r,\tau,\zeta.(0),\eta,\lambda,\bar\lambda)$

$\dot\zeta_r(0) = h(r,\zeta.(0),\zeta.(0),\lambda,\bar\lambda)$

oder $(0 \to t)$

$$\boxed{\dot\zeta_r(t) = h(r,\zeta.(t),\zeta.(t))} \qquad (h = h_{\lambda,\bar\lambda})$$

$\zeta.(t)|\lambda(r,0) \quad \zeta.(t)|\bar\lambda(r)$

ausführlich:

$$\dot\zeta_r(t) = h(r,\zeta_{r+r_1}(t),\ldots\zeta_{r+r_n}(t),\zeta_{r+\bar r_1}(t),\ldots,\zeta_{r+\bar r_s}(t))$$
$$r_i \in \lambda(0,0) \quad , \quad \bar r_i \in \bar\lambda(0)$$

$$\underbrace{\eta_r(t)}_{\Phi(r)} = g(r,\zeta_{r+s_1}(t),\ldots,\zeta_{r+s_m}(t))$$
$$s_i \in \lambda_0(0)$$

Neuronennetz von Chua : $h(r,\ldots)$ Linear

$$\dot\zeta_r(t) = \sum_{k_i \in \lambda(r,0)} A_{s_i}(r)\cdot\zeta_{s_i}(t) + \sum_{k_j \in \bar\lambda(r)} B_{s_i}(r)\,\zeta_{s_i}(t)$$

Bei Chua: $\lambda(r,0) = \bar\lambda(r) = \lambda_0(r)$

3 5 Felder im Kontinuum ($R = \mathbb{R}^3$)

3 5.1 Lineare Felder

Vorauss $\boxed{T = \mathbb{R},\ R = \mathbb{R}^3,\ Z = \mathbb{R}}$

$f(r,\tau,\cdot,\lambda)$ Linear

$\Rightarrow \Psi'(r) = f(r,\tau,\Psi,\lambda)$

$\Psi(r) = \int_{\bar r \in \lambda(r,\tau)} \delta(r-\bar r)\,\Psi(\bar r)\,d\bar r$

$= \int_{\bar r \in \lambda(r,\tau)} f(r,\tau,\delta(\cdot - \bar r))\cdot\Psi(\bar r)\,d\bar r$

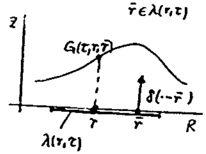

Def: $\boxed{f(r,\tau,\delta(\cdot-\bar r)) = G(\tau,r,\bar r)}$

Greensche Funktion
(Impulsantwort)

Lokaler Überführungsoperator

$$\boxed{f(r,\tau,\Psi,\lambda) = \int_{\bar r \in \lambda(r,\tau)} G(\tau,r,\bar r)\cdot\Psi(\bar r)\,d\bar r}$$

Einschränkung:

1) f homogen: $f(r,\tau,\Psi,\lambda) = f(0,\tau,\sigma^r(\Psi),\lambda)$
$(\sigma^r(\Psi)(r_0) = \Psi(r_0 + r))$

$\Rightarrow G(\tau,r,\bar r) = G(\tau,0,\bar r - r) = G(\tau,\bar r - r)$

2) λ homogen: $\lambda(r,\tau) = r + \lambda(0,\tau)$

$\Rightarrow \bar r - r \in \lambda(0,\tau)$

3

3) R ist isotrop $\quad (\bar{r}-r)\in\lambda(0,\tau) \Leftrightarrow |\bar{r}-r|\leq\psi(\tau)$

$\psi(\tau)$: Wirkungsradius

$$\Rightarrow \boxed{f(r,\tau,\psi,\lambda) = \int\limits_{|\bar{r}-r|\leq\psi(\tau)} G(\tau,|\bar{r}-r|)\,\psi(\bar{r})\,d\bar{r}}$$

3.5.2 Elektromagnetische Felder (homög. u. isotrope Medien)

Wirkungsradius: $\psi(\tau) = v\tau \quad (\Rightarrow R$ regulärer Raum$)$

$|\bar{r}-r|\leq v\tau \quad \Rightarrow \boxed{|\bar{r}-r|^2 - v^2\tau^2 = d^2 \leq 0} \quad v$ Ausbreitungsgeschwindigkeit

$$\Rightarrow \underbrace{\psi'(r)}_{\zeta(r,\tau)} = f(r,\tau,\psi,\lambda) = \int\limits_{|s|\leq v\tau} G(\tau,|s|)\,\psi(r+s)\,ds$$

Glatte Felder:

$$\psi(r+s) = \psi(r) + \psi_{x_i}(r)s_i + \left[\psi_{x_i x_j}(r) + \varepsilon(s)\right]s_i s_j$$

$(x_1,x_2,x_3) \quad (s_1,s_2,s_3)$

$$\Rightarrow \boxed{\frac{\partial\zeta}{\partial t} = a_0\zeta + a_2\Delta\zeta}\ , \quad \Delta = \frac{\partial^2}{\partial x_1^2}+\frac{\partial^2}{\partial x_2^2}+\frac{\partial^2}{\partial x_3^2}\ , \quad \zeta(r,t)=\psi$$

Diffusionsgleichung

mit: $a_0 = \lim\limits_{\tau\to 0}\left[\int\limits_{|s|\leq v\tau} G(\tau,|s|)\,ds - 1\right] \quad \left| \begin{array}{l} ds = ds_1 ds_2 ds_3 \\ s^2 = s_1^2+s_2^2+s_3^2 \end{array}\right.$

$a_2 = \lim\limits_{\tau\to 0}\frac{1}{\tau}\left[\int\limits_{|s|\leq v\tau} G(\tau,|s|)\,s_i^2\,ds\right]$ (unabh. von i)

Vorauss $\quad \int\limits_{|s|\leq v\tau} |G(\tau,|s|)|\,ds < \frac{K}{\tau}$

Verallg. Binäre Felder

$Z \subset Z_1 \times Z_2 \qquad Z_1 \subset Z_1^T$
$\qquad\qquad\qquad\quad Z_2 \subset Z_2^T$

$$\Rightarrow \begin{pmatrix}\dot\zeta_1\\ \dot\zeta_2\end{pmatrix} = \begin{pmatrix} c_{11} & c_{12}\\ c_{21} & c_{22}\end{pmatrix}\begin{pmatrix}\zeta_1\\ \zeta_2\end{pmatrix} + \begin{pmatrix} d_{11} & d_{12}\\ d_{21} & d_{22}\end{pmatrix}\begin{pmatrix}\Delta\zeta_1\\ \Delta\zeta_2\end{pmatrix}$$

$H(r,t) = \Phi(r) = g(r, \zeta_1(\cdot,t), \zeta_2(\cdot,t), \lambda_0)$

Spezialisierung: $\left| \begin{array}{l} \text{z.B. } c_{11}=c_{12}=c_{22}=0 \\ \qquad d_{11}=d_{21}=d_{22}=0 \\ \lambda_0(r) = r \end{array}\right.$

$g: \quad H = H(r,t) = a_1\zeta_1(r,t) + a_2\zeta_2(r,t)$

$$\Rightarrow \boxed{\frac{\partial^2 H}{\partial t^2} + k\,\Delta H = 0}$$ Wellengleichung (skalar) $\quad (k = d_{12}c_{21})$

$$\left.\boxed{\begin{array}{l} \dot\zeta = \underline{C}\,\zeta + \underline{D}\,\Delta\zeta \\ \text{(Vektorgleich.)} \\ H = a_1\zeta_1 + a_2\zeta_2 \end{array}}\right\}$$ Zustandsgleich. der Wellengleich $\quad \left(\zeta = \begin{pmatrix}\zeta_1\\ \zeta_2\end{pmatrix}\right.$

(1) 4.3 **Diskrete Felder** (stetige Zeit)

Lokaler Überführungsoperator (hom. Struktur)

$c'(r) \longrightarrow \dot{c}_t(r)$,
c_{t+1}

$\underline{\dot{c}_t(r) = f(c_t^n(\lambda(r))}$

Linearer Überf.-Operator

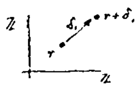

$$\dot{c}_t(r) = \sum_{i=1}^{n} b_i\,(c_t \circ \lambda_i)(r)$$
$$= \sum_{i=1}^{n} b_i\, c_t(r+\delta_i) \qquad \lambda_i(r) = r+\delta_i$$

Mathem. Analyse: | z-Transformation
| Quotientenkörper
| Laplace-Transformation

Beispiel:

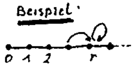

$$\dot{c}_t(r) = b_{-1}c_t(r-1) + b_0 c_t(r),$$

$$\left|\begin{array}{l} c_t^* = \dfrac{c_0^*(z)}{p-g(z)} \qquad g(z) = b_0 + b_{-1}z \\ c_t^*(t) = \underbrace{e^{+g(z)t}}_{h_t^*(z)}\, c_0^*(z) \end{array}\right.$$

c) **Nachbarschafts- u. Zellfunktion**

Zustand $c(r)$ in Zelle r nicht von allen $c(r_i)$ abhängig:

$$c'(r) = F(c)(r) = f(r, c)$$
$$= f(\underline{r-1, r, r+1}, c(r-1), c(r), c(r+1))$$
$$= \underline{f(\underline{\lambda(r)}, (c^n \circ \lambda)(r))} \qquad (c^n = c \times c \times \ldots \times c)$$

Allgemeiner:

| $\lambda: R \to R^n \quad \lambda(r) = (r_1, r_2, \ldots, r_n), \; r_1 = r$
| **Nachbarsch.-F't** λ
| **f: Zellfunktion**, **lokaler Überführungsoperator**

Zellautomat (Ort r)

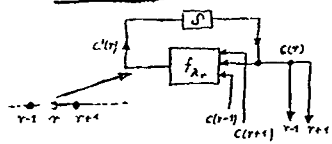

$$f_{\lambda_r} = f(\lambda(r), \cdot, \cdot)$$

3 (11)

Beispiel:

$$\left| \begin{array}{l} -L \frac{\partial i}{\partial t} = iR + \frac{\partial u}{\partial x} \\ -C \frac{\partial u}{\partial t} = uG + \frac{\partial i}{\partial x} \end{array} \right|$$

x: Ort
t: Zeit

u: Spannung
i: Strom

$$\underline{z(x,t+1) = \boxed{A\, z(x,t)}}$$

$$A = \begin{pmatrix} 1-\frac{R}{L} & \frac{1-T_{-1}}{L} \\ \frac{1-T_{-1}}{C} & 1-\frac{G}{C} \end{pmatrix} \qquad z(x,t) = \begin{pmatrix} i(x,t) \\ u(x,t) \end{pmatrix}$$

Realisierung

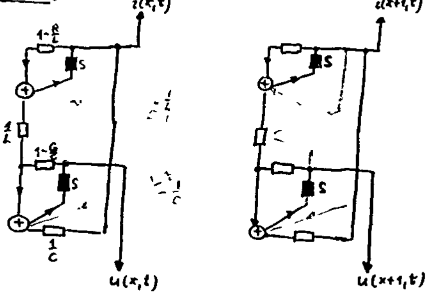

(B)

Lotka-Volterra-System (Ökologie)

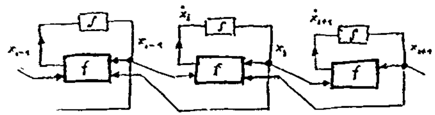

$$\frac{d}{dt} \ln x_i = e_i + \sum_j g_{ij} x_j$$
$$= f(x_{i-1}, x_i, x_{i+1}, \ldots)$$

(10)

IV

$$\frac{\partial z(u,v,t)}{\partial t} = \sum_{(m,n)\in B} C_{m,n} \frac{\partial^{m+n}}{\partial u^m \, \partial v^n} z(u,v,t)$$

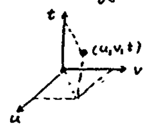

Näherung:

$$\Delta_t z(u,v,t) = \sum_{(m,n)\in B} C_{m,n} \Delta_u^m \Delta_v^n \; z(u,v,t)$$

$z(u,v,t+1) - z(u,v,t)$:

$$\boxed{z(u,v,t+1) = \sum_{(i,j)\in I} a_{i,j}\, z(u+i, v+j, t)}$$

$a_{i,j} = \psi(C_{m,n})$

$$\sum_{(i,j)\in I} a_{i,j} T_{i,j}\, z(u,v,t)$$

$B \longmapsto I$

Beispiel:

$$\frac{\partial z}{\partial t} = c_2 \frac{\partial^2 z}{\partial u^2} + c_1 \frac{\partial^2 z}{\partial v^2} + c_0 z$$

$B = \{(2,0), (0,2), (0,0)\}$

$I = \{(-1,0), (0,0), (+1,0), (0,+1), (0,-1)\}$

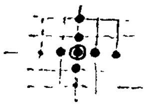

$\bullet \hat{=} I$
$\bullet \hat{=} B$

$a_{-1,0} = a_{1,0} = c_2$
$a_{0,1} = a_{0,-1} = c_1$
$a_{00} = c_0 - 2(c_1 + c_2) + 1$

(13)

Eindimensionale Struktur (Linear, ...)

$$z(u,t+1) = A_1 z(u-1,t) + A_0 z(u,t) + A_1 z(u+1,t) + B_0 x(u,t)$$

$$y(u,t) = C_0 z(u,t) + D_0 x(u,t)$$

λ: xxx
μ, λ', μ': x

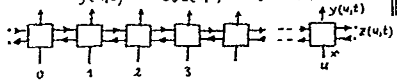

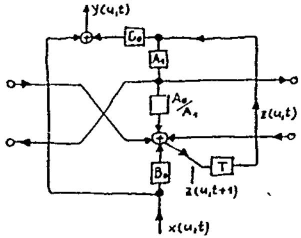

Lösung

$$z(u,t) = \sum_{n_1+n_2+n_3=t} \frac{(t-1)!}{n_1!\,n_2!\,n_3!} \times$$

$$\times A_1^{n_1+n_3} A_0^{n_2} x(u-n_1+n_3, 0)$$

Anfangsbed:

$$x(u,t) = \begin{cases} 0 & (t>0) \\ x_0 & (u=k, t=0) \end{cases}$$

$z(u,t) = 0 \quad (t=0)$

ANALYSIS OF NONLINEAR MICROWAVE CIRCUITS VIA THE TIME-DOMAIN VOLTAGE-UPDATE METHOD

H.D. Foltz, *J.H. Davis, and T. Itoh†

Although direct transient time-domain solutions of circuit equations (for example, SPICE-type programs) are sometimes employed to analyze microwave systems containing nonlinear devices, steady-state methods (for example, harmonic balance techniques) are preferable in cases involving high-Q resonant circuits and other narrow-band structures, for which steady-state methods have a significant advantage in computation time.

Many steady-state nonlinear techniques, such as (1) the common minimizing-or-optimizing-based piecewise harmonic-balance method and (2) the relaxation-based voltage-update method, operate primarily in the frequency domain. Unfortunately, most nonlinear solid-state devices are most easily treated in the time-domain. Analagous steady-state techniques, based on discrete time samples, can be formulated: (1) the waveform-balance technique, which is related to the piecewise harmonic-balance method, and (2) the time-domain voltage-update technique, which is relaxation-based. In this paper, the latter technique will be examined in more detail and compared to more conventional approaches.

In the time-domain version of the voltage-update, time samples representing the steady-state voltage waveform are applied to the nonlinear device(s). The resulting current samples are applied to the linear portions of the system, leading to a new set of voltage samples. Relaxation parameters are then applied to determine the starting samples for the next iteration, and the process is repeated until convergence is obtained.

Voltage-update techniques have a marked advantage over most other approaches in simplicity and speed per iteration, when applied to problems in which the frequency is known, such as amplifiers, frequency multipliers, and mixers They can also be applied, with some modifications, to variable-frequency problems such as oscillators.

Strategies for extending the range and speed of convergence for the relaxation procedure will be discussed, along with the relationship between frequency-domain and time-domain relaxation parameters. The results of several representative applications involving negative resistance devices and SIS junctions will be presented.

* The University of Texas, Electrical Engineering Research Laboratory, Austin, TX 78712

† University of California, Los Angeles, Department of Electrical Engineering, Los Angeles, CA 90024

Time Domain Voltage Update Method

H Foltz
The University of Texas at Austin

and

T Itoh
UCLA

for

International Workshop on

Discrete Time Domain Modeling
of
Electromagnetic Fields and Networks

October 24 25, 1991
Munich

OUTLINE

Time Domain Voltage Update Method.

- Relation to other nonlinear circuit methods
- Description of method
- Differences between frequency and time domain relaxation
- Sample applications

NF16

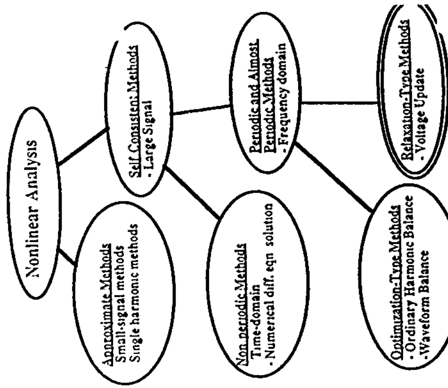

SELF-CONSISTENT LARGE-SIGNAL NONLINEAR CIRCUIT ANALYSIS

TRANSIENT SOLUTIONS	STEADY-STATE SOLUTIONS
Voltages not necessarily periodic	Voltages periodic
Usually time domain	Usually frequency domain or fixed length time domain
Example: SPICE	Example: EEsof LIBRA

NF1

STEADY-STATE METHODS FOR NONLINEAR CIRCUITS

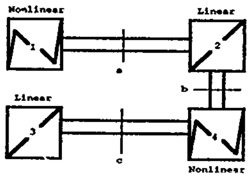

Divide circuit into a number of linear and nonlinear parts. Find voltages at each port (a,b,c) such that currents satisfy Kirchoff

RF2

CLASSIFICATION OF STEADY-STATE METHODS

METHOD OF SOLUTION

QUANTITIES TO BE MATCHED AT EACH PORT	Newton-type Root Finding, Continuation	Optimization Algorithms	Relaxation Algorithms
Current Fourier Coefficients	Harmonic Balance	Harmonic Balance	Voltage Update
Current Time Samples	Waveform Balance	Waveform Balance	Voltage Update

RF3

THE VOLTAGE UPDATE METHOD

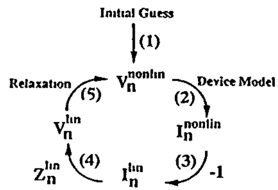

Iteration loop is repeated until convergence is obtained

RF4

THE VOLTAGE UPDATE METHOD

Relaxation is of the form

$$\text{new } V_n^{nonlin} = \text{old } V_n^{nonlin}(1-p_n) + p_n V_n^{lin}$$

where the V_n can be either the Fourier coefficients or the time samples

$\boxed{\#\text{ of variables} = \#\text{ of ports} \times (1 + 2 \times \#\text{ of harmonics})}$

RF5

VOLTAGE UPDATE VS. HARMONIC BALANCE

ADVANTAGES OF VOLTAGE UPDATE:
Very simple to program
Insensitive to numerical error
> Only one nonlinear circuit evaluation per iteration, vs. "N" evaluations for HB

ADVANTAGES OF HARMONIC BALANCE:
Generally fewer iterations are required (but each iteration is much longer)
Convergence is said to be more reliable

COMPARISON OF VOLTAGE UPDATE METHODS WITH OTHER METHODS

	Optimization or Continuation	Standard Voltage-Update	Voltage-Frequency Update with improved splits
Program	Complex	Very simple	Simple
Sensitivity to numerical errors	Varies, can be poor	Relatively Insensitive	Relatively Insensitive
Applicable to free-running oscillators	Yes	No	Yes
Iterations required for convergence	Few	Variable, can be high	Variable, can be high
Time per iteration	Lengthy	Very short	Short
Nonlinear evaluations per iteration	N	1	1
Reliability of convergence	Very good	Poor, some problems not solvable	Adequate: trial and error may be needed

VOLTAGE UPDATE VS. HARMONIC BALANCE

Steady State Analysis

Relaxation-type Voltage Update	Optimization-type Harmonic Balance
<u>Best for specific application programs:</u> Fast program turnaround; High efficiency	<u>Best for general purpose, turnkey programs:</u> Large amount of programming; High reliability

CONVERGENCE OF VOLTAGE UPDATE METHOD

Traditional problem with relaxation: poor convergence in high-Z or high-Q circuits

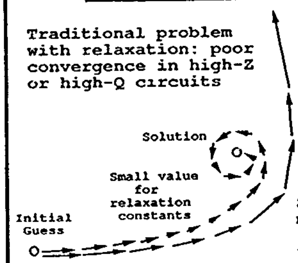

Some problems may not converge for any value unless algorithm is changed

CONVERGENCE IMPROVEMENT

(1) GET ROUGH ESTIMATE OF LARGE SIGNAL IMPEDANCE LOOKING INTO NONLINEAR DEVICE PORT

(2) FIND IMPEDANCE LOOKING INTO CORRESPONDING LINEAR CIRCUIT PORT

(3) CHOOSE RESISTORS TO MAKE MAGNITUDE OF DEVICE IMPEDANCE LARGER (ABOUT TWICE) THAN THE LINEAR CIRCUIT IMPEDANCE

THIS PROCEDURE ALLOWS CONVERGENCE WITH REASONABLE, POSITIVE VALUES FOR THE RELAXATION CONSTANTS

- MAKES DIVERGENT PROBLEMS CONVERGENT
- MAKES SLOWLY CONVERGENT PROBLEMS CONVERGE FASTER

TYPICAL RESULTS FOR SINGLE DEVICE OSCILLATOR WITH R-L C RESONANT CIRCUIT, $Z_{lin} = 10 \times Z_{nonlin}$

- NO RESISTORS: DIVERGES FOR ANY VALUE OF RELAXATION CONSTANTS
RESISTORS CONVERGENCE TO 1% IN 30 TO 40 ITERATIONS

SOLVING CONVERGENCE PROBLEMS

Simple technique to change splitting add pairs of cancelling resistances (R,-R) or impedances (Z,-Z)

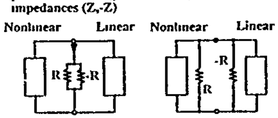

Parallel impedances are shown. Series pairs of cancelling impedances can also be used

No net effect on correct solution

Always possible to select resistances to ensure convergence

NF9

TIME DOM. VS. FREQ. DOM. RELAXATION

When all relaxation constants are the same, methods are equivalent:

Time Domain Relaxation (Diagonal Matrix) ⟷ Equivalent ⟷ Frequency Domain Relaxation (Diagonal Matrix)

When they are not all the same:

Time Domain → Freq Domain

Freq Domain (Diagonal Matrix) → Time Domain (Full Matrix) (Inefficient)

Exact equivalence can not be done efficiently

NF10

TIME DOM. VS. FREQ. DOM. RELAXATION

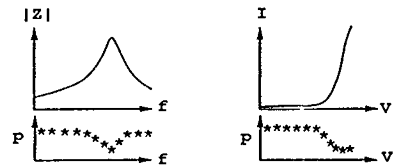

Frequency Domain:
Choose smaller relaxation constants at frequencies falling on high impedance points of LINEAR circuit

Time Domain:
Choose smaller relaxation constants for points that fall on high dynamic conductance points of NONLINEAR I-V curve

NF11

APPLICATIONS

Some applications which have been successfully handled using improved voltage-update algorithms:

- Schottky mixers and frequency multipliers
- SIS (Superconductor-Insulator-Superconductor) circuits
- Multiple device power combining circuits, including free-running and injection locked oscillators

MF12

TIME DOMAIN UPDATING

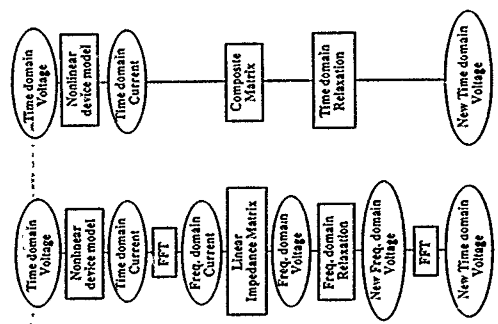

TIME DOMAIN UPDATING

MOST USEFUL WHEN FREQUENCY IS KNOWN

AMPLIFIERS
MIXERS
LIMITERS
INJECTION-LOCKED OSCILLATORS

COMPOSITE MATRIX IS FORMED ONLY ONCE AT BEGINNING OF PROBLEM.

COMPUTATION TIME FOR LINEAR PART OF CIRCUIT IS GREATLY REDUCED. NONLINEAR PART BECOMES MAIN PART OF ITERATION.

ONLY ONE EVALUATION OF THE NONLINEAR CIRCUIT IS REQUIRED PER ITERATION

TIME-DOMAIN LINEAR CIRCUIT DESCRIPTION

Time domain method can be applied to circuits described in frequency domain by forming composite matrix:

$$A = D^{-1} Z D$$

where D is DFT matrix and Z is impedance matrix. 'A' directly relates time voltage to time current.

Only has to be formed once for a given problem if fundamental frequency is fixed

MF13

PERIODIC POWER COMBINER

- Devices nominally half-wavelength apart
- Load impedance = device impedance / N
- Devices resonated with inductive stubs to be resistive at oscillation frequency

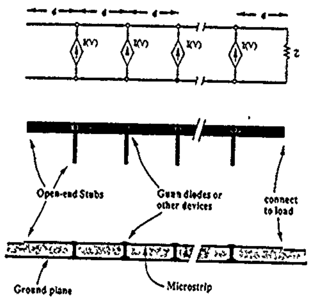

INJECTION-LOCKED POWER COMBINER

- MODEL INJECTION WITH CURRENT SOURCE AT END OF ARRAY

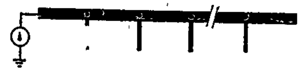

- NO NEED FOR FREQUENCY UPDATE FREQUENCY IS KNOWN
- USE TIME DOMAIN UPDATING
- USE PAIRS OF CANCELLING RESISTORS AT EACH DEVICE PORT TO IMPROVE CONVERGENCE

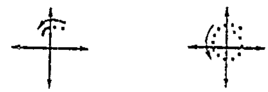

23

LOCKING BANDWIDTH VERSUS INJECTION LEVEL

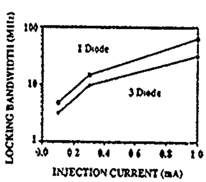

Multiple diode combiners require higher injection currents to obtain a given locking bandwidth

VARIATION OF OSCILLATION FREQUENCY WITH RESONANCE FREQUENCY OF INDIVIDUAL DEVICES

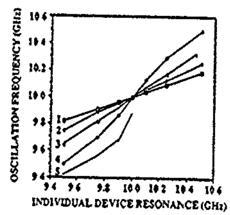

As the number of devices in the combiner increases, the oscillation frequency depends more on the devices and less on the periodicity

26

VARIATION OF TOTAL OUTPUT POWER WITH RESONANCE FREQUENCY OF INDIVIDUAL DEVICES

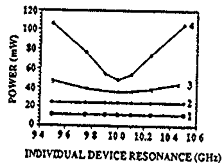

VARIATION OF POWER DISTRIBUTION AMONG DEVICES

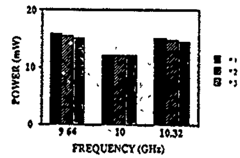

As the frequency is changed away from the center frequency where the structure is half-wave periodic, the distribution of power becomes unequal

TIME-DOMAIN LINEAR CIRCUIT DESCRIPTION

Time domain method blends naturally with linear circuits described directly in time domain:

EXAMPLE: Linear structure analyzed by a periodic FDTD technique.

Can combine relaxation solution to FDTD equations with relaxation solution to nonlinear-liner balance in one iteration loop

27

EFFECT OF DEVICE NON-UNIFORMITY:

FREQUENCY AND POWER OUTPUT VERSUS DEVICE AREA

(THREE DIODE COMBINER)

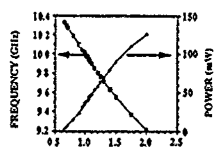

AREA OF PERTURBED DEVICE RELATIVE TO OTHER DEVICES IN COMBINER

CONCLUSIONS

Time Domain Voltage Update Method:

- Useful alternative to other steady-state methods

- Has been applied to wide variety of circuits

- Should combine easily with electromagnetic structures analyzed by time-domain techniques

HF15

MULTIPORT APPROACH FOR THE ANALYSIS OF MICROWAVE NON-LINEAR NETWORKS

M. I. Sobhy†, E. A. Hosny† and M. A. Nassef*

† Electronic Eng. Labs., University of Kent, Canterbury, CT2 7NT, U.K.

* Electrical Engineering Department, Military Technical College, Cairo, Egypt.

Abstract

The state and output equations of the overall networks are derived from the state and output equations of individual multiports and knowledge of the interconnections between them. A generalised lumped-distributed multiport is described by its associated state, output and non-linear equations in the time domain. Any network can be considered as composed of a set of multiports and independent sources. These equations have been incorporated into computer-aided procedure for the analysis of L/D networks. The procedure can be used for the simulation of any non-linear microwave circuit and offers the facility of developing a multiport equivalent circuit for any linear or non-linear device or sub-circuit. Several examples are successfully analysed using the developed general program.

OBJECTIVES

TO DERIVE A METHOD FOR ANALYSING NON-LINEAR MULTIPORTS.

- **DERIVE A METHOD OF MODELLING NON-LINEAR MULTIPORTS**
- **DEVELOP A LIBRARY OF SUCH MODELS**
- **COMBINE NON-LINEAR MULTI-PORTS FOR ANY INTER-CONNECTION.**
- **SOLVE THE EQUATIONS DESCRIBING THE WHOLE SYSTEM.**

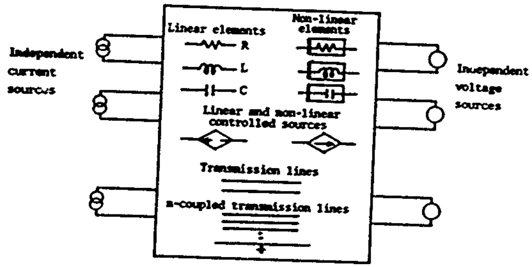

General lumped-distributed non-linear multiport

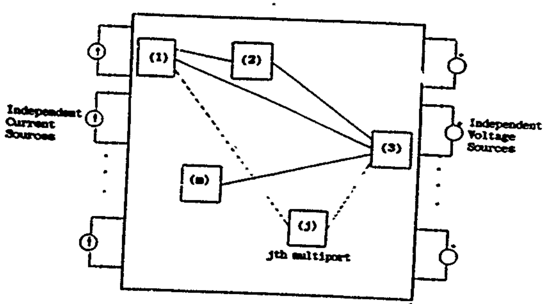

Overall network composed of m multiports, $1 \le j \le m$

LUMPED ELEMENTS

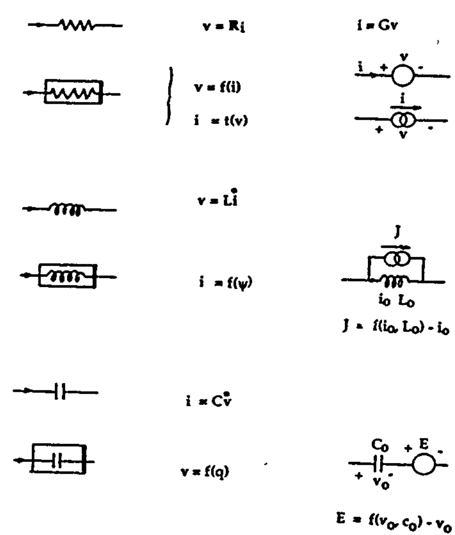

DISTRIBUTED ELEMENTS

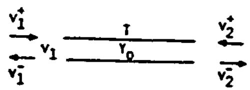

$v_1 = v_2^-(t-T) + v_1^-(t)$

$i_1 = Y_0[v_2^-(t-T) \;\; v_1^-(\cdot)]$

$v^+ = v^-(t-T)$

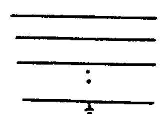

$v^+(t) = M_v \exp(A_a \ell_0)\, S_1(t-T)$

$v^-(t) = M_v\, S_1(t)$

M_v = mode matrix

A_a = attenuation matrix

$S_1(t)$ = state vector

STATE and OUTPUT EQUATIONS

STATE EQUATION

$$\begin{bmatrix} \dot{x}_1(t) \\ x_2(t+T_i) \end{bmatrix} = \begin{bmatrix} A_1 & A_2 \\ A_3 & A_4 \end{bmatrix} \begin{bmatrix} x_1(t) \\ x_2(t) \end{bmatrix} + B_1 u(t) + B_2 F(x_1, x_2, u)$$

OUTPUT EQUATION

$$y(t) = C \begin{bmatrix} x_1(t) \\ x_2(t) \end{bmatrix} + D_1 u(t) + D_2 F(x_1, x_2, u)$$

$x_1(t)$	is the lumped state vector of order n (voltages across capacitors and currents in inductors).
$x_2(t)$	is the distributed state vector of order m. (reflected voltages at transmission line ports.)
$u(t)$	is the input vector.
$F(x_1,x_2,u)$	are the non-linear functions.
T_i	is the delay on the i^{th} transmission line.
$y(t)$	is the output vector

$A_1, A_2, A_3, A_4, B_1, B_2, C, D_1, D_2$ are real matrices of compatible dimensions.

EQUILIBRIUM POINTS

CONDITIONS OF EQUILIBRIUM

$$\dot{x}_1(t) = 0$$

and

$$x_2(t + T_i) = x_2(t)$$

APPLYING TO STATE EQUATION WE GET

$$-\begin{bmatrix} A_1 & A_2 \\ A_3 & A_4 - I_m \end{bmatrix} \begin{bmatrix} x_1 \\ x_2 \end{bmatrix} = B_1 u + B_2 F$$

WHERE I_m IS A UNIT MATRIX OF ORDER m (NUMBER OF TRANSMISSION LINE PORTS).

SOLUTION GIVES EQUILIBRIUM POINT i.

$$x_{Qi} = \begin{bmatrix} x_{1Qi} \\ \hline x_{2Qi} \end{bmatrix}$$

STABILITY ANALYSIS

THE CHARACTERISTIC EQUATION

$$\begin{vmatrix} sI_n - A_{1i} & -A_{2i} \\ -A_{3i} & e^{sT}I_m - A_{4i} \end{vmatrix} = 0$$

gives the eigenvalues of the system for the i^{th} equilibrium point where

$$\begin{bmatrix} A_{1i} & A_{2i} \\ A_{3i} & A_{4i} \end{bmatrix}$$

is the Jacobian matrix of the State equation for the i^{th} equilibrium point.

The Generalised L/D Multiport

The jth multiport is described by

$$x^j = A^j x^j + B^j u^j + B^j u^j \,, \quad (1a)$$

$$y^j = C^j x^j + D^j u^j + D^j u^j \,, \quad (1b)$$

$$F^j = C^j x^j + D^j u^j + D^j u^j \,, \quad (1c)$$

where

$x = [x_1(t) : x_2(t)]$, $x_1(t)$ and $x_2(t)$ are the lumped and distributed state vectors of the jth multiport, respectively,

$x = [x_1(t) : x_2(t+T_k)]$, T_k is the delay of the kth transmission line,

$u = [i_{cp} : v_{vp}]^T$ is the input vector,

$y = [v_{cp} : i_{vp}]^T$ is the output vector,

u_n is the vector of the controlling voltages and currents of the non- linear elements,

$F_n = [f_n(x, u, u_n, t)]^T$ is the vector of the non-linear functions.
The subscripts cp and vp refer to the current driven or voltage driven ports.

INITIAL COMBINATION OF STATE EQUATIONS

$$x_p = \begin{bmatrix} x^1(t) \\ x_2^1(t+T) \\ \vdots \\ x_1^j(t) \\ \vdots \\ x_2^j(t+2) \\ \vdots \\ x_1^m(t) \\ x_2^m(t+T) \end{bmatrix}$$

$$A_p = \begin{bmatrix} [A_p^1] & & & \\ & \ddots & & \\ & & [A_p^j] & \\ & & & \ddots \end{bmatrix}$$

RESTRICTIONS DUE TO INTERCONNECTIONS

$$\begin{bmatrix} i_f \\ v_c \end{bmatrix} = \begin{bmatrix} O & D \\ -D_T & O \end{bmatrix} \begin{bmatrix} v_f \\ i_c \end{bmatrix}$$

WHICH IS A COMBINATION OF KIRCHOFF's FIRST AND SECOND LAWS.

Formulation of the Network Equations

The state, output and non-linear equations of the whole network consisting of a number of multiports is written in the form,

$$xp = Ap\,xp + Bp\,up + Bnp\,u \qquad (5a)$$

$$yp = Cp\,xp + Dp\,up + Dnp\,un \qquad (5b)$$

$$Fn = C1p\,xp + D1p\,up + 1np\,un \qquad (5c)$$

where

xp, xp, up, un and Fnp are real vectors, each vector contains the elements of the corresponding vectors of all multiports (e.g. xp = [x1..xm]T).

Ap, Bp, Bnp, Cp, Dp, Dnp, C1p, D1p and D1np are real quasidiagonal matrices, each matrix contains the elements of the corresponding matrices of all multiports.

STEPS FOR SOLUTIONS

- STORE (OR DERIVE) STATE AND OUTPUT EQUATIONS FOR EACH SUBNETWORK
- COMBINE ALL THE STATE AND OUTPUT EQUATIONS
- APPLY THE CONSTRAINTS ON THE INPUTS AND OUTPUTS OF THE INDIVIDUAL SUBNETWORKS DUE TO THE INTERCONNECTIONS.
- REARRANGE THE STATE VARIABLES.
- SOLVE THE STATE EQUATIONS FOR THE WHOLE NETWORK.

The advantages of this approach are summarized below:

1. A large network can be divided into smaller subnetworks and the equations for each subnetwork are derived separately.

2. A library of subnetworks can be developed and stored for future use without the need of an equivalent circuit. This includes transistors, FETs, diodes,..etc..

3. The equations characterising a non-linear device can be derived to match experimental data without the need to develop a physically realizable equivalent circuit. This gives a greater flexibility in modelling active devices.

4. The subnetworks developed can be used in either a direct integration subroutine or a harmonic balance subroutine.

Multi-port Number	Number of ports	Non-zero elements of the state and output matrices		Multiport Circuit
1 2 10	1	See Table I		$R_S = R_0 = R_L = 50\ \Omega$
3	4	A matrix: $a_{15}=a_{26}=a_{37}=a_{48}=-1$ $a_{51}=a_{62}=a_{72}=a_{82}=1$ C matrix: $c_{11}=c_{25}=-2Y_{o1}$ $c_{22}=c_{36}=-2Y_{o2}$ $c_{33}=c_{47}=-2Y_{o3}$ $c_{44}=c_{18}=-2Y_{o4}$	B matrix: $b_{12}=b_{23}=b_{34}=b_{41}=1$ $b_{51}=b_{62}=b_{73}=b_{84}=1$ D matrix: $d_{11}=Y_{o4}+Y_{o1}$ $d_{22}=Y_{o1}+Y_{o2}$ $d_{33}=Y_{o2}+Y_{o3}$ $d_{44}=Y_{o3}+Y_{o4}$	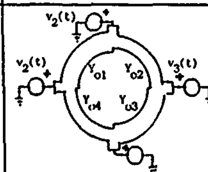 Hybrid Coupler $Y_{o1}=Y_{o3}=0.02$ S $Y_{o2}=Y_{o4}=0.02828$ S $T_1=T_2=T_3=T_4=35.714$ ps
4	2	See Table II		Phasing Line $Y_o=0.02$ S, $T=35.714$ ps

TABLE V Multiport Circuits of Diode Balanced Mixer ... Continued

5 6	2	A matrix $a_{13}=-a_{24}=-1$ $a_{31}=-a_{42}=(Y_{o1}-Y_{o2})/(Y_{o1}+Y_{o2})$ $a_{32}=a_{41}=2Y_{o1}/(Y_{o1}+Y_{o2})$ C matrix. $c_{11}=2Y_{o1}/(Y_{o1}+Y_{o2})$ $c_{12}=2Y_{o2}/(Y_{o1}+Y_{o2})$ $c_{23}=-2Y_{o1}$	B matrix: $b_{12}=1$ $b_{31}=b_{41}=1/(Y_{o1}+Y_{o2})$ D matrix $d_{11}=1/(Y_{o1}+Y_{o2})$	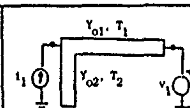 Matching Section $Y_{o1}=Y_{o2}=0.02$ S $T_1 = 11.429$ ps $T_2 = 45.818$ ps
7 8	2	B matrix. $b_{11}=1/c_o$ C matrix $c_{11}=1$ D_{1n} matrix $d_{1n11}=1$	B_n matrix $b_{n11}=-1/c_o$ D_n matrix $d_{n21}=1$ F_n vector $F_n=\{J\ V_{co}\}^T$, $V_{co}=-v_c^2/4V_c$ $J=J_o[\exp(-v/v_T)-1]$	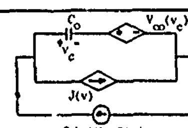 Schottky Diode $J_o=10^{-6}$A $V_T=.68$ v $V_B=0.8$, $C_o=.15$ pF
9	2	A matrix $a_{93}=-1/C_1$, $a_{23}=-1/C_2$ $a_{31}=-a_{32}=1/L$ C matrix: $c_{11}=c_{22}=1$	B matrix $b_{11}=1/C_1$ $b_{22}=1/C_2$	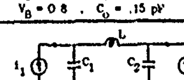 Third order lumped-filter L = 63.408 nH $C_1=C_2=22.803$ pF

TABLE V: Multiport Circuits of Diode Balanced Mixer

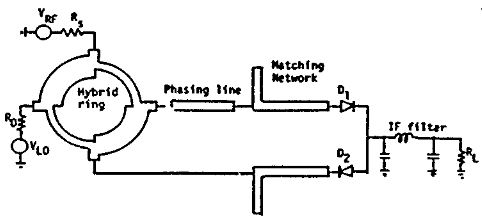

(a) Schematic diagram of balanced mixer

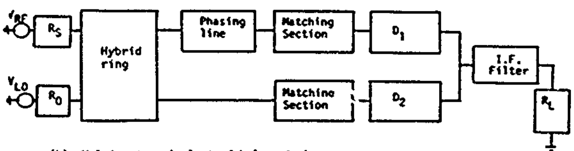

(b) Multiport equivalent of balanced mixer

Circuit diagram and multiport equivalent of balanced mixer

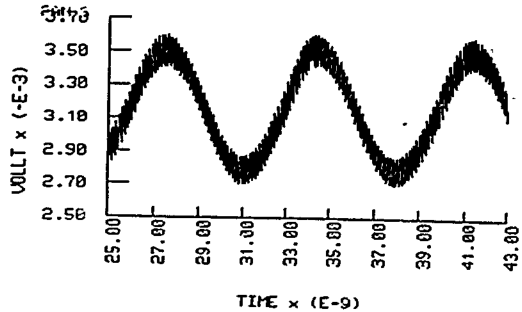

Simulated output of microwave mixer

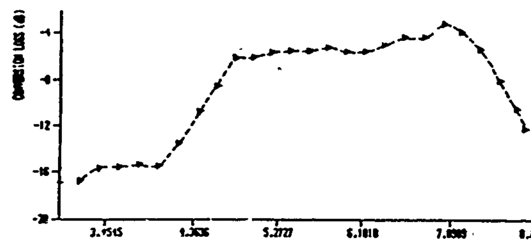

Frequency response of microwave mixer

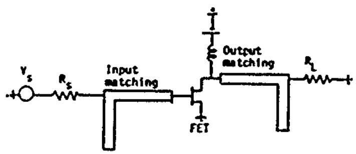

(a) Schematic diagram of frequency doubler

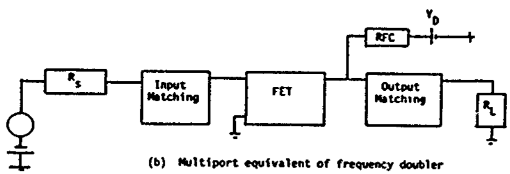

(b) Multiport equivalent of frequency doubler

Circuit diagram and multiport equivalent of frequency doubler

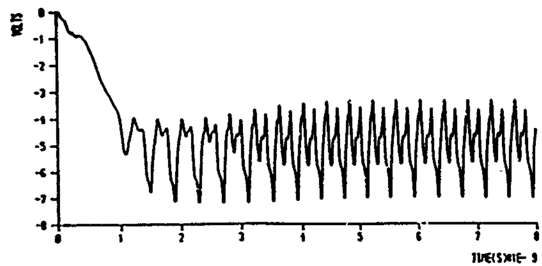

Output waveform of frequency doubler

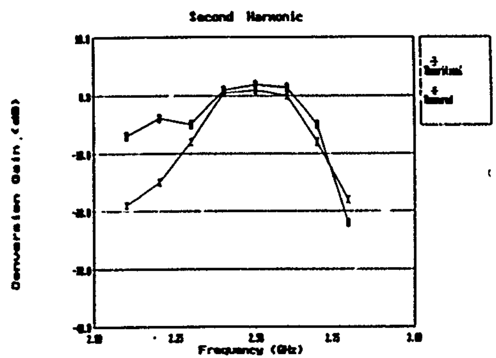

Frequency response of frequency doubler

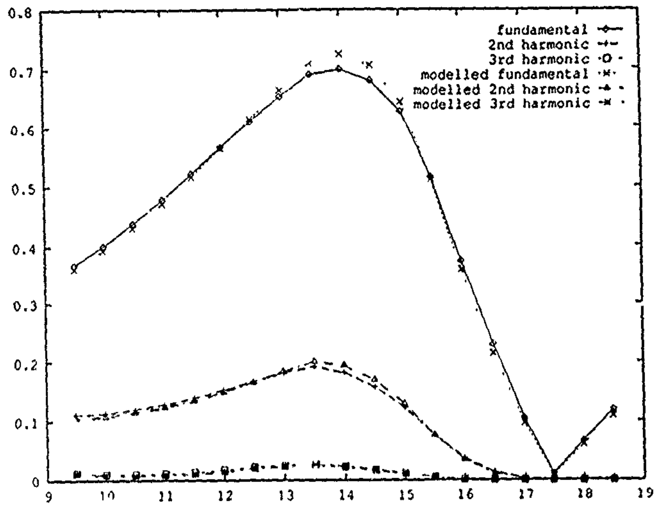

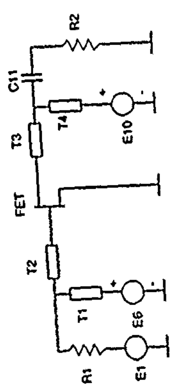

CIRCUIT OF A NON-LINEAR FET AMPLIFIER

R1 = 50 Ohm

R2 = 50 Ohm

T1 = 50 Ohm 28.5ps

T2 = 50 Ohm 8.28ps

T3 = 50 Ohm 10.5ps

T4 = 50 Ohm 4.7ps

C11 = 1 pF

E1 = Input voltage source

E6 = Gate bias dc source = 0 V

E10 = Drain bias dc source = 3 V

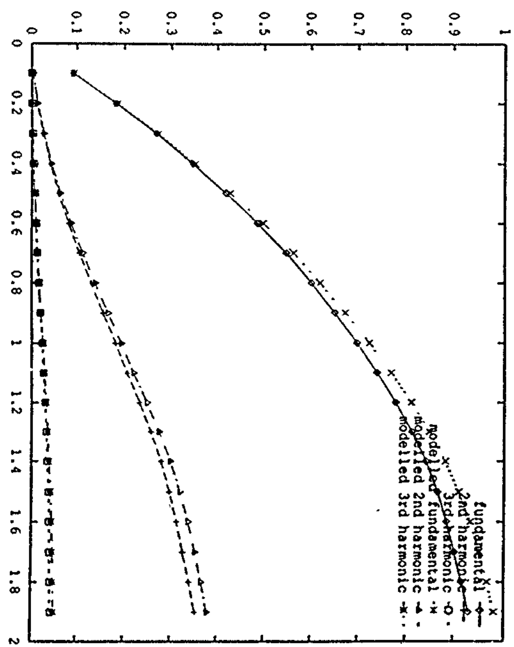

- NON-LINEAR LUMPED-DISTRIBUTED NETWORKS CAN NOW BE ANALYSED IN THE TIME DOMAIN AS AN INTERCONNECTION OF MULTIPORTS.

- THE OVERALL NETWORK IS DIVIDED INTO A NUMBER OF SUBNETWORKS AND EACH SUBNETWORK IS CHARACTERISED SEPARATELY.

- A LIBRARY OF SUBNETWORKS CAN BE DEVELOPED FROM ACTIVE ELEMENTS SUCH AS TRANSISTORS. FETs, DIODES...etc. WITH VERY LITTLE STORAGE REQUIRED.

- THE NON-LINEAR MULTIPORTS CAN BE USED IN EITHER A DIRECT INTEGRATION SUBROUTINE OR USING THE HARMONIC BALANCE METHOD.

Efficient Analytical-Numerical Modeling Of Ultra-Wideband Pulsed Plane Wave Scattering From a Large Strip Grating

Lawrence Carin and Leopold B. Felsen
Weber Research Institute/ Electrical Engineering Department
Polytechnic University
Farmingdale, NY 11735

Summary: Ultra-wideband (UWB) pulsed plane wave scattering from a large but finite strip grating in free space is analyzed in the frequency domain via decomposition into plane wave spectra, implemented numerically by the method of moments, and then inverted into the time domain (TD). To make this procedure practical under UWB conditions, closed form expressions are derived for interaction integrals involving widely separated expansion and testing functions. These closed forms are based on a judicious choice of the basis functions, and on asymptotic methods for reducing the integrals. Although large separation distances are assumed, the expressions have been found to be accurate for separations as small as 0.1 wavelengths. The TD self terms can also be evaluated efficiently. To test the frequency domain algorithm, comparisons are made with available data in the literature for surface currents and far field scattering from multiple strips. New short pulse TD results are shown as well.

Transient currents and fields of wire antennas with diodes

N. Scheffer, Telefunken Systemtechnik VR3 E51, Sedanstr.10, 7900 Ulm

1. Numerical method

The electric field integral equation for a wire antenna can be written in matrix notation for the time step t_ν as

$$(\mathbf{Z}+\mathbf{Z}_\nu^L)\cdot\mathbf{I}_\nu=\mathbf{E}_\nu^i+\mathbf{E}_\nu^s. \qquad (1)$$

The unknown quantitiy in (1) is the current distribution $\mathbf{I}_\nu=\begin{pmatrix} I_{1\nu} \\ I_{2\nu} \\ \vdots \\ I_{N\nu} \end{pmatrix}$ of the antenna. The antenna is devided into N segments. The impedance matrix Z is time independent.

$$\mathbf{Z}_\nu^L=\begin{pmatrix} R_1 & & 0 \\ & R_2 & \\ & & \ddots \\ 0 & & R_N \end{pmatrix}$$

represents a diagonal matrix containing the nonlinear loads.

The components of $\mathbf{E}_\nu^i$ are the tangential components of the incident electric field and $\mathbf{E}_\nu^s$ are the tangential components of the scattered electric field. Introducing the admittance matrix $\mathbf{Y}=\mathbf{Z}^{-1}$ and

$$\mathbf{I}_\nu^0=\mathbf{I}_\nu|_{\mathbf{Z}_\nu^L=0}=\mathbf{Y}\cdot(\mathbf{E}_\nu^i+\mathbf{E}_\nu^s) \qquad (2)$$

equation (1) can be written as

$$(\mathbf{E}+\mathbf{Y}\cdot\mathbf{Z}_\nu^L)\cdot\mathbf{I}_\nu=\mathbf{I}_\nu^0. \qquad (3)$$

E repesents the unity matrix.
For the special case, that the antenna is loaded at exactly two segments m and n with R_m and R_n, the currents in the loaded segments are

$$I_{m\nu}=\frac{(Y_{nn}R_n+1)I_{m\nu}^0-Y_{mn}R_nI_{n\nu}^0}{(Y_{mm}R_m+1)(Y_{nn}R_n+1)-Y_{mn}Y_{nm}R_mR_n} \qquad (4)$$

$$I_{n\nu}=\frac{(Y_{mm}R_m+1)I_{n\nu}^0-Y_{nm}R_mI_{m\nu}^0}{(Y_{nn}R_n+1)(Y_{mm}R_m+1)-Y_{nm}Y_{mn}R_nR_m} \qquad (5)$$

The currents in the unloaded segments $i\neq m,n$ are

$$I_{i\nu}=I_{i\nu}^0-Y_{im}R_mI_{m\nu}-Y_{in}R_nI_{n\nu}. \qquad (6)$$

2. The time dependent current distribution

The above method of calculation is used to examine a dipole. The dipole contains two diodes and is centerfed by a source voltage with Gausssian pulse shape as shown in Fig. 1.
The two diodes are described by resistors

$$R_m=\begin{cases} 0\Omega & , I_m^0\geq 0 \\ 100k\Omega & , I_m^0<0 \end{cases}$$

$$R_n=\begin{cases} 0\Omega & , I_n^0\geq 0 \\ 100k\Omega & , I_n^0<0 \end{cases}$$

Fig. 2 shows the two current pulses arriving at the antenna ends after passing the diodes almost undistortedly. The arrows mark the positions of the diodes. In Fig. 3 the current pulses have arrived at the reversed biased diodes after they have been reflected at the antenna ends. Fig. 4 shows the reflection at the reversed biased diodes.

3 The electric nearfield

It is possible to reduce the fieldline equation $d\vec{r}\times\vec{E}=0$ to a potential function

$$U=\rho\int_{-\infty}^{z}H_\varphi dz \;,\quad \rho=\sqrt{x^2+y^2}$$

because of the cylinder symmetry.

An electric fieldline is then described by $U=const$. H_φ is derived in the appendix. Fig. 5 shows the electric fieldlines located on concentric spheres around the generator. The pulse has just arrived at the antenna end. In Fig. 6 the reflection at the antenna end is considered: the fieldlines are now located on concentric spheres around the source and the antenna end. Fig. 7 shows the reflection at the diode: a new sphere around the diode is visible. In Fig. 8 multiple reflections for a late time step can be observed.

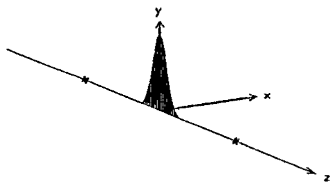

Fig. 1

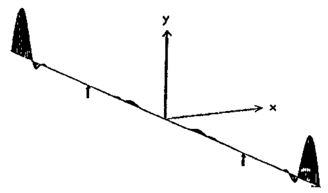

Fig. 2

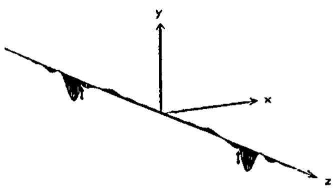

Fig. 3

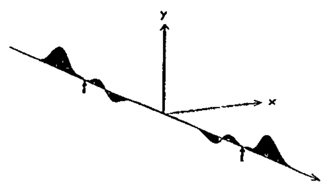

Fig. 4

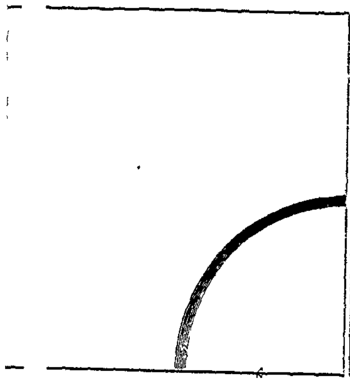

Fig. 5

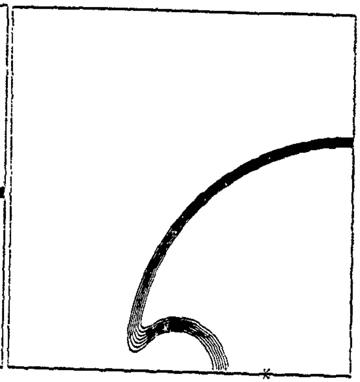

Fig. 6

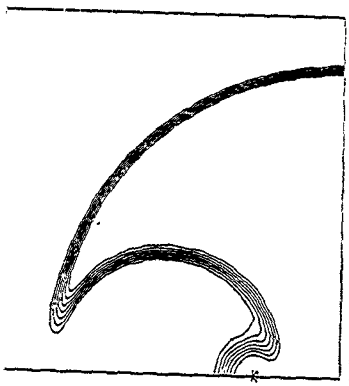

Fig. 7

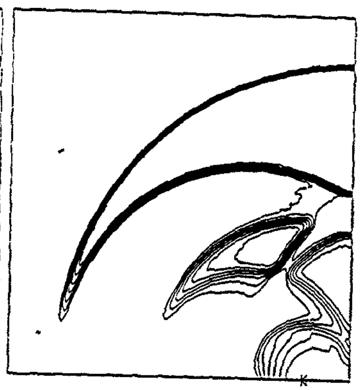

Fig. 8

Calculating Frequency Domain Data by Time Domain Methods

by M. Dehler, M. Dohlus, T. Weiland
Technische Hochschule Darmstadt Theorie Elektromagnetischer Felder (FB18)

Abstract

We show the calculation of far field patterns and scattering parameters by means of time domain methods. In order to obtain a mode excitation, the eigensolution of the discrete waveguide eigenvalue problem in combination with an adequate processing at the boundaries is used.

Far Field Transforms

In general the electric field of radiating structures can be written for large distances as

$$\vec{E}_{far}(r,\Theta,\phi) = \frac{e^{-jkr}}{r}\vec{F}(\Theta,\phi), \tag{1}$$

where $k = \omega^2\mu\epsilon$ is the wave number and r, Θ, ϕ denote spherical coordinates.

For the calculation of the far field transform $\vec{F}(\Theta,\phi)$, one needs to determine the complex time harmonic field amplitudes. $\vec{F}(\Theta,\phi)$ can be determined by a convolution of Greens function and tangential electric and magnetic amplitudes on a closed surface surrounding the radiating structure.

$$\vec{F}(\Theta,\phi) = \frac{j\omega}{4\pi}\oint_{\partial V} e^{jk\vec{r}_r\vec{r}'}\left\{\vec{r}_r \times (\vec{c}_r \times (\vec{n}\times\underline{\vec{B}})) - \frac{1}{c}\vec{c}_r \times (\vec{n}\times\underline{\vec{E}})\right\}dA\,, \tag{2}$$

The computation of the complex field amplitudes by a Fast Fourier Transform requires sampling and storage of the tangential electric and magnetic field values at the integration surface and is only feasible for small mesh sizes. Therefore these amplitudes are obtained by using time harmonic excitation sources and a direct sampling of the harmonic fields. Another way is to perform a monochromatic, single frequency fourier transform of the time domain fields.

Filter Design

The transversal electric field in a waveguide is described for the time harmonic case by the mode expansion

$$\vec{E}(x,y,z,t) = \mathrm{Re}\left\{e^{j\omega t}\sum_\nu \underline{\vec{E}}_\nu(x,y,j\omega)\left(\underline{a}_\nu(j\omega)\,e^{-\gamma_\nu(j\omega)z} + \underline{b}_\nu(j\omega)\,e^{\gamma_\nu(j\omega)z}\right)\right\} \tag{3}$$

which can be formulated for general time dependency with double convolutions:

$$\vec{E}(x,y,z,t) = \sum_\nu \vec{E}_\nu(x,y,t) * \left(a_\nu(t) * P_\nu(t,z) + b_\nu(t) * P_\nu(t,-z)\right) \tag{4}$$

with $P_\nu(t,z)$ being the inverse Fourier transform of $\exp(\gamma_\nu(j\omega)$. The knowledge of $\underline{A}_\nu(j\omega) = \underline{a}_\nu(j\omega) + \underline{b}_\nu(j\omega)$ is essential for the calculation of the tangential boundary field $\underline{\vec{E}}(x,y,0,j\omega)$ at the interface $z = 0$. The stimulation wave $\underline{a}_\nu(j\omega)$ is known, but $\underline{b}_\nu(j\omega)$ has to be calculated from

$$\underline{B}_\nu(j\omega) = \underline{a}_\nu(j\omega)e^{-\gamma_\nu(j\omega)\delta z} + \underline{b}_\nu(j\omega)e^{\gamma_\nu(j\omega)\delta z}\,. \tag{5}$$

$\underline{B}_\nu(j\omega)$ can be obtained by mode expansion of the field in the plane $z = \delta z$. The modes $\underline{\vec{E}}_\nu(x,y,j\omega)$ and the propagation constants are calculated by a 2D eigenvalue solver. The case of frequency dependent $\underline{\vec{E}}_\nu$ is problematic because the expansion of sampled fields $\vec{E}(x,y,z,t_\mu)$ is only possible in the steady state. In the other case $B_\nu(t_\mu)$ is yielded directly and

$$A_\nu(t) = [1 - P_\nu(t,2\delta z)] * a_\nu(t) + P_\nu(t,\delta z) * B_\nu(t) \tag{6}$$

can be calculated by single convolutions. This method is applicable for homogeneously filled waveguides and for modes with weak frequency dependency. A simplification of the algorithm is possible, if the convolution can be approximated in the desired frequency range by a low order digital filter.

TIME DOMAIN ANALYSIS OF INHOMOGENEOUSLY LOADED STRUCTURES USING EIGENFUNCTION EXPANSION

MICHAŁ MROZOWSKI
TECHNICAL UNIVERSITY OF GDAŃSK, TELECOMMUNICATION INSTITUTE
80-952 GDAŃSK, POLAND, TEL.: +(048 58) 472 549, FAX: +(048 58) 47 19 71

SUMMARY

At present there are two algorithms, namely the TLM and FD-TD, which are used to solve Maxwell's equations in time domain. In this contribution we shall present new methods which may broaden the range of options available in time domain analysis of 2-D and 3-D structures. A wave is treated as a superposition of eigenmodes (eigenfunctions) of the homogeneous Laplace equation. An inhomogeneity in the structure perturbs the field and causes the coupling of eigenmodes. Eigenmodes are chosen so that they fulfil the Helmholtz equation either on the entire homogeneous domain or on homogeneous subdomains. An advantage of this approach is that it allows to obtain time domain algorithms which, in contrast to TLM and FD-TD methods, do not exhibit the numerical dispersion.

Outline of time domain eigenfunction expansion algorithms.

Based on the concept briefly described above, a number of algorithms can be proposed. We shall start with an algorithm called a complete eigenfunction expansion (CEE). Let us consider a set of coupled differential equations reflecting the form of Maxwell equations

$$\frac{d}{dt}f = \mathcal{L}_1 g \qquad \frac{d}{dt}g = \mathcal{L}_2 f \tag{1}$$

where $\mathcal{L}_1$, $\mathcal{L}_2$ are linear operators.
In the FD-TD algorithm the above equations are discretized both in time and space. In the CEE algorithm the discretization is only in time. As a result we get

$$f^n = f^{n-1} + \Delta t \mathcal{L}_1 g^{n-1/2} \qquad g^{n+1/2} = g^{n-1/2} + \Delta t \mathcal{L}_2 f^n \tag{2}$$

The unknown functions f, g are now expanded into series of complete set of orthonormal functions.

$$f = \sum a_i f_i \qquad g = \sum b_i g_i \tag{3}$$

Expansion function are defined on the entire domain. A sensible choice for the electromagnetic fields is are the eigenfunctions of Laplace equation with suitable boundary conditions. Substituting (3) into (2) we get

$$\sum a_i^n f_i = \sum a_i^{n-1} f_i + \Delta t \mathcal{L}_1 \sum b_i^{n-1/2} g_i \tag{4}$$
$$\sum b_i^{n+1/2} g_i = \sum b_i^{n-1/2} g_i + \Delta t \mathcal{L}_2 \sum a_i^n f_i$$

Taking the inner product with the expansion functions results in

$$a_i^n = a_i^{n-1} + \Delta t < \mathcal{L}_1 g^{n-1/2}, f_i > \tag{5}$$
$$b_i^{n+1/2} = b_i^{n-1/2} + \Delta t < \mathcal{L}_2 f^n, g_i >$$

The above equations can be cast into the following matrix form

$$\underline{a}^{n} = \underline{a}^{n-1} + \Delta t \underline{A}\, \underline{b}^{n-1/2} \tag{6}$$
$$\underline{b}^{n+1/2} = \underline{b}^{n-1/2} + \Delta t \underline{B}\, \underline{a}^{n}$$

where $\underline{a}$ and $\underline{b}$ are the vectors containing expansion coefficients and $\underline{A}$ and $\underline{B}$ are dense matrices with elements

$$A_{ij} = < \mathcal{L}_1 g_j, f_i > \qquad B_{ij} = < \mathcal{L}_2 f_j, g_i > \tag{7}$$

Another version of the eigenfunction expansion algorithm is obtained if the discretization is in time and one spatial coordinate and the expansion is done with respect to two remaining spatial coordinate. This algorithm we shall call partial eigenfunction expansion (PEE). In this technique the space is sliced into subdomains and the fields are expanded on each subdomain (slice) into series of local expansion functions. In the PEE method one obtains a set of equations similar to (6) except that matrices $\underline{A}$ and $\underline{B}$ are sparse.

Compared with the FD-TD method the CEE and PEE algorithms show the time evolution of the expansion coefficients rather then field components at nodes. Such an approach allows one to investigate propagation of particular modes and their mutual interactions. Moreover, in contrast to FD-TD and TLM techniques, both algorithms proposed in this contribution do not exhibit numerical dispersion.

Efficient numerical implementation of eigenfunction expansion algorithms: CEE-FFT and PEE-FFT.

One drawback of the CEE and PEE algorithms that they may lead to higher numerical cost then FD-TD and TLM. The CEE involves matrix multiplication hence, assuming that expansion is done using L eigenfuncions, the cost of one time step is of order $O(L^2)$. For the PEE this cost is lower as the matrices involved are sparse. In the FD-TD and TLM method with N nodes, the numerical cost is of order $O(N)$. Consequently, eigenfunction expansion techniques may be regarded as an alternative to classical time domain algorithms only when $L^2 \sim N$. This condition will be fulfilled in slightly and moderately perturbed homogeneous structures. Nevertheless, much more efficient version of CEE and PEE may be obtained if the expansion functions are sine and cosines. Equations (6) imply that at each step one evaluates the inner products $< \mathcal{L}_1 g^{n-1/2}, f_i >$ and $< \mathcal{L}_2 f^{n}, g_i >$. For sine and cosine functions the inner product can be computed in a very efficient way using the technique described in [1]. In this technique the inner products are computed in a sequence of inverse and forward FFTs. The numerical cost of such computations is low and therefore the overall performance of the CEE-FFT and PEE-FFT algorithms is better than original CEE and PEE methods.

Conclusions. New algorithms of the time domain analysis of inhomogeneously loaded microwave structures have been described. The methods proposed are based on the expansion of fields into complete series of orthogonal eigenfunctions. The resulting equations show the time evolution of the expansion coefficients and consequently allow one to investigate propagation of separate modes and their mutual interactions. The algorithms proposed in this contribution do not exhibit numerical dispersion and allow coarser time discretization than the equivalent FD-TD or TLM program.

[1] M. Mrozowski, "IEEM FFT - A fast and efficient tool for rigorous computations of propagation constants and field distributions in dielectric guides with arbitrary cross-section and permittivity profiles", *IEEE Trans. Microwave Theory Tech.*, vol. MTT-39, Feb. 1991.

The Hilbert Space Formulation of the TLM Method

Peter Russer, Michael Krumpholz [1]

Abstract

The Hilbert space representation of the TLM method for time domain computation of electromagnetic fields and the algebraic computation of the discrete Green's function are investigated. The complete field state is represented by a Hilbert space vector. The space and time evolution of the field state vector is governed by operator equations in Hilbert space. The discrete Green's functions may be represented by a Neumann series in space– and time–shift operators. The Hilbert space representation allows the description of the geometric structures by projection operators, too. The system of difference equations governing the time evolution of the electromagnetic field in configuration space is derived from the operator equation for the field state vector in the Hilbert space.

1 Introduction

The TLM (transmission line matrix) method developed and first published in 1971 by Johns and Beurle is a discrete time domain method for electromagnetic field computation [1,2,3]. In this paper, the Hilbert space representation of the TLM method is presented and applied to the algebraic computation of discrete Green's functions. The Hilbert space representation is a very general and powerful concept in field theory [4]. Whereas in the electromagnetic theory Hilbert space methods are mainly used for solving the field equations as for example in the moment method [5], in quantum theory, the fundamental theoretical concepts have been formulated in Hilbert space [6,7].

The state of a discretized field can be represented by a vector in the Hilbert space. The specification of the mesh node connections and the boundary con-

[1]Lehrstuhl für Hochfrequenztechnik, Technische Universität München, Arcisstrasse 21, D-8000 Munich 2, Fed. Rep. Germany

ditions is done by operators in the Hilbert space. The Hilbert space representation also allows the description of geometric structures by projection operators. The space and time evolution of the field state vector is governed by operator equations.

In field theory, the field propagation in spatial domains may be treated using Green's functions [8]. The concept of Green's functions may also be applied to discrete time domain field computation [9]. Discrete time domain Green's functions allow to model the relation between the field values on the boundaries if the knowledge of the field in the spatial domains beyond the boundaries is not required.

In this paper, the algebraic computation of the discrete Green's function is investigated. Our approach is based on a Hilbert space representation of the space– and time discretized electromagnetic field. The discrete Green's functions may be represented by a Neumann series in space– and time–shift operators. The system of difference equations governing the time evolution of the electromagnetic field in configuration space is derived from the operator equation for the field state vector in the Hilbert space. First results are presented for the two–dimensional case.

2 The Two–dimensional TLM Method

The electromagnetic field is discretized within space and time. The space is modelled by a mesh of transmission lines connecting the sample points in space. The field computation algorithm consists of two steps:

- The propagation of wave pulses from the mesh nodes to the neighbouring nodes.
- The scattering of the wave pulses in the mesh nodes.

In the following, we restrict our considerations to the two–dimensional case with the transverse electric field. In the shunt TLM model, voltage wave amplitudes are used instead of total voltage and current. The voltage wave amplitudes of the incident and the reflected waves are given by ${}_k\boldsymbol{a}_{m,n}$ and ${}_k\boldsymbol{b}_{m,n}$. The left index k denotes the discrete time coordinate and the right indices m and n denote the two discrete space coordinates. We consider the TLM mesh to be composed by elementary TLM shunt node four-ports as shown in Fig. 1, where each of the four arms is of length $\Delta l/2$. The scattering in this elementary four-port is connected with the time delay Δt.

The scattering of the wave pulses is described by

$$ {}_{k+1}\begin{bmatrix} b_1 \\ b_2 \\ b_3 \\ b_4 \end{bmatrix}_{m,n} = S \; {}_{k}\begin{bmatrix} a_1 \\ a_2 \\ a_3 \\ a_4 \end{bmatrix}_{m,n} \tag{1} $$

with the scattering matrix S given by

$$ S = \begin{bmatrix} -\frac{1}{2} & \frac{1}{2} & \frac{1}{2} & \frac{1}{2} \\ \frac{1}{2} & -\frac{1}{2} & \frac{1}{2} & \frac{1}{2} \\ \frac{1}{2} & \frac{1}{2} & -\frac{1}{2} & \frac{1}{2} \\ \frac{1}{2} & \frac{1}{2} & \frac{1}{2} & -\frac{1}{2} \end{bmatrix} \tag{2} $$

With the scattering, a time delay of Δt is associated and therefore, the time index k is incremented by one. The scattered pulses are the incident pulses of the neighbouring elementary cell. This is described by

$$ \begin{aligned} {}_{k}a_{1,m,n} &= {}_{k}b_{2,m-1,n} \\ {}_{k}a_{2,m,n} &= {}_{k}b_{1,m+1,n} \\ {}_{k}a_{3,m,n} &= {}_{k}b_{4,m,n-1} \\ {}_{k}a_{4,m,n} &= {}_{k}b_{3,m,n+1} \end{aligned} \tag{3} $$

3 The Discrete Field State Space

In the TLM model, the field state at a given discrete time is described completely by specifying the amplitudes of the four wave pulses incident to each mesh node . The space of the voltage wave amplitudes of the incident and the reflected waves ${}_{k}a_{i,m,n}$ and ${}_{k}b_{i,m,n}$ is the four-dimensional real vector space $\mathcal{R}^4$. In order to develop our formalism in a more general way we introduce the

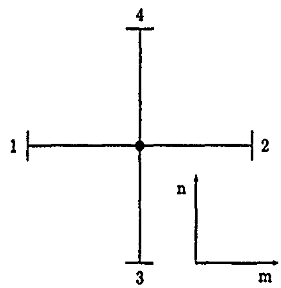

Figure 1: A two-dimensional TLM shunt node four-port.

four-dimensional complex vector space C^4 for representing the wave amplitudes ${}_ka_{m,n}$ and ${}_kb_{m,n}$.

In order to describe the whole mesh state, we introduce the Hilbert space $\mathcal{H}_m$ which allows to map each mesh node onto an ortonormal set of base vectors of $\mathcal{H}_m$. The time states are represented by the Hilbert space $\mathcal{H}_t$. With each pair of discrete spatial coordinates (m,n), a basis vector of $\mathcal{H}_m$ is associated and with each k, a basis vector of $\mathcal{H}_t$ is associated. We now introduce the state space $\mathcal{H}$ given by the Cartesian product of C^4, $\mathcal{H}_m$ and $\mathcal{H}_t$

$$\mathcal{H} = C^4 \otimes \mathcal{H}_m \otimes \mathcal{H}_t \tag{4}$$

The space $\mathcal{H}$ is a Hilbert space, too. The complete time evolution of the field state within the whole three-dimensional space-time may now be represented by a single vector in $\mathcal{H}$. Using the bra-ket notation introduced by Dirac [6], the orthonormal basis vectors of $\mathcal{H}$ are given by the bra-vectors $|k;m,n\rangle$. The ket-vector $\langle k;m,n|$ is the Hermitian conjugate of $|k;m,n\rangle$. The orthogonality relations are given by

$$\langle k_1;m_1,n_1|k_2;m_2,n_2\rangle = \delta_{k_1,k_2}\delta_{m_1,m_2}\delta_{n_1,n_2} \tag{5}$$

The incident and reflected voltage waves are represented by

$$|a\rangle = \sum_{k=-\infty}^{+\infty} \sum_{m=-\infty}^{+\infty} \sum_{n=-\infty}^{+\infty} {}_k\begin{bmatrix} a_1 \\ a_2 \\ a_3 \\ a_4 \end{bmatrix}_{m,n} |k; m, n\rangle \tag{6}$$

and

$$|b\rangle = \sum_{k=-\infty}^{+\infty} \sum_{m=-\infty}^{+\infty} \sum_{n=-\infty}^{+\infty} {}_k\begin{bmatrix} b_1 \\ b_2 \\ b_3 \\ b_4 \end{bmatrix}_{m,n} |k; m, n\rangle \tag{7}$$

in the Hilbert space $\mathcal{H}$. We define the shift operators $\boldsymbol{X}$, $\boldsymbol{Y}$ and their Hermitian conjugates $\boldsymbol{X}^\dagger$ and $\boldsymbol{Y}^\dagger$ by

$$\begin{aligned} \boldsymbol{X}\,|k; m, n\rangle &= |k; m+1, n\rangle \\ \boldsymbol{X}^\dagger\,|k; m, n\rangle &= |k; m-1, n\rangle \\ \boldsymbol{Y}\,|k; m, n\rangle &= |k; m, n+1\rangle \\ \boldsymbol{Y}^\dagger\,|k; m, n\rangle &= |k; m, n-1\rangle \end{aligned} \tag{8}$$

The operators $\boldsymbol{X}$ and $\boldsymbol{Y}$ shift the field state by one interval Δl in the positive m– and n–direction, respectively. Their Hermitian conjugates $\boldsymbol{X}^\dagger$ and $\boldsymbol{Y}^\dagger$ shift the field state in the opposite direction.

We define the time shift operator $\boldsymbol{T}$. The time shift operator increments k by 1 i.e. it shifts the field state by Δt in the positive time direction. If the time shift operator is applied to a vector $|k; m, n\rangle$, we obtain

$$\boldsymbol{T}\ |k; m, n\rangle = |k+1; m, n\rangle \tag{9}$$

We introduce the connection operator $\boldsymbol{\Gamma}$ given by

$$\boldsymbol{\Gamma} = \begin{bmatrix} 0 & \boldsymbol{X} & 0 & 0 \\ \boldsymbol{X}^\dagger & 0 & 0 & 0 \\ 0 & 0 & 0 & \boldsymbol{Y} \\ 0 & 0 & \boldsymbol{Y}^\dagger & 0 \end{bmatrix} \tag{10}$$

With the connection operator $\boldsymbol{\Gamma}$, equation (3) yields the operator equation

$$|b\rangle = \boldsymbol{\Gamma}\,|a\rangle \tag{11}$$

describing the mesh connections. The operator Γ is hermitian and unitary:

$$\Gamma = \Gamma^{\dagger} = \Gamma^{-1} \tag{12}$$

Therefore we obtain from eqs. (11) and (12)

$$|a\rangle = \Gamma\ |b\rangle \tag{13}$$

We now express eq. (1) in the Hilbert space notation by

$$|b\rangle = \boldsymbol{T}\ \boldsymbol{S}\ |a\rangle \tag{14}$$

This equation describes the simultaneous scattering within all the mesh node four-ports according to Fig. 1. The scattering by a mesh node causes the unit time delay Δt.

Fig. 2 shows an example of a spatial domain within a TLM mesh. This spatial domain is specified by a given set of mesh four-ports. A spatial domain D in our TLM mesh may be specified by projection operators. We define the domain projection operator $\boldsymbol{P}_D$ which projects a state vector $|a >$ on the domain D:

$$\boldsymbol{P}_D\,|a\rangle = |a\rangle_D \tag{15}$$

This projection operator may be written in dyadic notation as the sum of the projection operators on the nodes belonging to the domain D:

$$\boldsymbol{P}_D = \sum_{m\in D}\sum_{n\in D} |k;m,n\rangle\,\langle k;m,n| \tag{16}$$

In the same way, we define the inner domain projection operator $\boldsymbol{P}_I$ and the boundary projection operator by

$$\begin{aligned} \boldsymbol{P}_I\,|a\rangle &= |a\rangle_I && (17)\\ \boldsymbol{P}_B\,|a\rangle &= |a\rangle_B && (18) \end{aligned}$$

with

$$\begin{aligned} \boldsymbol{P}_I &= \boldsymbol{P}_I\boldsymbol{P}_D && (19)\\ \boldsymbol{P}_B &= \boldsymbol{P}_B\boldsymbol{P}_D && (20)\\ \boldsymbol{P}_B + \boldsymbol{P}_I &= \boldsymbol{P}_D && (21) \end{aligned}$$

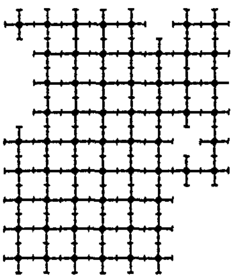

Figure 2: A spatial domain within the TLM mesh.

The inner domain projection operator projects the circuit space $\mathcal{H}$ on the inner ports of the domain D. Since the projection operator $\boldsymbol{P}_I$ and the connection operator $\boldsymbol{\Gamma}$ are commuting, i.e.

$$[\boldsymbol{P}_I, \boldsymbol{\Gamma}] = 0 \tag{22}$$

we obtain

$$|b\rangle_I = \boldsymbol{\Gamma}\,|a\rangle_I \tag{23}$$

Applying diakoptics to TLM structures requires the computation of the wave pulses scattered at the domain boundaries. The initial conditions or boundary conditions are given by the wave pulses incident on the boundary ports. We apply the projection operators $\boldsymbol{P}_I\boldsymbol{P}_D$ and $\boldsymbol{P}_B\boldsymbol{P}_D$ in order to seperate the field states $|a\rangle$ and $|b\rangle$ into the inner field states $|a\rangle_I$ and $|b\rangle_I$ and the boundary states $|a\rangle_B$ and $|b\rangle_B$. From eq. (14) we obtain

$$\begin{aligned} |b\rangle_B &= \boldsymbol{T}\,\boldsymbol{S}_{BB}\ |a\rangle_B + \boldsymbol{T}\,\boldsymbol{S}_{BI}\ |a\rangle_I \\ |b\rangle_I &= \boldsymbol{T}\,\boldsymbol{S}_{IB}\ |a\rangle_B + \boldsymbol{T}\,\boldsymbol{S}_{II}\ |a\rangle_I \end{aligned} \tag{24}$$

with

$$\begin{aligned} \boldsymbol{S}_{BB} &= \boldsymbol{P}_B\,\boldsymbol{S}\,\boldsymbol{P}_B \\ \boldsymbol{S}_{BI} &= \boldsymbol{P}_B\,\boldsymbol{S}\,\boldsymbol{P}_I \\ \boldsymbol{S}_{IB} &= \boldsymbol{P}_I\,\boldsymbol{S}\,\boldsymbol{P}_B \\ \boldsymbol{S}_{II} &= \boldsymbol{P}_I\,\boldsymbol{S}\,\boldsymbol{P}_I \end{aligned} \tag{25}$$

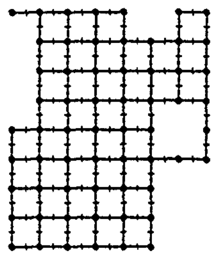

Figure 3: The inner ports of a TLM domain.

Using eqs. (23) and (24), we eliminate the inner domain states $|a\rangle_I$ and $|b\rangle_I$ and obtain

$$|b\rangle_B = \left[\boldsymbol{T}\boldsymbol{S}_{BB} + \boldsymbol{T}\boldsymbol{S}_{BI}\,(1 - \boldsymbol{\Gamma}\boldsymbol{T}\boldsymbol{S}_{II})^{-1}\,\boldsymbol{\Gamma}\boldsymbol{T}\boldsymbol{S}_{IB} \right] |a\rangle_B \qquad (26)$$

This is the relation between the incident and scattered boundary state. It describes the evolution of the boundary field state without knowledge of the inner field state. It has to be considered that the operator equation (26) is nonlocal with respect to both space and time. We expand the operator $(1 - \boldsymbol{\Gamma}\boldsymbol{T}\boldsymbol{S}_{II})^{-1}$ into a Neumann series [10,11] and obtain

$$(1 - \boldsymbol{\Gamma}\boldsymbol{T}\boldsymbol{S}_{II})^{-1} = \sum_{l=0}^{\infty} \boldsymbol{T}^{l}\,(\boldsymbol{\Gamma}\boldsymbol{S}_{II})^{l} \qquad (27)$$

Inserting this into eq. (26) yields the *boundary state evolution equation*

$$|b\rangle_B = \boldsymbol{G}\,|a\rangle_B \qquad (28)$$

with the boundary field evolution operator $\boldsymbol{G}$ given by

$$\boldsymbol{G} = \left[\boldsymbol{T}\boldsymbol{S}_{BB} + \boldsymbol{S}_{BI}\left(\sum_{l=0}^{\infty} \boldsymbol{T}^{l+2}\,(\boldsymbol{\Gamma}\boldsymbol{S}_{II})^{l} \right) \boldsymbol{\Gamma}\boldsymbol{S}_{IB} \right] \qquad (29)$$

The boundary field operator $\boldsymbol{G}$ gives the relation between the boundary state vector $|a\rangle_B$ representing the wave pulses incident on the boundary and the boundary state vector $|b)_B$ representing the wave pulses reflected through the boundary. Eq. (28) is the general formulation of the boundary element problem in the Hilbert space. Since the Neumann series is an infinite geometrical series in space- and time-shift operators, the boundary field operator is nonlocal with respect to space and time.

4 The Discrete Two-dimensional Green's function

As an example, we derive the discrete Green's function for the half-plane. The discrete Green's function for the half-plane is given by the projection of the boundary state evolution operator equation (28) onto configuration space for a point-like initial state $|a)_B$. The half-plane (Fig. 4) is defined by the domain projection operator $\boldsymbol{P}_D$ given by

$$\boldsymbol{P}_D = \sum_{k,n} \sum_{m=0}^{\infty} |k;m,n)\,(k;m,n| \tag{30}$$

As in the shunt TLM-model, voltage wave amplitudes instead of total voltages are used, a new Green's function for wave amplitudes has to be defined. For a boundary problem, the Green's function in discrete formulation is given by the convolution

$$_k\,b_{\mathrm{n}} = {}_k\,G_{\mathrm{n}} * {}_k\,a_{\mathrm{n}'} \tag{31}$$

where $_k\,a_{\mathrm{n}}$ is the column vector of the incident impulse functions at the time $k\Delta t$ and at the boundary node number n. $_k\,b_{\mathrm{n}}$ is the column vector of the scattered output wave impulses at the time $k\Delta t$ and at the n^{th} boundary node. $_k\,G_{\mathrm{n}}$ is the discrete Green's function for an arbitrary boundary with n boundary nodes. It describes the relation between the incident and the scattered wave amplitudes in the boundary ports.

For the half-plane, the boundary is given by $m = 0$ and $n = -\infty,\ldots,-1,0,1,\ldots,\infty$. Therefore eq. (31) yields

$$_k\,b_n = \sum_{n'=-\infty}^{\infty} \sum_{k'=-\infty}^{\infty} {}_{k-k'}\,G_{n-n'}\ \ {}_{k'}\,a_{n'} \tag{32}$$

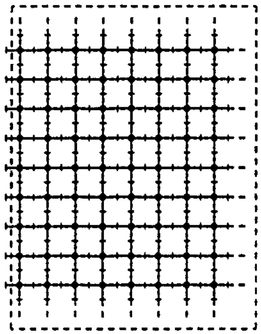

Figure 4: The homogeneous two-dimensional half-space.

The boundary state evolution equation (28) may be expressed by the discrete Green's function, eq. (32), via

$$|b\rangle_B = G\,|a\rangle_B \tag{33}$$

where the boundary field evolution operator is given by

$$G = \begin{bmatrix} 1 & 0 & 0 & 0 \\ 0 & 0 & 0 & 0 \\ 0 & 0 & 0 & 0 \\ 0 & 0 & 0 & 0 \end{bmatrix} \sum_{n=-\infty}^{\infty} \sum_{k=-\infty}^{\infty} {}_{k-k'}G_{n-n'}\,|k;0,n\rangle\,\langle k';0,n'| \tag{34}$$

In order to calculate the Green's function for the boundary of the half-plane, we start from an impulsive excitation at $n' = 0$, $k' = 0$ given by

$$|a\rangle_{B,k_0=0} = \begin{bmatrix} 1 \\ 0 \\ 0 \\ 0 \end{bmatrix} |0;0,0\rangle \tag{35}$$

Mapping eqs. (28) with (29) and (35), (33) with (34) and (35) to configuration space by multiplying both equations from the left side with $\langle k;0,n|$, we obtain a system of partial difference equations which can be solved by transforming it to frequency- and momentum-space.

We obtain an algebraic expression for the Green's function

$$
\begin{aligned}
{}_kG_n &= \frac{1}{2}\delta_{k,n+1} - \frac{1}{2}\delta_{k,n-1} + \frac{1}{2}\,{}_{k+1}I_n - \frac{1}{2}\,{}_{k-3}I_n \\
&\quad + \sum_{j=0}^{k-1} \frac{1}{8}\,{}_{k-1-j}I_{n+2+j} - \frac{1}{4}\,{}_{k-1-j}I_{n+j} \\
&\qquad + \frac{1}{8}\,{}_{k-1-j}I_{n-2+j} \\
&\quad + \sum_{j=0}^{k-2} \frac{1}{8}\,{}_{k-2-j}I_{n+1-j} - \frac{1}{4}\,{}_{k-2-j}I_{n-1-j} \\
&\qquad + \frac{1}{8}\,{}_{k-2-j}I_{n-3-j}
\end{aligned}
\tag{36}
$$

with $n = 0, 1, 2, \ldots \infty$; $k = 2, 3, 4, \ldots \infty$ and

$$
{}_kG_{-n} = {}_kG_n \tag{37}
$$

for $n \leq 0$.

The function ${}_kI_n$ is given by

$$
\begin{aligned}
{}_kI_n &= 2\sum_{l=0}^{k}\sum_{s=0}^{[l/2]}\sum_{r=0}^{k-l}(-1)^{n+s}\left(\frac{1}{2}\right)^{3l+3r-4s}\binom{l}{s}\binom{2l-2s}{l} \\
&\qquad \times \binom{2r}{r}\binom{k-l+r}{2r}\binom{2l-4s+2r}{l-2s+r-n}
\end{aligned}
\tag{38}
$$

In Fig. 4, ${}_kG_n$ is depicted for $n = -9\ldots, -1, 0, 1, \ldots 9$; $k = 1, 2, \ldots 10$.

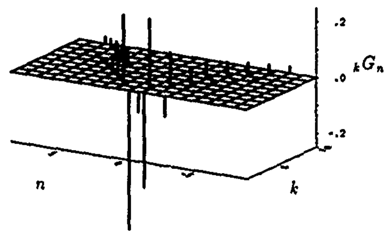

Figure 5: Values of the Green's function

References

[1] P.B. Johns, R.L. Beurle, "Numerical Solution of 2-Dimensional Scattering Problems using a Transmission-Line Matrix", Proc. IEE, vol.118, no. 9, pp 1203-1208, Sept 1971.

[2] W.J.R. Hoefer, "The Transmission Line Matrix Method-Theory and Applications", IEEE Trans. Microwave Theory Tech., vol. MTT-33, no.10,pp.882-893, Oct 1985.

[3] W.J.R. Hoefer, "The Transmission Line Matrix (TLM) Method", Chapter 8 in "Numerical Techniques for Microwave and Millimeter Wave Passive Structures", edited by T. Itoh, New York, 1989, J. Wiley, New York 1989, pp. 496-591.

[4] K.E. Gustafson, "Partial Differential Equations and Hilbert Space Methods", J. Wiley, New York 1987.

[5] R.F. Harrington, "Field Computation by Moment Methods", Krieger, Malabar, Florida, 1982.

[6] P.A.M. Dirac, "Quantum Mechanics", fourth edition, Oxford University Press, Oxford

[7] J.v. Neumann, "Mathematische Grundlagen der Quantenmechanik", Springer, Belin, 1932.

[8] R.E. Collin, "Field Theory of Guided Waves", second edition, IEEE Press, New York 1991, pp. 55–172.

[9] W.J.R. Hoefer, "The Discrete Time Domain Green's Function or John's Matrix – a new powerful Concept in Transmission Line Modelling", International Journal of Numerical Modelling : Electronic Networks, Devices and Fields, Vol. 2, 215-225, 1989.

[10] J. Weidmann, "Lineare Operatoren in Hilberträumen", B.G. Teubner, Stuttgart, 1976, pp. 96–105.

[11] H. Heuser, "Funktionalanalysis", B.G. Teubner, Stuttgart, 1986, pp. 106–113.

Solving eigenvalue and steady-state problems using time-domain models

Gunnar Nitsche
Lehrstuhl für Nachrichtentechnik
Ruhr-Universität Bochum
D-4630 Bochum 1
Germany

Time-domain modelling of partial differential equations has become popular in the last years for several reasons. The detailed time-domain behaviour, however, is often not of primary concern, but one is more interested in the eigenvalues and eigenfunctions of a system or its steady-state response to a sinusoidal excitation. These kinds of problems are usually approached by methods based on the discrete Fourier transform.

A new alternative approach to efficiently compute the low frequency eigenmodes of a time-domain model approximating a physical system will be proposed. The method is based on principles known from digital signal processing, in particular from parametric spectrum estimation, so it is not surprising that the achievable accuracy is much higher than the accuracy of the non-parametric Fourier transform approach. The algorithm works in the general lossy case even for a very large number of unknowns and can easily be extended to calculate steady-state solutions for several different frequencies simultaneously.

Restaurant Guide

Near the TU there are some restaurants and coffee-houses were you can go to. Some of these are listed below. The number is related to the numbers on the map. So you can easily find your location.

1. CANTON *chinese restaurant,* Theresienstr. 49
2. BEI MARIO *pizzeria, italian restaurant,* Luisenstr.
3. BELLA ITALIA *pizzeria, italian restaurant,* Türkenstr.
4. HIÊǸ *Vietnamese food,* Schellingstr. 91
5. CAFE ALTSCHWABING *coffee house, bistro,* Schellingstr.
6. WEINSCHATULLE *restaurant,* Theresienstr.
7. MC DONALDS *fast food,* Augustenstr.

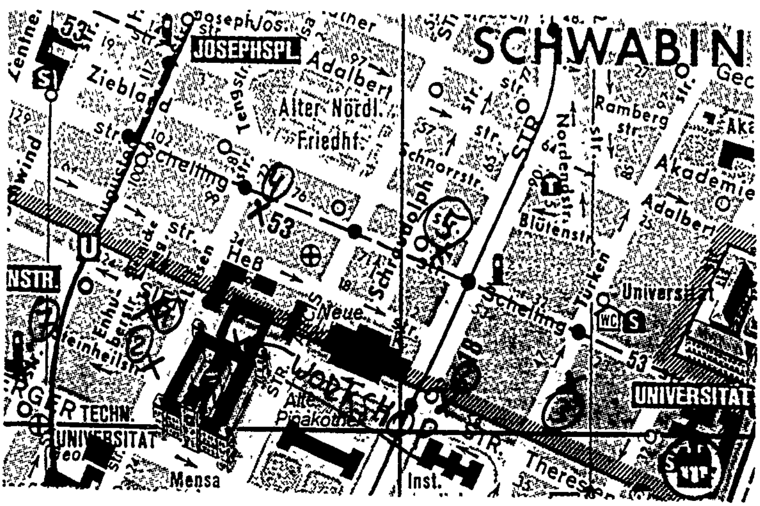

On thursday evening there is a social event consisting of a Song Recital with Piano and dinner for all workshop participants at the restaurant "Seehaus", Englischer Garten (see the map below). We recommend you to reach the Seehaus by car or taxi coming from the Mittlerer Ring.